Formation Water Chemistry and Modeling of Fluid-Rock Interaction for Improved Oil Recovery in Aux Vases and Cypress Formations, Illinois Basin

Ilham Demir

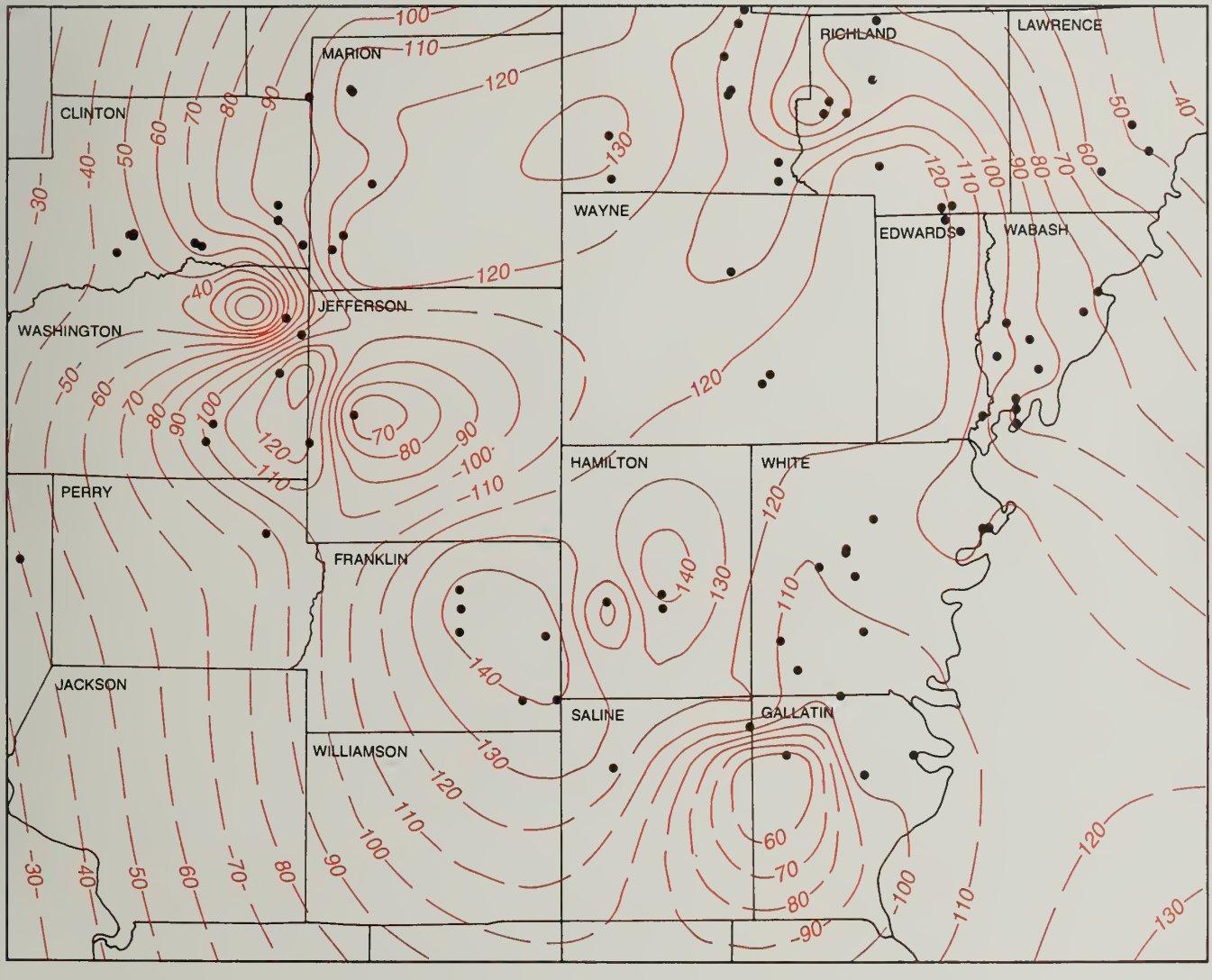

Illinois Petroleum 148
1995

Department of Energy and Natural Resources
ILLINOIS STATE GEOLOGICAL SURVEY

Formation Water Chemistry and Modeling of Fluid-Rock Interaction for Improved Oil Recovery in Aux Vases and Cypress Formations, Illinois Basin

Ilham Demir

Illinois Petroleum 148
1995

ILLINOIS STATE GEOLOGICAL SURVEY
Jonathan H. Goodwin, Acting Chief

Natural Resources Building
615 East Peabody Drive
Champaign, Illinois 61820-6964

DISCLAIMER

This report was prepared by the Illinois State Geological Survey (ISGS) for a project sponsored by the State of Illinois and the U.S. Department of Energy (USDOE). It presents reasonable interpretations of available scientific data. Any opinions, findings, conclusions, or recommendations expressed herein are those of the author and do not necessarily reflect the views of the USDOE. Neither the ISGS, any member of the ISGS staff, the Illinois Department of Energy and Natural Resources (ENR), nor the USDOE assumes any liability with respect to the use, or for any damages resulting from the use, of any information contained in this report. Use of trademarks and brand names in this report does not constitute endorsement of any product by the ISGS, ENR, or USDOE.

Editor — E. Anne Latimer
Graphic Artist — Michael W. Knapp
Graphic Artist — Vicki Reinhart

Printed by the authority of the State of Illinois/1995/1000

printed with soybean ink on recycled paper

CONTENTS

FIGURES

TABLES

ABSTRACT

Geochemical characterization of oil reservoir formation waters is important in the study of the diagenetic history of sedimentary basins, and in reservoir analysis for application of improved oil recovery techniques. This study focused on the practical application of formation water chemistry of two important oil-producing reservoir rocks, the Mississippian Aux Vases and Cypress Formations, in Illinois.

A total of 99 formation water samples was collected from oil wells in 36 fields producing from the Aux Vases or Cypress Formations. Two more samples were collected from oil-water separation tanks. The samples were analyzed for various geochemical parameters on site and in the laboratory. The analytical results suggested that high salinities in Aux Vases and Cypress formation waters resulted at least partly from halite dissolution, and were subsequently modified by diagenetic reactions. Relationships among the chemical compositions of formation waters, the mineralogical compositions of their host rocks, and depth suggested that dissolved cation concentrations in the formation waters are controlled predominantly by dissolution and recrystallization of calcite, as well as by leaching or dissolution of clay minerals. Albitization of detrital plagioclase and probably partial dolomitization of calcite also affected cation concentrations. Clay minerals and feldspars have apparently released potassium (K) and magnesium (Mg) into the formation waters; the implication is that clay minerals in the Aux Vases and Cypress Formations are largely detrital and/or were formed diagenetically prior to the emplacement of present subsurface waters in the reservoir. Variations in solute concentrations in wells producing from the same formation in the same field may indicate a lack of communication between different parts of the same reservoir.

Electrical resistivity and total dissolved solids (TDS) content data for the formation waters are used to calculate water saturation and permeability of the reservoirs, two important parameters for reservoir analysis and management. Empirical relationships between the resistivity, TDS, and temperature of the Aux Vases and Cypress formation waters were developed. The areal distribution of all available resistivity and TDS values was mapped and used to estimate both resistivity and TDS in areas where no data were available.

Computer simulations of mineral precipitation and/or dissolution reactions and accompanying porosity changes that would take place in improved oil recovery processes were conducted for several scenarios. These simulations were used to assess potential formation damage that can be caused by disturbance of the oil reservoir's original physical-chemical state during primary production or improved oil recovery processes.

INTRODUCTION

Assessing the chemical composition of saline formation waters can be important in delineating the diagenetic history of sedimentary basins, which in turn is useful for oil exploration and production. Because of the marine origin of most sediments, the origin of saline formation waters was thought to be seawater trapped in the pores of the sediments. Recent studies by Bethke and Marshak (1990), however, have provided evidence that, in many cases, the dissolution of evaporites in gravity-driven groundwater may be the primary mechanism for generating saline formation waters. Bethke and Marshak proposed that tectonic deformations along the continental margins of North America induced long-range, subsurface water migration. Long-range migration implies that hydrocarbon reservoirs can be located in areas

hundreds of miles away from the source rock. Long-range migration provides opportunity for the migrating fluids (trapped seawater or meteoric water) to evolve chemically as a result of reaction with the host sediments and mixing with waters of different compositions, and as a result of changes in their pressure and temperature along the migration path. During each process, existing minerals may dissolve and new ones may precipitate, which can change the porosity and permeability of the host rocks and leave various chemical signatures in the fluid composition.

Attempts to use the chemical composition of formation waters to infer paleoflow paths and/or diagenetic reactions have been made by numerous investigators (Clayton et al. 1966, Graf et al. 1966, Collins 1975, Hitchon et al. 1971, Carpenter 1978, Frape et al. 1984, Morton and Land 1987, Sanders 1991, Stueber and Walter 1991, Land and Macpherson 1992, Macpherson 1992, Moldovanyi and Walter 1992, Stueber et al. 1993). Because the chemical composition of formation waters often reflects the mineralogical composition of their host reservoirs, maps of geochemical parameters often delineate changes in permeability, lithologic variations, diagenetic changes and, therefore, possibly identify stratigraphic traps and structural features. Collins (1975) reported that petroleum accumulation is often correlated with salinity transition zones. Moldovanyi and Walter (1992) perhaps summarized the importance of formation water chemistry best by stating that "a more complete understanding of processes active during the evolution of sedimentary basins emerges when diagenetic studies of sedimentary rocks are integrated to geochemical trends in subsurface waters."

Knowledge of the formation fluid chemistry can also be used to prevent formation damage and improve the recovery of oil from existing fields. Differences in the chemical composition of formation fluid from different wells within a reservoir in the same field can indicate mineralogical heterogeneity or lack of communication, and thus help in delineating separate flow units within a reservoir. Formation water chemistry can be used to determine whether injection water has reached a producing well during secondary oil recovery. Mineral precipitation and dissolution reactions that occur in reservoirs as a result of water, alkali, and CO_2-floodings, acidizing, and other enhanced oil recovery processes can be investigated by using geochemical data as input for geochemical modeling.

This study demonstrates how formation water chemistry can be used to improve oil production in the Mississippian Aux Vases and Cypress Formations in Illinois. Figure 1 shows stratigraphic positions of the Aux Vases and Cypress Formations. Chemical data on the formation waters were used to interpret reservoir geology, determine reservoir properties (porosity, permeability, water saturation), and assess formation damage. Data on formation water chemistry were also input to a computerized mathematical and geochemical model to simulate the mineral dissolution and precipitation reactions during improved oil recovery processes. The effects of the mineral dissolution and precipitation on reservoir porosity were determined by using the computer simulation results; implications for oil production were also assessed.

ANALYTICAL PROCEDURES

Sampling of Formation Waters

A total of 99 formation water samples was collected from oil wells producing from the Aux Vases (52 samples) and Cypress (47 samples) Formations. Two other samples of formation waters (one from the Cypress Formation and another from the Waltersburg Formation) that were used as injection waters for the Aux Vases and

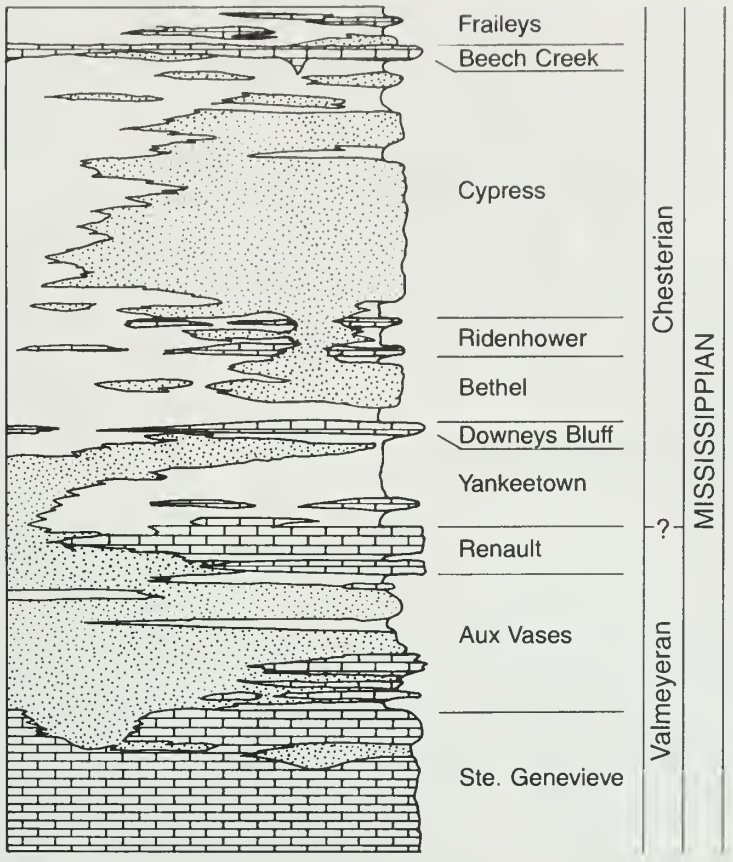

Figure 1 Generalized upper Valmeyeran and Chesterian geologic column (Mississippian System) of southern Illinois (from Leetaru 1990).

Cypress reservoirs were collected from separation tanks. Each sample is identified by well API number and field name in appendix B. Arrangements with oil companies were made to discontinue chemical treatments (corrosion inhibitors, acidizing, etc.) of the wells at least 4 hrs (usually 24 hrs) before they were sampled. The samples remained isolated from the atmosphere as much as possible to minimize oxidation and degassing until they were tested for pH, Eh, and resistivity and processed for laboratory chemical analyses. The procedure for collecting formation fluids is based on a USGS method (Lico et al. 1982), illustrated in figure 2 , and outlined in appendix A (see also ISGS 1993).

Analyses of Formation Waters and Reservoir Rocks

An inductively coupled plasma spectrometer was used to analyze the formation water samples for sodium (Na), calcium (Ca), magnesium (Mg), potassium (K), strontium (Sr), barium (Ba), lithium (Li), iron (Fe), manganese (Mn), boron (B), silicon (Si), aluminum (Al), lead (Pb), titanium (Ti), vanadium (V), cobalt (Co), nickel (Ni), copper (Cu), zinc (Zn), zirconium (Zr), cadmium (Cd), beryllium (Be), chromium (Cr), arsenic (As), selenium (Se), molybdenum (Mo), and antimony (Sb).

Concentrations of anions and ammonium (NH_4^+) were determined using standard ASTM-EPA procedures (ASTM 1976, U.S. EPA 1975, 1985): chloride (Cl^-) by the titrimetric-mercuric nitrate method; bromide (Br^-) and iodide (I^-) by a titrimetric method; sulfate (SO_4^{2-}) by the turbidimetric method; nitrate (NO_3^-) by spectrophotometric-cadmium reduction method; carbonate (CO_3^{2-}) and bicarbonate

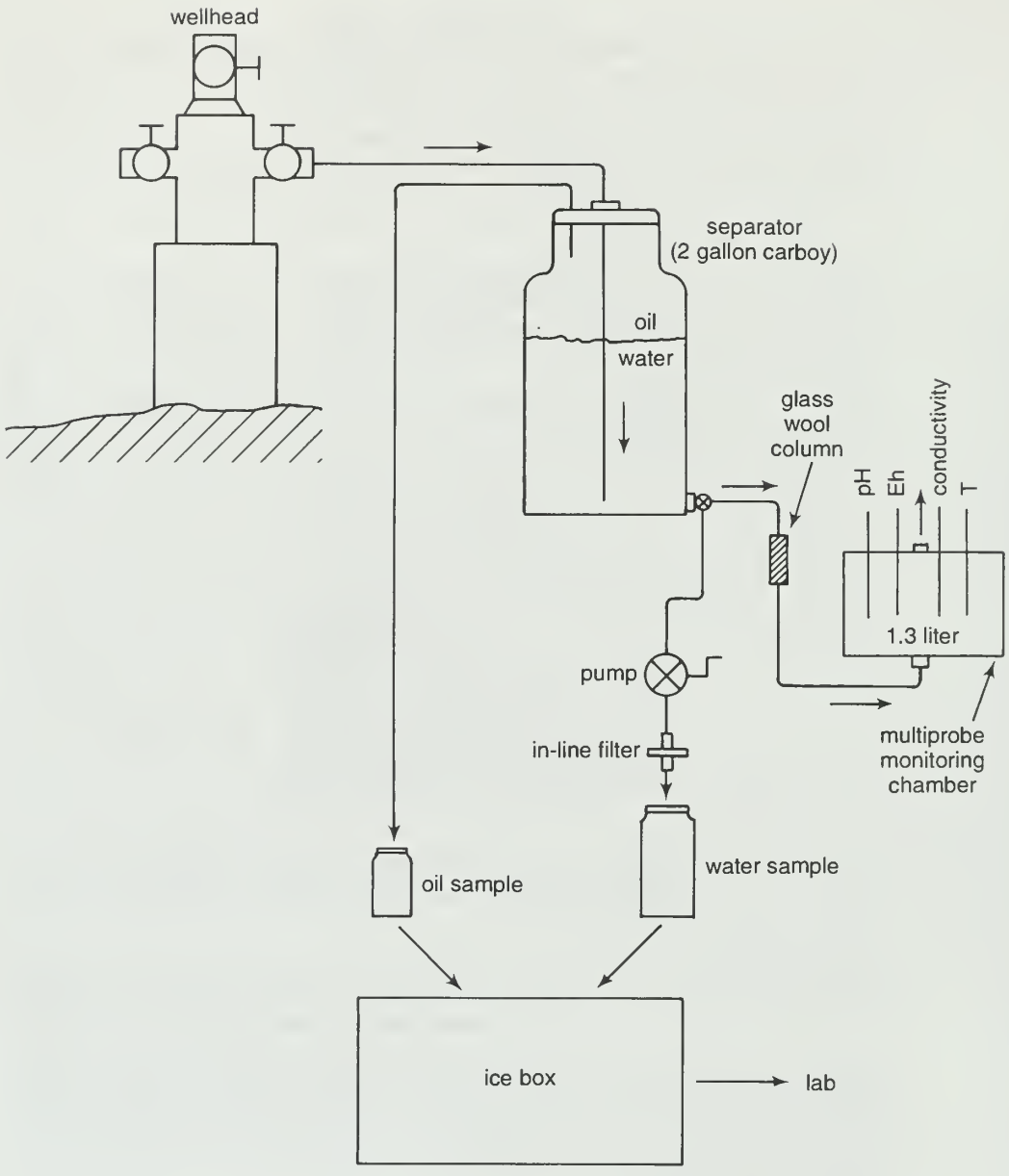

Figure 2 Schematic of the setup for collecting formation fluids in the field.

(HCO_3^-) by a titrimetric method; and NH_4^+ by potentiometric-ion selective electrode method. Details of these methods are in ISGS (1993).

Mineralogical data for the reservoir rocks were determined using X-ray diffraction techniques (ISGS 1993). The sources of the core samples analyzed for mineralogical composition are given in appendix C.

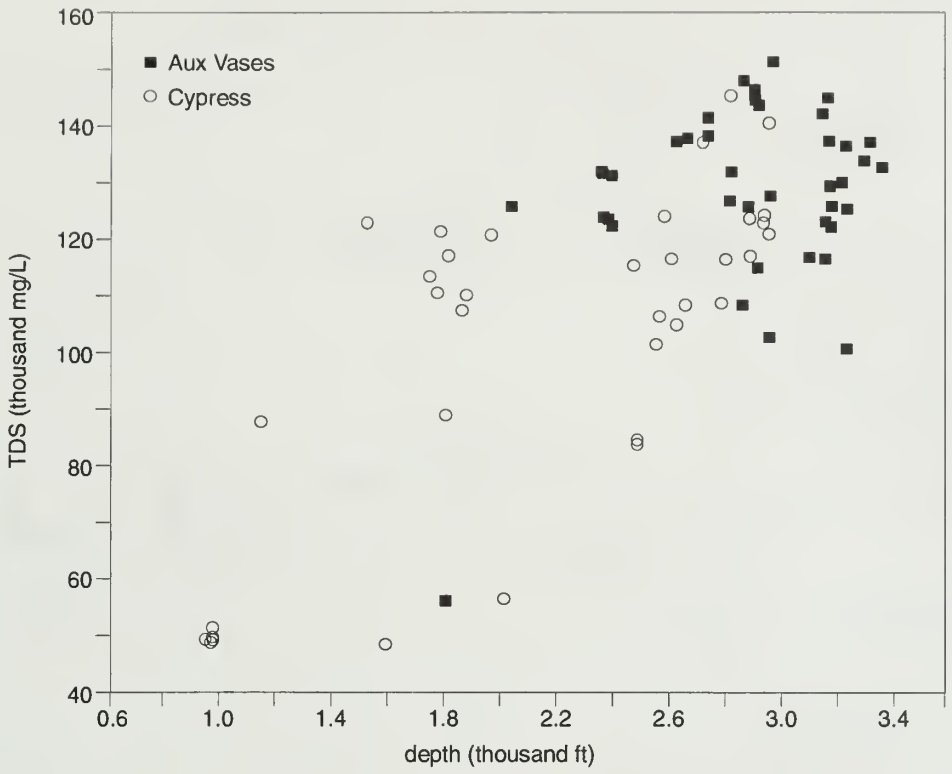

Figure 3 Relationship between total dissolved solids (TDS) content and depth of Aux Vases and Cypress formation waters in Illinois.

APPLICATIONS OF FORMATION WATER CHEMISTRY

Geological Interpretations

Diagenetic reactions Geological interpretations of reservoir rocks were based on data on natural processes not affected by anthropogenic processes, such as waterflooding of the reservoirs. Therefore, only geochemical data on formation water samples from wells judged not to have been affected by waterflooding or other improved oil recovery processes were used as a basis for geological interpretation.

The total dissolved solids (TDS) contents of the Aux Vases and Cypress formation waters are significantly higher (43,325–151,399 mg/kg, appendix B) than that of seawater (~35,400 mg/kg, Drever 1988), and tend to increase toward the deeper parts of the Basin (figs. 3–5). The origin of the high TDS levels in the Illinois Basin has been debated extensively in the literature (Clayton et al. 1966, Graf et al. 1966, Bethke 1986, Bethke and Marshak 1990, Walter et al. 1990, Stueber and Walter 1991, Stueber et al. 1993). Dissolution of evaporites, membrane filtration through shales, evaporated seawater, density stratification, and diagenetic reactions have been invoked to explain the high TDS levels in formation waters in the Illinois Basin and elsewhere. In most cases, a combination of several processes is likely.

One way of investigating the sources of high TDS or salinities in formation waters is to examine the relationship of chlorine (Cl) to bromine (Br). During evaporation, the Cl/Br ratio of seawater remains constant until halite precipitation begins (Carpenter 1978). Although a small amount of Br can replace Cl in the halite crystal structure, the Cl/Br ratio of halite is much greater than that of seawater. The Cl/Br

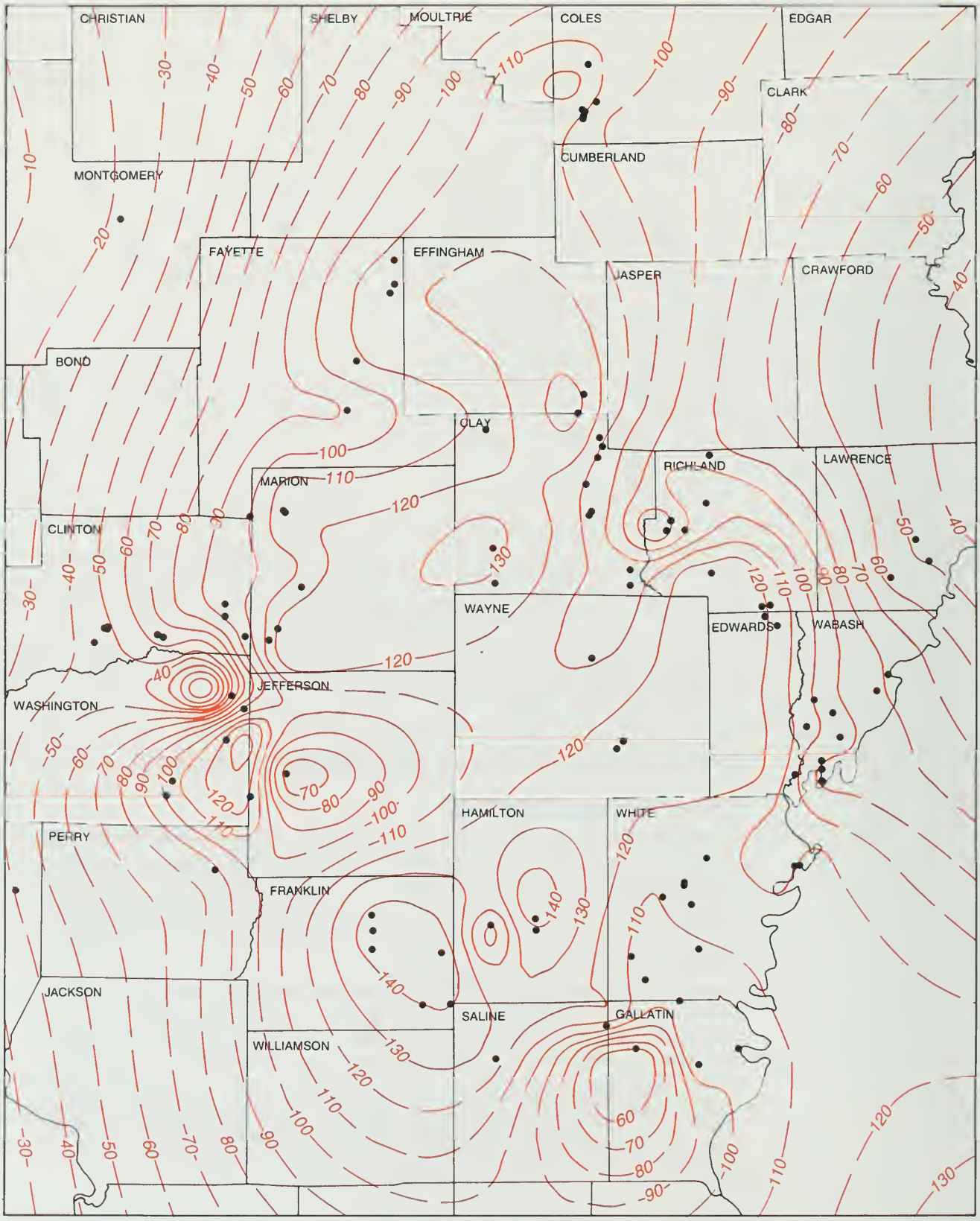

Figure 4 Areal distribution of TDS in Cypress formation waters.

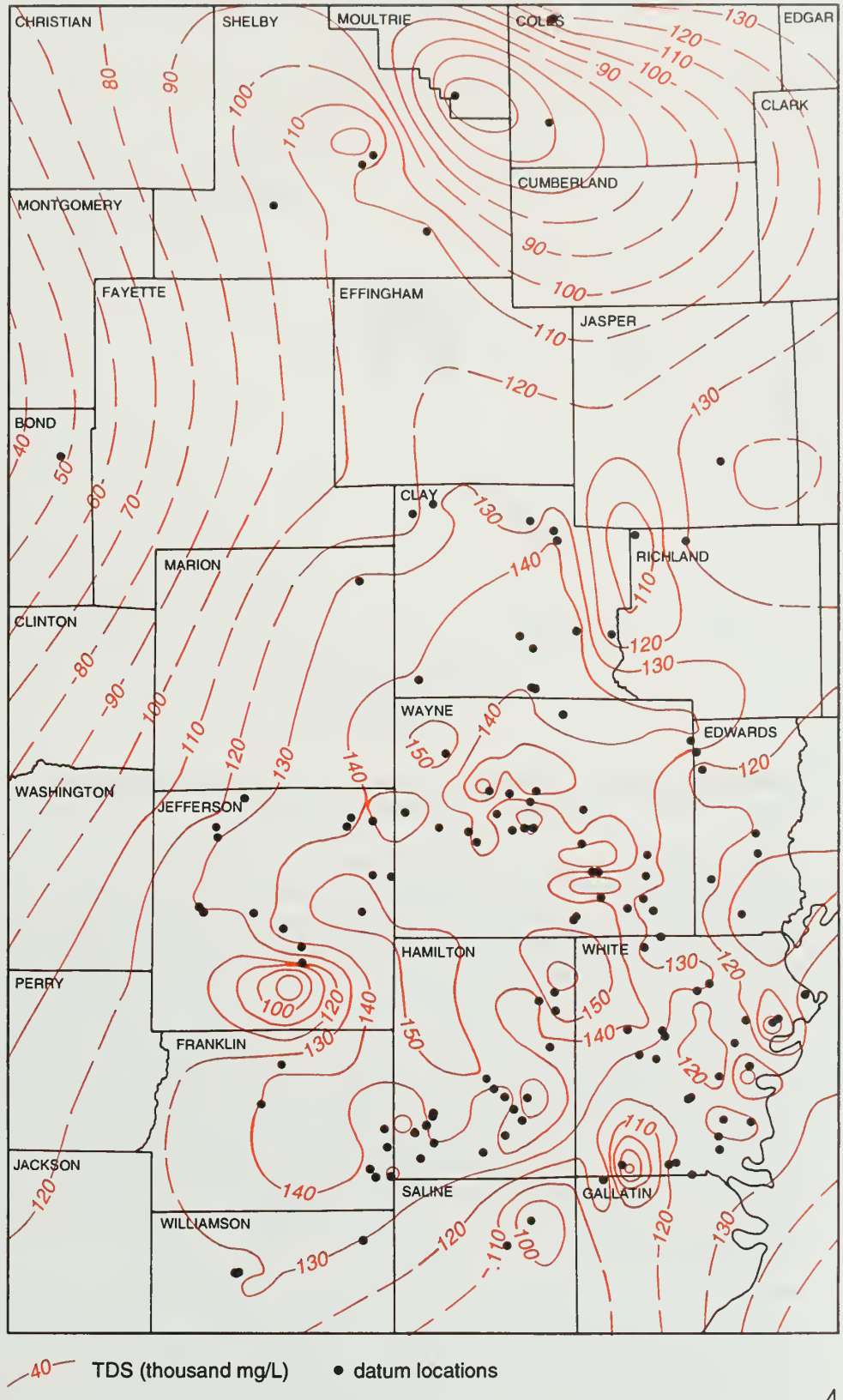

Figure 5 Areal distribution of TDS in Aux Vases formation waters.

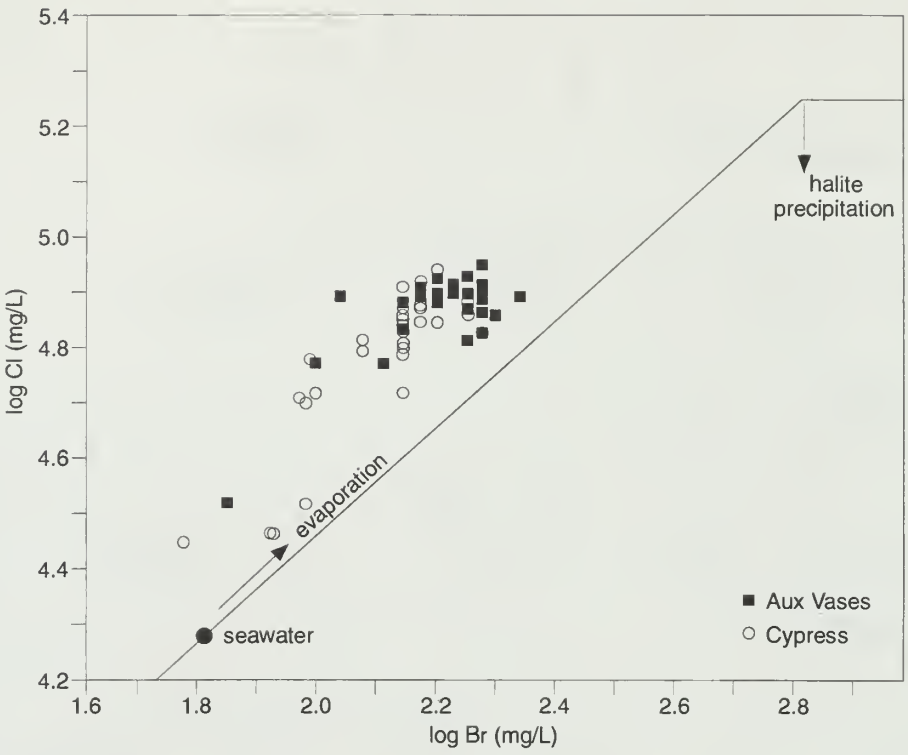

Figure 6 Relationship between Cl and Br in Aux Vases and Cypress formation waters (seawater evaporation trajectory is from Carpenter 1978).

ratio of seawater, therefore, decreases during the precipitation of halite. If a brine forms by congruent dissolution of halite, the Cl/Br ratio of the brine can be up to 30 times that of seawater (Walter et al. 1990). On the other hand, incongruent halite dissolution (halite recrystallization) can produce fluids that have Cl/Br ratios lower than the ratio in the seawater. The Cl/Br ratio of these fluids also varies depending on the Br content of the original halite, the value of the distribution coefficient for Br in halite, and the ratio of rock to water (Land and Prezbindowski 1981, Stoessell and Carpenter 1986, Hanor 1987, Walter et al. 1990). Waters from the Aux Vases and Cypress Formations are enriched in Cl relative to the evaporation trajectory of seawater (fig. 6), suggesting the presence of a congruent halite dissolution component in these waters. Incongruent halite dissolution would have resulted in a lower Cl/Br ratio in the brine relative to the seawater evaporation trajectory. Data in figure 6 and the scarcity of evaporite sediments in the Illinois Basin, therefore, suggest that halite recrystallization, if any, was not significant enough to influence the salinities of the brines in the Aux Vases and Cypress Formations.

Bethke (1986) proposed that formation waters have high salinities in the Illinois Basin due to extensive reaction between the rocks, particularly halite deposits, and meteoric water introduced into the basin from elevated recharge areas formed by the uplift of the Pascola Arch southwest of the basin. Although the Illinois Basin has few evaporitic sediments, Walter et al. (1990) suggested that the dissolution of small amounts of halite in Mississippian sediments could account for an average of about 30% of Na and Cl concentrations in the formation fluids of the Mississippian clastics. Oxygen and hydrogen isotope studies by Clayton et al. (1966) indicated that meteoric water may have mixed with seawater trapped in the pores of sediments during the compaction and tectonic deformation of the Illinois Basin. If this is the

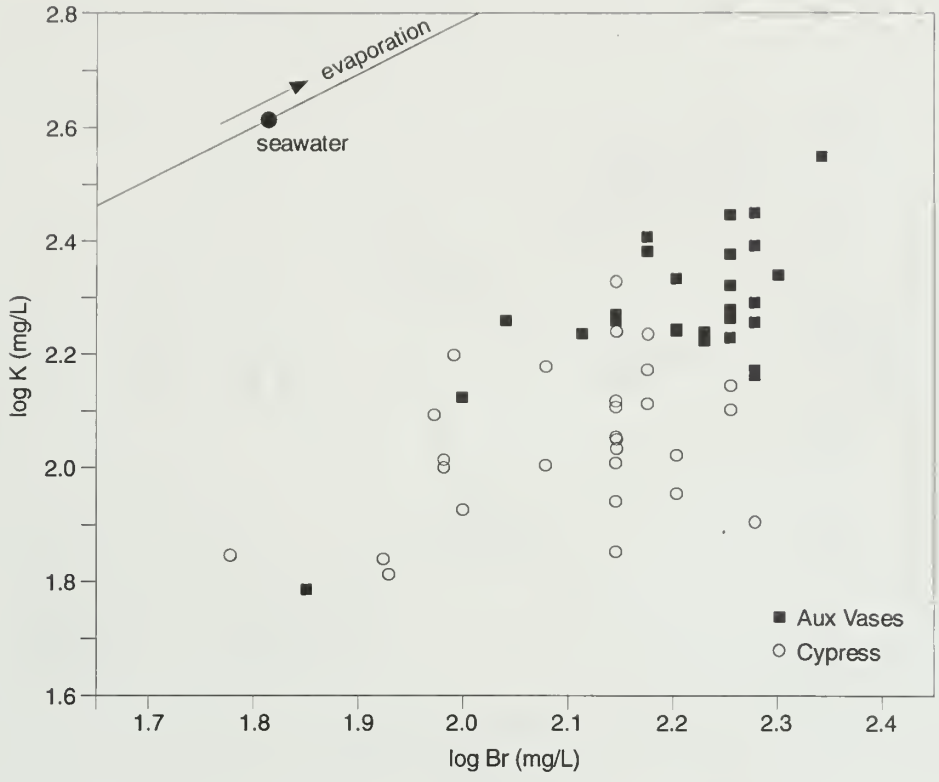

Figure 7 Relationship between K and Br in Aux Vases and Cypress formation waters (seawater evaporation trajectory is from Carpenter 1978).

case, the seawater in the mixture apparently had not evaporated to the halite saturation point (fig. 6).

Relationships between Br and other elements, such as potassium (K), magnesium (Mg), calcium (Ca), and strontium (Sr), in formation waters can be used to infer the nature of diagenetic reactions in the subsurface (Rittenhouse 1967, Carpenter 1978, Das et al. 1990). Aux Vases and Cypress formation waters are depleted of potassium (K) and magnesium (Mg) relative to the evaporation trajectory of seawater (figs. 7, 8). This relationship suggests that the original trapped seawater was replaced or mixed with waters containing low ratios of K/Br and Mg/Br, and/or modified by diagenetic reactions. The diagenetic reactions invoked to explain the Mg and K depletion include dolomitization of calcite and conversion of low-K clay minerals, such as kaolinite, to high-K clay minerals, such as illite, and to authigenic K-feldspar (Stueber and Walter 1991, Stueber et al. 1993). The diagenetic depletion of K and Mg in the formation waters, relative to the evaporation trajectory of seawater, appears to have occurred primarily before these waters were placed into the Aux Vases and Cypress Formations.

Levels of dissolved K and Mg increased slightly after placement of the waters in the Aux Vases and Cypress Formations for the following reasons. Although there is considerable scatter in data, the formation waters of the Aux Vases generally contain higher concentrations of K and Mg than those of the Cypress (figs. 7, 8). Furthermore, K- and Mg-bearing minerals such as illite, illite/smectite, chlorite, and K-feldspar are, on average, more abundant in the Aux Vases core samples than in the Cypress core samples (fig. 9). These observations, shown in figures 7 to 9, suggest that the clay and feldspar minerals in the Aux Vases samples and possibly those in the Cypress samples contributed K and Mg to the formation fluids by dissolution or

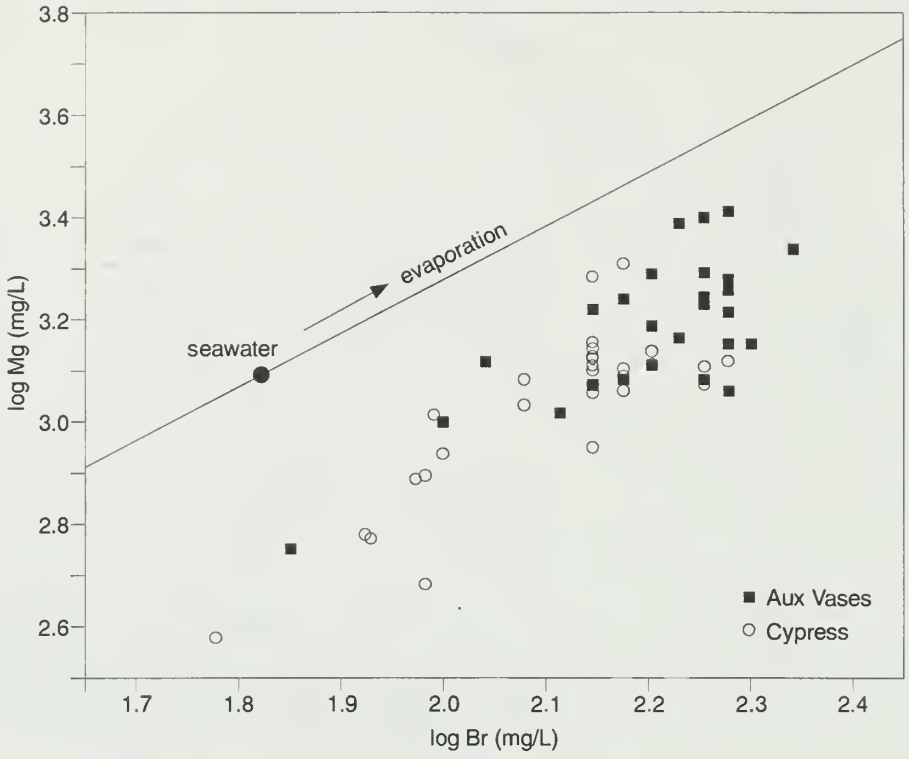

Figure 8 Relationship between Mg and Br in Aux Vases and Cypress formation waters (seawater evaporation trajectory is from Carpenter 1978).

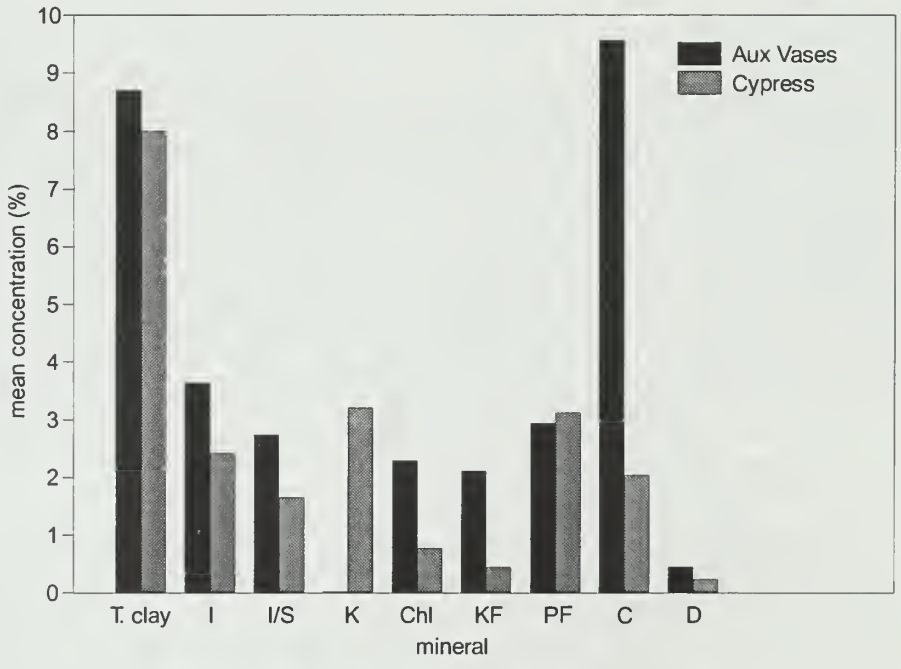

Figure 9 Mean concentrations of minerals (excluding quartz) in Aux Vases (25 cores) and Cypress (14 cores) Formations core samples. T. clay = total clay; I = illite; I/S = illite/smectite; K = kaolinite; Chl = chlorite; KF = potassium feldspar; PF = plagioclase; C = calcite; D = dolomite.

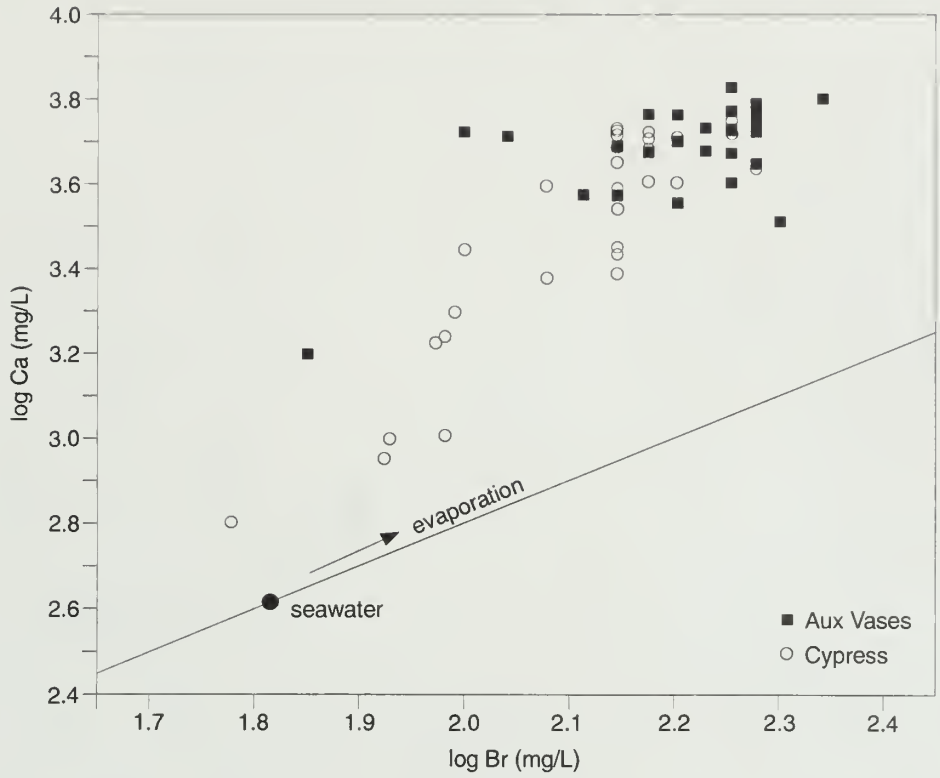

Figure 10 Relationship between Ca and Br in Aux Vases and Cypress formation waters (seawater evaporation trajectory is from Carpenter 1978).

leaching. Differences in the amounts of dissolved K and Mg in Aux Vases and Cypress formation waters cannot be explained by dilution of generally shallower Cypress formation waters with meteoric water. The reason is the concentration of Mg and K does not significantly correlate with depths of the formation waters (r^2 = 0.141 for Mg, r^2 = 0.386 for K). Furthermore, dilution with meteoric water alone would not affect the K/Br or Mg/Br ratios. It then follows that clay minerals and K-feldspar in the Aux Vases and Cypress Formations are detrital and/or formed diagenetically prior to the placement of the present subsurface waters.

Decreased concentration of Mg (fig. 8) and increased concentration of Ca (fig. 10) relative to the seawater evaporation trajectory indicate the possible dolomitization of some calcite in the Aux Vases and Cypress Formations, or dolomitization of limestones within, just above, or below the Aux Vases-Cypress section. Choquette and Steinen (1980) estimated that extensive dolomitization in the Ste. Genevieve Limestone underneath the Aux Vases Formation began early during burial history of the limestone, perhaps at a depth of 100 meters or less. Mattes and Mountjoy (1980) suggested that, in many cases, dolomitization that begins near the surface may continue, or even accelerate, as increasing burial depth and temperature reduce kinetic obstacles to the formation of ordered dolomite. Dolomitization of limestone as it was buried, however, could not be the only mechanism by which Ca was enriched in the Aux Vases and Cypress formation waters because the correlation between Ca/Mg ratio and depth of formation waters is not strong enough (fig. 11). Furthermore, dolomitization alone would have resulted in a negative correlation between Ca and Mg, the opposite of the positive correlation shown in figure 12.

The albitization of detrital plagioclase was proposed by Land and Prezbindowski (1981, 1985) as another mechanism that increases Ca levels in formation waters.

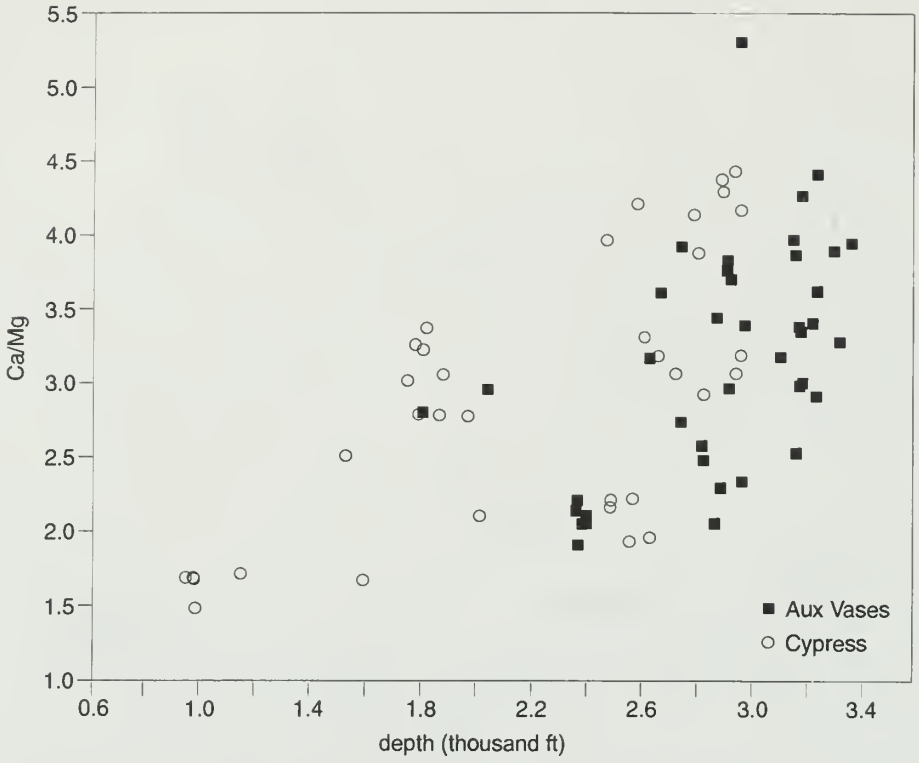

Figure 11 Relationship between the ratio of Ca (mg/L) to Mg (mg/L) and depth of Aux Vases and Cypress formation waters.

Although the albitization hypothesis is consistent with the fact that albite is the major plagioclase in the Aux Vases and Cypress Formations, it cannot alone explain the positive correlation between Ca and Mg (fig. 12). A reasonable suggestion, therefore, is that partial dissolution of minerals in the Aux Vases and Cypress Formations, albitization of plagioclase, and dolomitization of calcite all played a role in controlling the levels of Ca and Mg in the formation waters.

In summary, the levels of dissolved K and Mg in the brines were controlled by partial dissolution of K-feldspar and clay minerals, and in the case of Mg, also by the dolomitization of calcite. Dissolution of calcite, induced by increased partial pressure of CO_2 gas resulting from the breakdown of kerogen, would release calcium ion (Ca^{2+}) and increase bicarbonate (HCO_3^-) into solution. Because the HCO_3^- concentration is too low to balance Ca^{2+} in Aux Vases and Cypress formation waters, calcite dissolution could be only partly responsible for the concentration of Ca in solution. Therefore, in addition to calcite dissolution, albitization of detrital plagioclase and probably dolomitization released Ca^{2+} into the waters of the Aux Vases and Cypress Formations.

Because strontium (Sr) substitutes for Ca in the crystal structure of Ca-bearing minerals, Ca and Sr would be released the same time such minerals dissolve. This mechanism alone would result in a statistically significant positive correlation between Ca and Sr in the solution. Such a correlation exists for the Cypress Formation but not for the Aux Vases Formation (fig. 13). Then, the enrichment of Sr relative to the seawater evaporation trajectory (fig. 14) suggests that dissolution of Ca-bearing minerals raised Sr levels in the Cypress formation waters. In Aux Vases formation waters, however, calcite recrystallization, which is known to

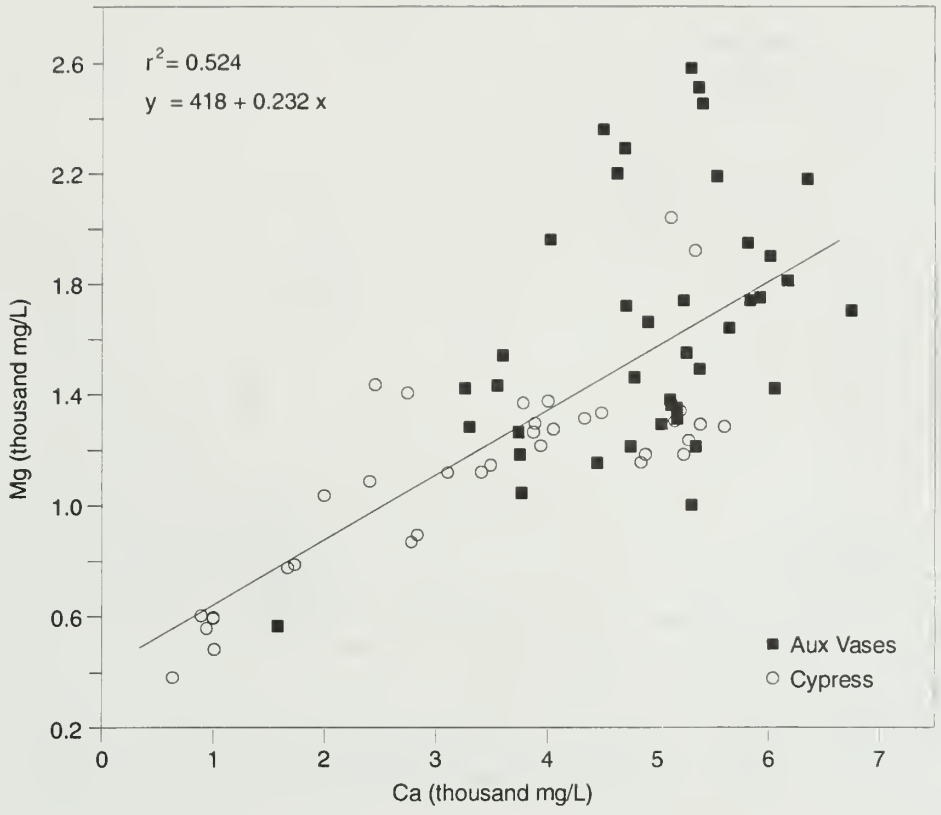

Figure 12 Relationship between Mg and Ca in Aux Vases and Cypress formation waters.

replace Sr with Ca in the crystal structure of calcite, was probably an important mechanism for raising Sr levels in the solution.

Heterogeneity studies Knowledge of formation water chemistry is useful in heterogeneity studies of oil-producing fields. Variations in solute concentrations in wells producing from the same reservoir in the same field may indicate a lack of communication or mineralogical heterogeneity between different parts of the reservoir within the field. For example, in the Dale Consolidated Field, the sulfate (SO_4^{2-}) concentration in sample EOR-B13 of formation water and iron (Fe) concentrations in samples EOR-B13 and EOR-B107 are much higher than those in other Aux Vases samples in the same field (appendix B). Bicarbonate (HCO_3^-) and SO_4^{2-} concentrations in sample EOR-B34 (a Cypress sample) are considerably lower than those in other Cypress samples in Mattoon field (appendix B).

Although the TDS in brines generally increases with depth at which the samples were taken, the data points are scattered widely in the TDS-depth plot (fig. 3). This scattering may be primarily due to structural and stratigraphic irregularities in the basin and, to a lesser degree, to sampling and analytical errors. For example, sample EOR-B74 from the New Harmony Consolidated Field had a very low TDS value (43,325 mg/L) for the depth of 2,873 ft (appendix B) at which it was taken. Although the well is within a recent waterflood area, production statistics showed that the waterflood had not reached the well at the time of sampling (Finnel, EQUINOX Oil Company, personal communication 1992). If that was the case, then the low TDS value in this pool was probably due to the mixing of brine with fresh

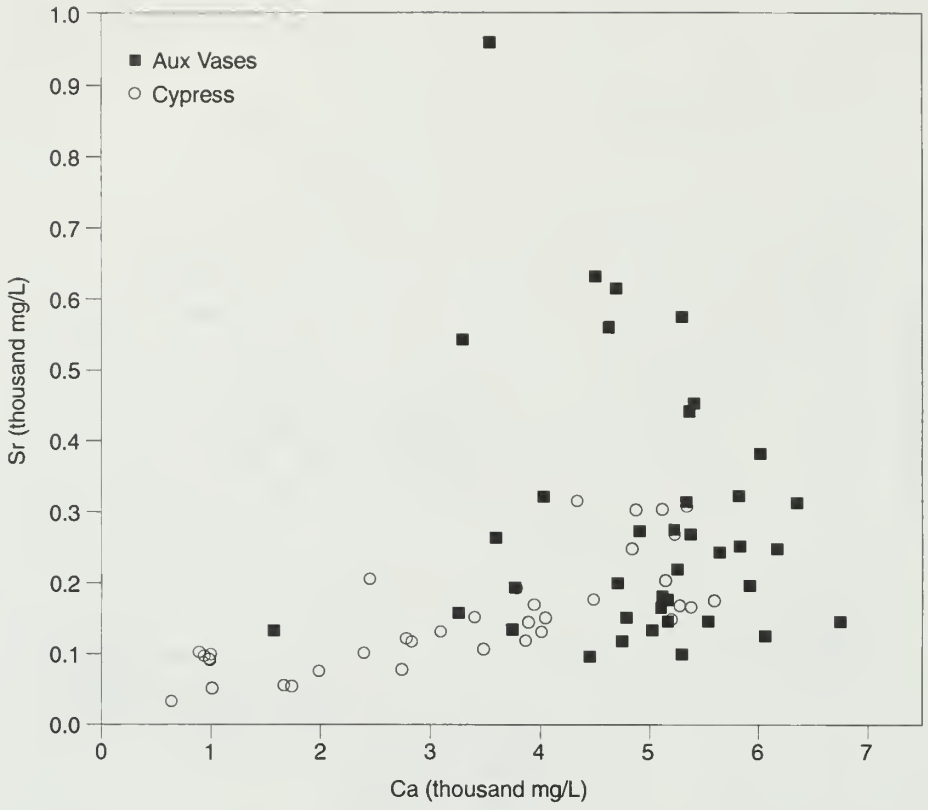

Figure 13 Relationship between Sr and Ca in Aux Vases and Cypress formation waters.

meteoric water. Such an occurrence would suggest the presence of a recharge zone, such as a high permeability zone or a fault extending to the surface. An extremely low flow rate in this well suggested the swelling of clay minerals and/or the conversion of anhydrite to gypsum, both of which can be initiated by freshwater intrusion. A similar interpretation is valid for a Mattoon Field well (sample EOR-B35, appendix B) that produces oil from an average depth of 1,808 feet. This well has a TDS content of only 56,100 mg/L, which is much lower than the TDS values generally encountered in similar depths (appendix B, fig. 3).

Only a few examples of using formation water chemistry for geological interpretation are discussed in this report. Users of this formation water data will likely have other ideas about possible geological and stratigraphic interpretations.

Formation Water Chemistry and Reservoir Properties

Resistivity–TDS–temperature relationships An empirical relationship between water resistivity (R_w) and TDS content (fig. 15) was established using field measurements of formation water resistivities (ohm-m) and laboratory TDS data (mg/L) for 56 oil wells. The empirical relationship between water resistivity and TDS is as follows:

$$\log R_w = 2.841 - 0.788 \log (\text{TDS}) \text{ at } 25\,^{\circ}\text{C} \qquad [1]$$

Equation (1) was used to calculate water resistivity values for more than 300 additional wells for which TDS values (obtained from DOE and ISGS databases) were available. The areal distribution of all measured and calculated resistivities for Aux Vases and Cypress formation waters unaffected by waterflooding or other

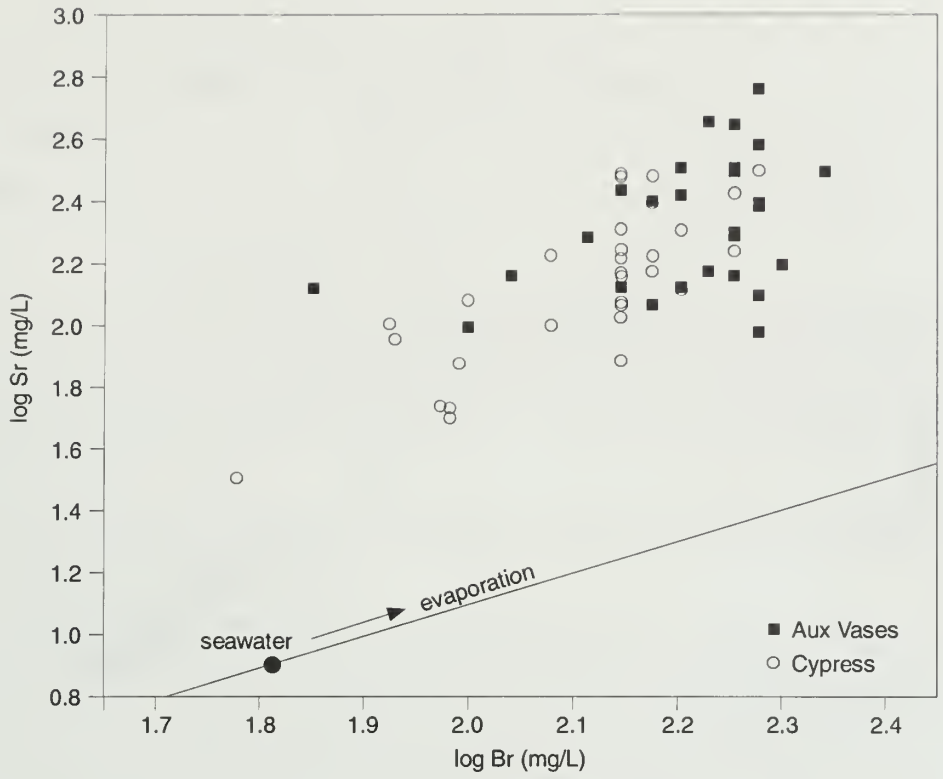

Figure 14 Relationship between Sr and Br in Aux Vases and Cypress formation waters (seawater evaporation trajectory is from Carpenter 1978).

improved oil recovery processes was mapped (figs. 16, 17). The resistivity values on figures 16 and 17 and in appendix B are for formation water at 25 °C.

Two more empirical equations were developed for the Aux Vases and Cypress formation waters. One equation is used to determine resistivity at different water temperatures if the resistivity of water at 25 °C is known; the other is used to determine resistivity at a given temperature if TDS is known. The equations are based on laboratory and field measurements of temperatures (18–60 °C), resistivities (0.0362–0.1832 ohm-m), and TDS (48,697–148,028 mg/L) of ten samples. If the water resistivity at 25 °C is known, the water resistivity at another temperature can be calculated by using the formula:

$$R_{w(T)} = 1.5(R_{w(25)})^{0.987}/(1.017)^{T} \quad [2]$$

where

$R_{w(T)}$ = water resistivity in ohm-m at temperature T (°C)
$R_{w(25)}$ = water resistivity in ohm-m at 25 °C

If TDS is known, the resistivity at a given temperature can be calculated by using the expression:

$$R_{w(T)} = 957/((TDS)^{0.778} \times (1.017)^{T}) \quad [3]$$

where

$R_{w(T)}$ = water resistivity in ohm-m at temperature T (°C)
TDS = total dissolved solid concentration in mg/L

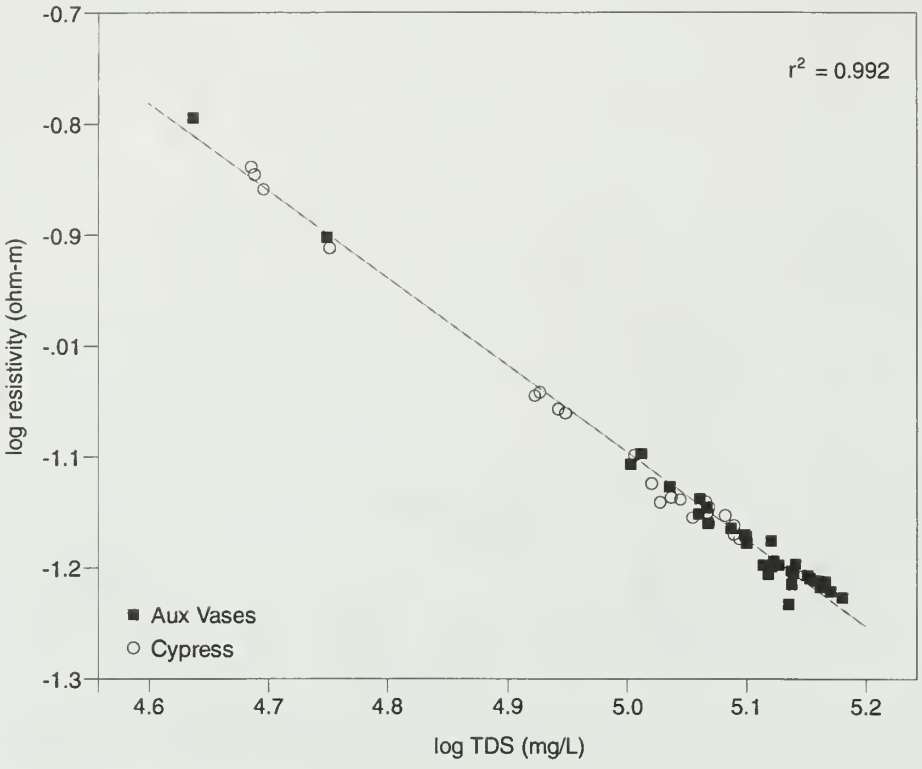

Figure 15 Relationship between Aux Vases and Cypress formation water resistivities and TDS. The r^2 is the square of the correlation coefficient.

For these computations, formation water resistivities were determined in the field before degassing and oxidation could affect the sample composition. Therefore, the formation water resistivities determined for this study are more accurate than those measured in the laboratory or estimated from spontaneous potential logs. The formation water resistivities calculated by using the above equations are also fairly accurate because only very little scatter is observed in the data used to calculate the R_w to TDS relationships (fig. 15). Furthermore, these equations do not require the use of correction factors for the ionic composition of the water. Correction factors are needed when resistivities are calculated from published charts which are based on artificial brines (Schlumberger 1989, p. 4–5).

Resistivity and reservoir properties Accurate resistivity values are important for calculating water saturation and permeability, two important parameters that affect oil production. Water saturation in nonshaley rocks is commonly calculated using the Archie (1942) water saturation equation:

$$S_w = (F_R R_w / R_t)^{1/2} \qquad [4]$$

where

S_w = water saturation (%)
R_w = water resistivity (ohm-m)
R_t = total resistivity of formation (ohm-m)
F_R = formation resistivity factor

The formation resistivity factor is related to the porosity by

$$F_R = 1/\phi^m \quad [5]$$

where

m = cementation exponent
ϕ = porosity (%)

The value of m is 2.0 for sandstones that have no clay matrix; it can be as low as 1.5 in sandstones that contain substantial amounts of clay matrix (Leetaru 1990). Once water saturation is calculated, the rock permeability can also be estimated from empirical relationships of water saturation, porosity, and permeability (Schlumberger 1989, p. 138–139).

The resistivity maps (figs. 16, 17) can be used to estimate formation water resistivities in the Aux Vases and Cypress Formations in undrilled areas or in wells for which no resistivity data are available.

TDS and reservoir properties Water saturation (S_w) of a reservoir can also be determined by using the TDS of formation waters and a Dual-Spacing TDT-K Thermal Decay Time log (Schlumberger 1989, p. 128–130). From a plot of the ratio curve and neutron cross section recorded by the TDT-K Thermal Decay Time log, apparent water salinity (AWS) can be determined. For gas-saturated formations or gas-filled casings, the ratio curve cannot be used and porosity (if known) can be used in lieu of the ratio curve. Once the AWS (mg/L) is determined, the S_w (%) of a formation that has no or a small amount of clay can be calculated from the TDS (mg/L) (referred to as connate water salinity in Schlumberger charts):

$$S_w\ (\%) = \text{AWS/TDS} \quad [6]$$

Again, the permeability can be computed from S_w and porosity (Schlumberger 1989, p. 138–139). The TDS maps in figures 4 and 5 can be used to estimate TDS values for undrilled areas or for wells for which no data are available. The TDS can also be used to estimate water resistivities (equations 1–3). If water and formation resistivities and cementation exponent are known, and S_w is calculated from equation [6], the porosity of the formation can be computed using equations [4] and [5].

As shown in the following section, TDS values and chemical compositions of formation waters are also needed to evaluate and prevent the swelling of clay minerals when another water is injected into the reservoir for improved oil recovery.

Formation Water Chemistry and Formation Damage

Knowledge of the formation water chemistry is important in diagnosing and solving hydrocarbon production problems such as formation damage. Disturbance of an oil reservoir's physical-chemical state due to reservoir temperature and pressure changes and reactions with externally introduced fluids can cause serious formation damage.

Minerals that commonly precipitate in reservoirs and boreholes and thus reduce oil production are calcite or aragonite ($CaCO_3$), gypsum ($CaSO_4 \cdot 2H_2O$) or anhydrite ($CaSO_4$), celestite ($SrSO_4$), barite ($BaSO_4$), and various Fe-sulfide minerals (Collins 1975, Collins and Kayser 1985). Therefore, concentrations of Ca^{2+}, Sr^{2+}, Ba^{2+}, Fe^{2+}, SO_4^{2-}, HCO_3^-, and CO_3^{2-} and the pH and Eh in formation waters and injection fluids should be considered when designing improved oil recovery processes.

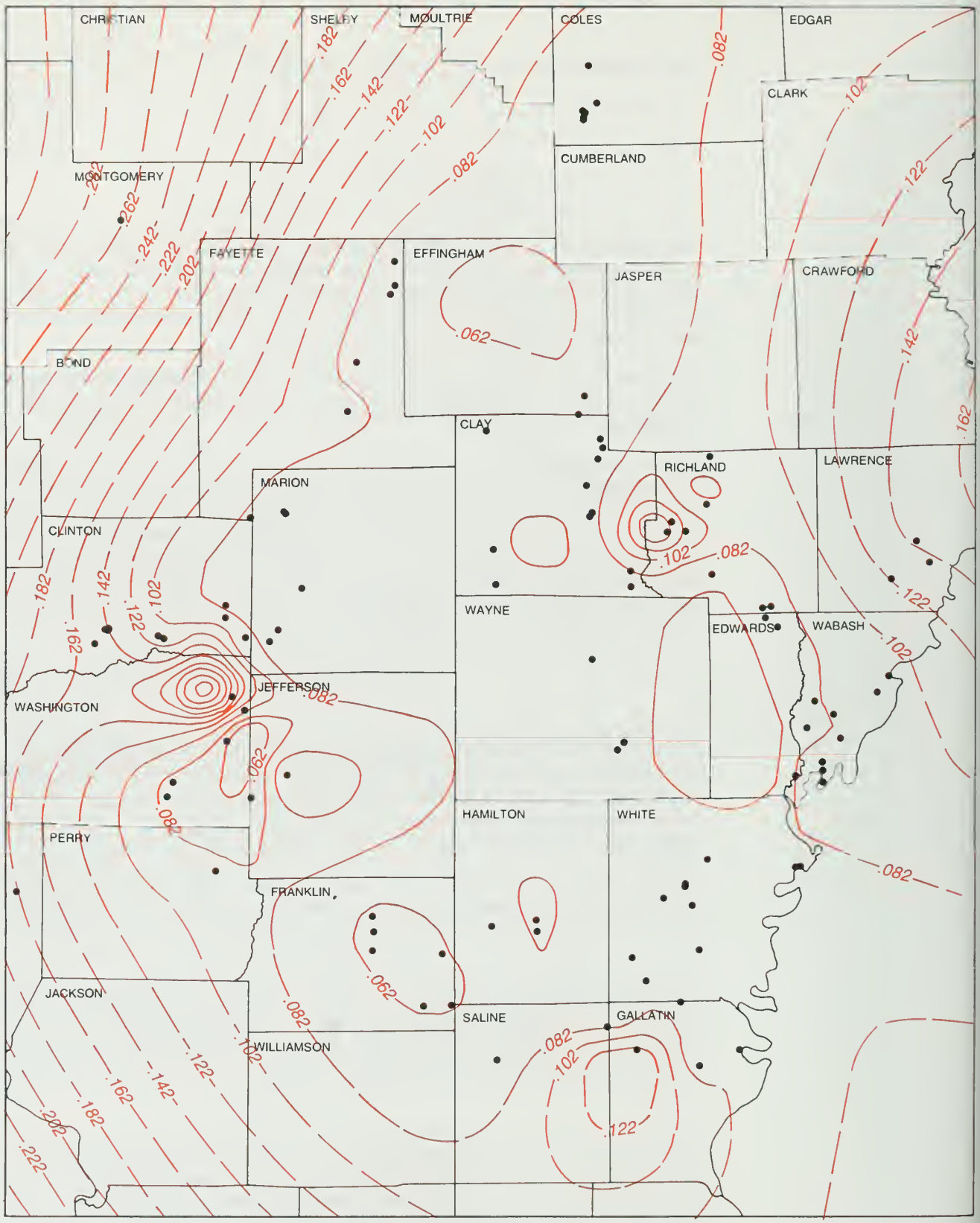

Figure 16 Areal distribution of Cypress formation waters resistivities.

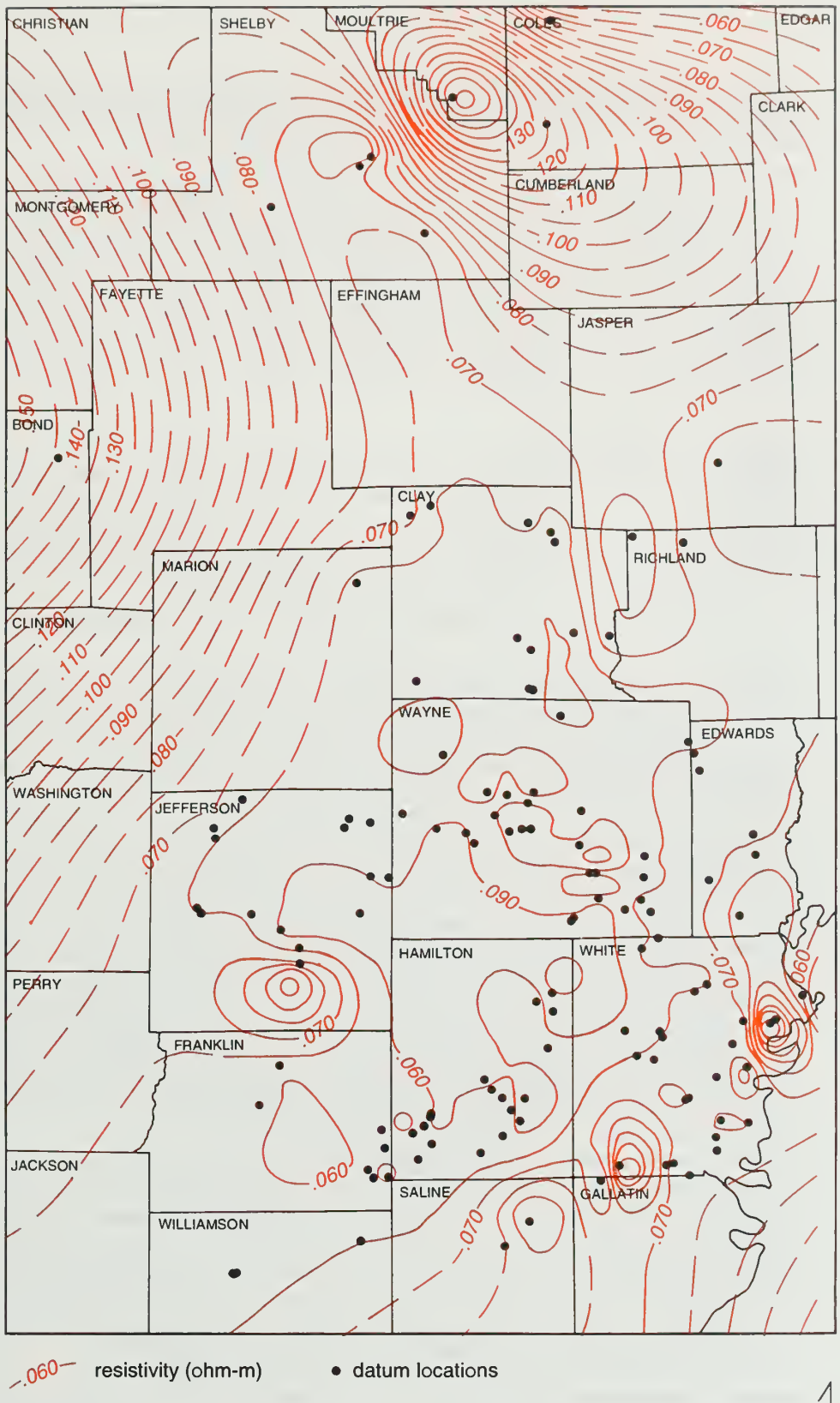

Figure 17 Areal distribution of Aux Vases formation waters resistivities.

Table 1 Saturation indexes (SI)[a] of minerals that have the potential for formation damage in five Aux Vases and five Cypress formation water samples. See appendix B for detailed information on the samples and text for computation of reservoir temperature and pressure.

			Saturation indexes				
Sample	Formation	Field	Calcite	Gypsum	Celestite	Barite	Fe-sulfide[b]
EOR-B17	Cypress	Bartelso	0.4	-3.3	-2.8	0.8	2.1, 2.2, 11.0
EOR-B36		Mattoon	0.3	-0.5	-0.5	0.2	2.1, 2.2, 11.5
EOR-B52		Clay City	0.8	-0.3	-0.4	0.0	2.5, 2.6, 11.1
EOR-B73		New Harmony	-0.7	-1.8	-1.5	1.3	2.0, 2.1, 11.4
EOR-B101		Dale Cons.	-0.5	-0.3	-0.3	0.0	2.5, 2.7, 12.1
EOR-B9	Aux Vases	King	0.3	-0.4	-0.3	0.3	1.5, 1.6, 10.6
EOR-B35		Mattoon	0.5	-2.0	-1.6	0.4	2.2, 2.3, 10.7
EOR-B70		Carmi North	-1.0	-0.7	-0.5	0.3	2.0, 2.1, 11.5
EOR-B93		Clay City	0.1	-0.2	-0.3	0.5	2.1, 2.2, 11.3
EOR-B99		Eldorado	0.1	-0.7	-0.3	0.1	2.5, 2.6, 11.7

[a] SI>0, supersaturated; SI=0, equilibrium; SI<0, undersaturated.
[b] The first, second, and third numbers belong to pyrothite, troilite, and pyrite, respectively.

Saturation indexes of these minerals in five Aux Vases and five Cypress formation water samples (randomly chosen from the north, south, west, east, and middle of the oil-producing area of the state) were calculated by using the geochemical model SOLMINEQ.88 (Kharaka et al. 1988). An introduction to SOLMINEQ and other geochemical modeling codes is included in the next section.

In addition to the chemical composition of the formation waters, the reservoir temperature and pressure must be known for input into the geochemical modeling program. Reservoir temperatures were estimated using a geothermal gradient of 0.67 °C per 100 feet (Pollack and Watts 1976). Fluid pressures were estimated using a hydraulic potential gradient of 0.465 psi per foot (0.032 bar/ft) (Dickinson 1953). Concentrations of dissolved organic species (acetate, oxalate, succinate, methane) commonly found in oil field waters and concentration of dissolved hydrogen sulfide were arbitrarily chosen to fall within the concentration ranges published in Carothers and Kharaka (1978), Kharaka et al. (1986), Moldovanyi and Walter (1992) and Duan et al. (1992). Concentrations used were 93 mg/L for acetate, oxalate, and succinate; 800 mg/L for methane; and 680 mg/L for hydrogen sulfide.

The saturation indexes in table 1 suggest that most samples are saturated or supersaturated with respect to calcite, barite, and Fe-sulfides. The Fe-sulfide saturation or supersaturation, which is largely controlled by dissolved hydrogen sulfide ($H_2S(aq)$), can occur even if $H_2S(aq)$ concentrations as low as 4 mg/L are used in the modeling. The estimated concentrations for the organic species are probably the least accurate. Excluding these species from the geochemical modeling calculations, however, did not make a noticeable difference in the degree of saturation of the samples with respect to the minerals noted above.

Supersaturation shown in table 1 suggests that factors such as common ion effects, ion pairs, or kinetic or activation energy barriers prevented the minerals involved from precipitating. The thermodynamic potential for mineral precipitation exists, however, if physical and chemical parameters, such as temperature, pressure, pH, Eh, and ionic strength, change. The processes that could change the temperature,

pressure, pH, Eh, and ionic strength of formation waters and the effects of these changes on the solubility and thus precipitation of the minerals that commonly cause formation damage are discussed below.

The solubility of anhydrite and celestite tends to decrease, but that of barite tends to increase, as temperature increases (Blount and Dickson 1969, Fletcher et al.1981, Templeton 1960, Collins and Kayser 1985). Reservoir temperature can change during secondary oil recovery; for example, a steam-flood operation raises the reservoir temperature whereas a waterflood operation lowers it. Injecting other cold fluids, such as acid, can also lower the reservoir temperature around the bore hole. Reservoir temperature also decreases during normal primary production as a result of the drop in pressure around a well bore; the pressure drop reduces the fluid temperature because of an increase in the vapor pressure of formation water.

The solubility of anhydrite was reported to decrease with decreasing pressure in solutions having dissolved NaCl concentration ranges (Fulford 1968, Collins 1975, Collins and Kayser 1985) commonly found in the Illinois Basin formation waters. Decreased reservoir pressure during normal primary production, or reduced pressure around a borehole due to degassing, therefore, could trigger anhydrite precipitation.

The pH and Eh of formation waters are important parameters influencing the solubilities of minerals. If pH is sufficiently lowered by processes such as injection of CO_2 or acid, calcite dissolves. The dissolution of calcite generally improves porosity and permeability in reservoirs containing clean calcite. For reservoirs containing a substantial amount of clay minerals dispersed within the calcite cement, calcite dissolution can release clay minerals, which can migrate and plug pore throats, and thus cause a reduction in permeability. The change in Eh, commonly caused by the introduction of injection fluids that have Eh values different from that of the reservoir, could lead to oxidation or reduction of certain aqueous species. For example, oxidation of H_2S in high Ca brines could lead to precipitation of calcium sulfate.

Ionic strength, a parameter that is a measure of the combined effect of TDS and the ionic composition of a fluid, significantly influences the solubility of minerals. The solubility of Ca-, Ba-, and Sr-sulfate minerals in dominantly NaCl solutions generally increases with increasing ionic strength of the solution (Davis and Collins 1971, Collins 1975, Collins and Kayser 1985) at the TDS ranges of Aux Vases and Cypress formation waters. This increase in solubility is mainly the result of decreased ionic activities of Ca, Ba, Sr, and SO_4 caused by the formation of ion complexes, ion pairs, and ionic interactions in the solution. If ionic activities of elements making up of a mineral decreases in a solution, the solubility of that mineral in contact with the solution generally increases. Diluting reservoir waters by injecting fresher waters in waterflood operations reduces their overall ionic strength. This reduction greatly increases the chance of sulfate-mineral precipitation in the reservoirs, especially when either the injection water or formation water, or both, contain a substantial amount of sulfate.

Ionic strength also affects the swelling of clay minerals and the anhydrite-gypsum transformation. Injection of fresher (lower TDS) waters into a reservoir can cause clay minerals to swell, depending on the ionic strength of the injected water. Furthermore, lowering the TDS content of a brine increases the activity of water in it. This increased water activity promotes the conversion of anhydrite (if present) to gypsum, which has a molar volume 1 to 1.5 times greater than that of anhydrite.

The swelling of clay minerals and transformation of anhydrite to gypsum can reduce the permeability of the reservoir rock and, thus, petroleum production.

Using the geochemical data produced by this study (appendix B) and the general guidelines discussed above, oil producing or oil field service companies can evaluate the potential production problems for each well, pool, or field. Once the potential problem is identified, preventive measures, such as using scale inhibitors or choosing compatible fluids, can be taken.

SIMULATION OF FLUID-ROCK INTERACTIONS DURING IMPROVED OIL RECOVERY

The consequences of chemical reactions that take place during improved oil recovery processes are difficult to predict because of the complexity of the systems involved. A vast number of reactions that may take place simultaneously in such systems can be simulated only with the help of quantitative, computerized mathematical-geochemical models. Important advances have been made in computerized geochemical modeling since the pioneering works of Garrels and Thompson (1962) and Helgeson et al. (1969, 1970). The purpose of computerized geochemical modeling is to understand solution chemistry and predict the results of fluid-rock interactions.

The two main types of geochemical models are speciation-solubility models and reaction path models. Speciation-solubility models are used to describe the equilibrium distribution of aqueous species and the saturation state of the solution with respect to various minerals. Mineral saturation states provide a measure of the thermodynamic potential of mineral precipitation or dissolution. The speciation solubility models commonly used include SOLMINEQ (Kharaka and Barnes 1973, Kharaka et al. 1988), WATEQ series (Truesdell and Jones 1974, Plummer et al. 1976, Ball et al. 1981, Ball and Nordstrom 1991), MINEQL and MINTEQ series (Westall et al. 1976, Felmy et al. 1984, Allison et al. 1991), and EQ3NR (Wolery 1992a,b). Speciation-solubility models are static; that is, they treat aqueous systems as isolated systems and ignore the exchange of mass and energy with the surrounding environment. Reaction path models, on the other hand, are dynamic because they model reversible and irreversible reactions by which mass and energy are exchanged between aqueous solutions and their surroundings in an open system. Reaction path models are used to predict the dissolution and precipitation of minerals and the evolution of fluid composition during consecutive stages (reaction steps) of fluid-rock interaction en route to complete equilibrium. The reaction path models can be instructed not to precipitate a mineral, thus putting that mineral into disequilibrium with the water-rock systems. Rate data (rate of the dissolution or precipitation of a mineral), if available, can be included in reaction path calculations to understand the kinetics of water-rock interactions.

The first published reaction path model, PATH1, was developed by Helgeson et al. (1970). Since then reaction path modeling has progressed significantly. Reaction path models commonly used at present are EQ3/6 (Wolery 1979, 1992b), REACT (Bethke 1992), PHREEQE (Parkhurst et al. 1980), PHRQPITZ (Plummer et al. 1988), and SOLVEQ/CHILLER (Reed 1982, Spycher and Reed 1989a,b).

REACT was the reaction path model used in this study to simulate the chemical aspects of improved oil recovery processes in the Aux Vases and Cypress Formations. Data on chemical composition, pH, Eh, density, and temperature of formation and injection fluids, and on mineralogical composition of the reservoir rocks were

input to the model. The density of the fluids was calculated using the geochemical model SOLMINEQ88 (Kharaka et al. 1988). For a given unit volume of reservoir rock, changes in volume were calculated for those minerals that were predicted by the reaction path model to precipitate and/or dissolve. The change in mineral volume was then used to calculate change in porosity. The reaction path model used in this study cannot calculate changes in permeability. Because mineral dissolution and precipitation reactions take place in pores that are accessible to the injection fluids, change in porosity implies change in permeability. Predicted changes in other parameters, such as pH, oxygen fugacity, iron concentration, and TDS also are reported, and their implications for reservoir properties are discussed.

Assumptions

When data on the mineralogy and fluid chemistry were incomplete, several assumptions and estimations were made to complete the input file for the geochemical modeling used in this study. Because the concentrations of gases in the formation fluids were not measured, estimated values had to be used. The concentration of CH_4 in the formation water was assumed, on the basis of data given in Duan et al. (1992), to be about 0.05 or 0.06 mol/kg (~800 or 960 mg/L) of water. The concentration of H_2S was assumed to be 0.02 mol/kg (680 mg/L) of water, a value close to the highest H_2S concentration reported in Moldovanyi and Walter (1992).

The average mineralogical composition determined from a core in a given field was assumed to represent the mineralogy of the reservoir in that field. The formation waters were assumed to be in equilibrium with quartz, calcite, and clay minerals and not in equilibrium with feldspars. Also, because no or very little thermodynamic data were available on mixed-layered clays of various compositions, the mixed-layered illite/smectite was assumed to be half illite and half smectite for modeling purposes. Because cristobalite and tridymite are stable silica polymorphs only at high temperatures (870 °C), they were not expected to precipitate under the conditions modeled in this study. The model was, therefore, instructed to suppress the precipitation of cristobalite and tridymite.

Initial simulation runs indicated that for some of the models, dolomite and/or some metamorphic or hydrothermal minerals would precipitate under the conditions of thermodynamic equilibrium. Past studies (Land 1983, Sibley et al. 1987) indicated, however, that dolomite precipitation would be highly unlikely at temperatures and time scales of the models used in this study because of kinetic barriers. Metamorphic or hydrothermal minerals were also not expected to form under the reservoir conditions modeled. The model was, therefore, instructed to suppress the precipitation of dolomite and metamorphic and hydrothermal minerals, such as graphite, paragonite, pyrophyllite, and others.

REACT computes geochemical reactions at standard (atmospheric) pressure; the effect of pressure on such reactions is negligible under most reservoir conditions. Therefore, the effect of reservoir pressure was ignored in all REACT runs. If needed, additional assumptions specific to each geochemical modeling were made.

Acid Treatment of a Production Well in Energy Field

The Morgan Coal no. 3 well in Energy Field, Williamson County, Illinois, was treated with 500 gallons of mud-cleaning acid (MCA), which contained about 15% hydrochloric acid (HCl). The field operator told the ISGS that production declined after the treatment; however, the treatment of other wells in the same field with MCA containing 7.5% HCl helped production somewhat. Experimental data on the effect of MCA and injection waters were reported by Haggerty and Seyler (in preparation).

Table 2 Mineralogical composition and porosity of the producing sandstone interval in the Morgan Coal no. 2 well, Energy Field.

	Minerals (wt. %, except the last row)								Porosity
Depth (ft)	Illite	Illite/smectite	Chlorite	Quartz	K-feldspar	Plagioclase	Calcite	Other	(%)
-387.6	1.6	0.9	2.4	81	0.0	8.2	6.0	4.7	21.3
-388.4	1.2	1.1	1.9	57	0.2	8.2	31.0	5.7	21.7
-390.1	1.4	0.7	2.5	85	0.6	2.6	6.7	0.6	23.6
-392.7	0.8	0.3	1.7	73	0.2	7.8	17.0	0.4	23.3
-394.7	1.0	0.5	3.0	76	0.4	6.3	13.0	0.0	20.6
-395.2	1.6	0.9	4.1	63	0.0	2.5	27.0	tr	13.6
Average (wt.%)	1.3	0.7	2.6	73	0.2	5.9	16.8	1.9	–
Average (vol.%)	1.3	0.8	2.3	71	0.3	6.0	16.1	1.8	22.0[a]

[a] 22.1 was rounded to 22 in geochemical modeling computations.
tr = trace.

Core and formation water data, necessary for creating an input file for geochemical modeling, were available for the Morgan Coal no. 2 (table 2) and Airport Morgan Coal no. 2 (sample EOR-B6, appendix B) wells, respectively. These two wells are in the same pool as the Morgan Coal no. 3 well. We assumed that the reservoir mineralogy and chemistry for the Morgan Coal no. 3 well were similar to those of the other two wells.

The MCA was assumed to be composed of 15% HCl and 0.1 molal KCl (clay stabilizer); the types and concentrations of the other components of MCA were not provided by the suppliers. Chlorite in the reservoir rock was assumed to be in the form of daphnite, an Fe-chlorite, to test whether the dissolution of an Fe-rich chlorite would lead to ferric oxide precipitation during the MCA treatment. The smectite in the reservoir rock was assumed to be beidellite, and because of the high Ca content in the formation water, the dominant interlayer cation in the smectite was interpreted to be Ca. Despite flushing by the operator, some residual acid was arbitrarily assumed to have remained about 2 days in the reservoir and to have reacted with the formation before it was consumed completely or flushed away by the formation fluid.

Analysis of the formation water sample (sample EOR-B6, appendix B), which provided data for the geochemical modeling, was conducted at room temperature (about 25 °C). The first step in modeling the reaction of MCA with the reservoir was to simulate the heating of the formation water up to the reservoir temperature (36 °C). This step calculates the distribution of the aqueous species at the reservoir temperature. In the second step, the reaction of MCA with the formation water and minerals at the reservoir temperature was modeled. Quartz, amorphous silica, and plagioclase (low albite) were set to form or dissolve according to a kinetic rate law using the rate data of Rimstidt and Barnes (1980) and Knauss and Wolery (1986). K-feldspar, calcite, and clay minerals were allowed to react freely until the system reached thermodynamic equilibrium. The calcite was expected to react quickly with the MCA. During the acid treatment, chlorite was suspected to react with acid relatively quickly, and other clay minerals probably reacted very slowly. Rate data were available for the precipitation or dissolution of quartz but not for chalcedony, a cryptocrystalline quartz. Chalcedony was, therefore, suppressed to allow the precipitation or dissolution of quartz to proceed only according to the rate law. Precipitation of hematite was also suppressed because the first ferric iron minerals to form would normally be ferric hydroxides, not hematite.

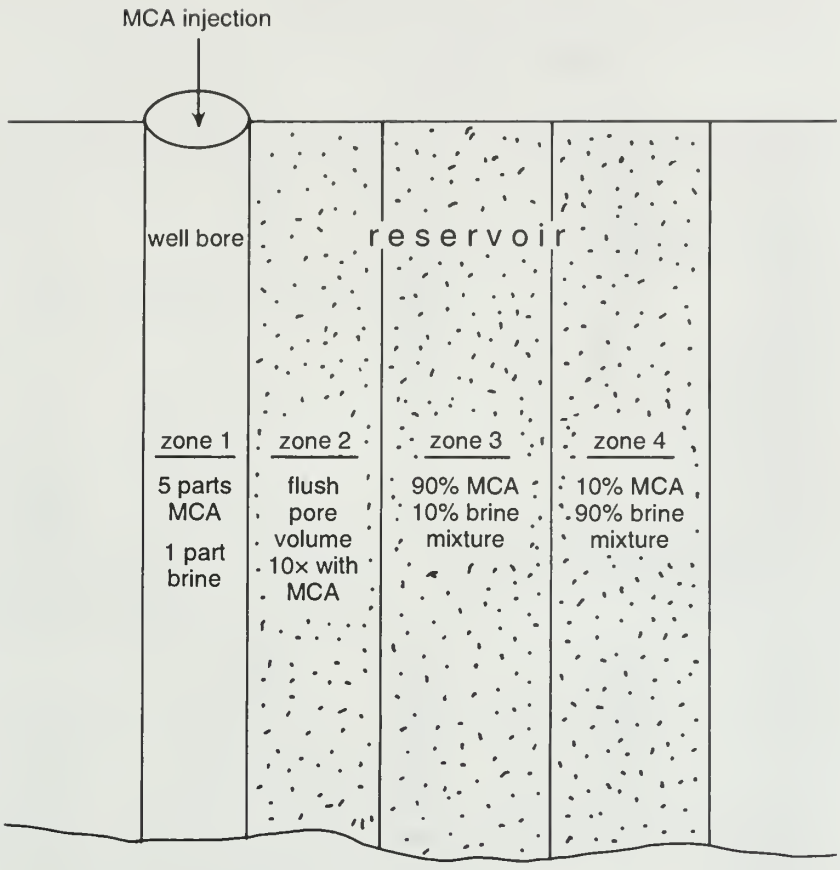

Figure 18 Hypothetical zones (not to scale) around an Energy Field well in which reactions were simulated.

Reaction path computations (geochemical modeling) of the MCA treatment process discussed above were made for four hypothetical zones (fig. 18).

Zone 1 In the well bore, the formation water and MCA were assumed to be mixed at a ratio of 5 parts MCA to 1 part formation water.

Zone 2 Immediately next to the well bore, MCA presumably flushed out the formation water and reacted with the reservoir rock. The volume of MCA that reacted with the reservoir rock was arbitrarily assumed to be ten times the volume of pore water flushed out.

Zone 3 Surrounding zone 2 in the reservoir was assumed to be a fluid mixture of 90% MCA and 10% formation water. The mixture was assumed to have reacted with the reservoir minerals.

Zone 4 Farther into the reservoir, a fluid mixture of 10% MCA and 90% formation water was assumed to be present and to have reacted with the reservoir minerals.

Geochemical reactions in the above four zones were simulated twice, once for 15% HCl-MCA and once for 7.5% HCl-MCA. MCA mixed with hydrofluoric acid (HF) is not commonly used in Illinois.

Results First, the reaction path computations predicted the original equilibrium concentrations of reservoir minerals before their reactions with the injection fluid

Table 3 Mineral volume corresponding to each kg (917 cm^3) of pore water (at a 50% water saturation), or 1834 cm^3 total pore volume, before and after treatment of a producing well in Energy Field with 15% HCl-MCA.

	Original volume (cm^3)		Final volume (cm^3)	
Mineral	Measured	Predicted	Predicted	Net change[a]
Zone 2				
Quartz	4703	4703	4703	0
Albite	393	393	393	0
Calcite	1060	1057	147	-913
Chlorite	154	123	0	-154
Illite	112	68	0	-112
Smectite	26	67	0	-26
K-feldspar	17	17	0	-17
Kaolinite	0	49	161	+161
Mordenite-K	0	0	115	+115
Pyrite	0	tr	0.1	+0.1
Siderite	0	0	83	+83
Net change in total mineral volume				-863
% Change in total pore volume[b]				+47.1
Final porosity (%)[c]				32.4
Zone 3				
Quartz	4703	4703	4703	0
Albite	393	393	393	0
Calcite	1060	1057	239	-821
Chlorite	154	123	0	-154
Illite	112	68	0	-112
Smectite	26	67	0	- 26
K-feldspar	17	17	0	-17
Kaolinite	0	49	161	+161
Mordenite-K	0	0	115	+115
Pyrite	0	tr	0.2	+0.2
Siderite	0	0	84	+84
Net change in total mineral volume				-770
% Change in total pore volume[b]				+42
Final porosity (%)[c]				31.2
Zone 4				
Quartz	4703	4703	4703	0
Albite	393	393	393	0
Calcite	1060	1057	1053	-7
Chlorite	154	123	102	-52
Illite	112	68	92 (muscovite)[d]	-20
Smectite	26	67	90	+64
K-feldspar	17	17	0	-17
Kaolinite	0	49	39	+39
Pyrite	0	tr	0.2	+0.2
Siderite	0	0	2	+2
Strontianite	0	0.3	0.3	+0.3
Net change in total mineral volume				+9.5
% Change in total pore volume[b]				-0.5
Final porosity (%)[c]				21.9

[a] Difference between original measured values and values after reaction path ended.
[b] (net change in total mineral volume/original total pore volume) x 100.
[c] (1 + (% change in total pore volume/100)) x (original porosity).
[d] Model assumes muscovite is a proxy for illite.
tr = trace.

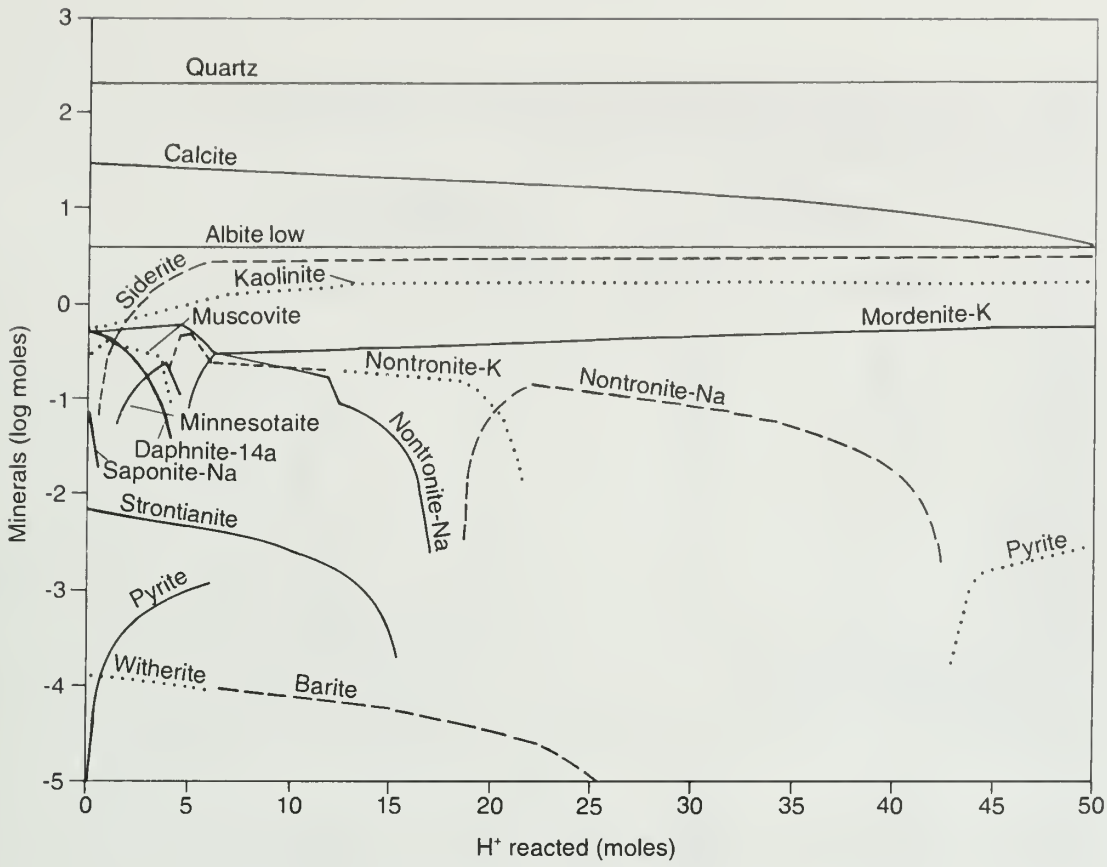

Figure 19 Predicted changes in mineralogical compositions along the reaction path when 1 part of pore water is flushed with 10 parts of 15% HCl-MCA in an Energy Field well.

began (column 3, tables 3 and 4). Feldspars were entered in the input file as reactants (out of equilibrium with the system) to prevent the model from adjusting the concentration of these minerals during the equilibrium step. The model predicted that kaolinite and trace amounts of pyrite and strontianite would be present in the reservoir, in addition to the original measured minerals (column 2, tables 3 and 4). This prediction was consistent with the results of Nesbitt (1980, 1985), who suggested that formation waters from Pennsylvanian and Mississippian strata in the Illinois Basin are in equilibrium with kaolinite. Even if the minerals predicted by the model are not in the reservoir, the model's prediction simply implies that the formation water was saturated with respect to these minerals. Figure 19 shows how the mineralogical composition would change between the first (equilibrium) step (column 3, table 3) and the last step (column 4, table 3) of the reaction path.

The above discussion of the implications of a mineral assemblage predicted by the model and changes in the mineralogical composition along the reaction path are also applicable to all other geochemical modeling cases included in this study.

The predicted results of chemical reactions in the four hypothetical zones defined above were as follows:

Zone 1 Mixing 5 parts of 15% or 7.5% HCl-MCA with 1 part of formation water did not result in precipitation or supersaturation of any mineral in the well bore.

Zone 2 Table 3 shows the amounts of minerals that formed and/or dissolved when the pore volume of the reservoir was flushed with a volume of MCA ten times the pore volume. Quartz and albite did not react significantly with the MCA solution. As

Table 4 Mineral volume corresponding to each kg (917 cm^3) of pore water (at a 50% water saturation), or 1834 cm^3 total pore volume, before and after treatment of a production well in Energy Field with 7.5% HCl-MCA .

	Original volume (cm^3)		Final volume (cm^3)	
Mineral	Measured	Predicted	Predicted	Net change[a]
Zone 2				
Quartz	4703	4703	4703	0
Albite	393	393	393	0
Calcite	1060	1057	699	-361
Chlorite	154	123	0	-154
Illite	112	68	0	-112
Smectite	26	67	29	+3
K-feldspar	17	17	0	-17
Kaolinite	0	49	165	+165
Mordenite-K	0	0	86	+86
Siderite	0	0	80	+80
Net change in total mineral volume				-310
% Change in total pore volume[b]				+16.9
Final porosity (%)[c]				25.7
Zone 3				
Quartz	4703	4703	4703	0
Albite	393	393	393	0
Calcite	1060	1057	735	-325
Chlorite	154	123	0	-154
Illite	112	68	0	-112
Smectite	26	67	29	+3
K-feldspar	17	17	0	-17
Kaolinite	0	0	161	+161
Mordenite-K	0	0	115	+115
Pyrite	0	tr	0.2	+0.2
Siderite	0	0	90	+90
Net change in total mineral volume				-239
% Change in total pore volume[b]				+13
Final porosity (%)[c]				24.9
Zone 4				
Quartz	4703	4703	4703	0
Albite	393	393	393	0
Calcite	1060	1057	1056	-4
Chlorite	154	123	109	-45
Illite	112	68	90 (muscovite)[d]	-22
Smectite	26	67	87	+61
K-feldspar	17	17	0	-17
Pyrite	0	tr	0.2	+0.2
Kaolinite	0	0	37	+37
Strontianite	0	0.3	0.3	+0.3
Net change in total mineral volume				+10.5
% Change in total pore volume[b]				-0.6
Final porosity (%)[c]				21.9

[a] Difference between original measured values and values after reaction path ended.
[b] (net change in total mineral volume/original total pore volume) x 100.
[c] (1 + (% change in total pore volume/100)) x (original porosity).
[d] Model assumes muscovite is a proxy for illite.
tr = trace.

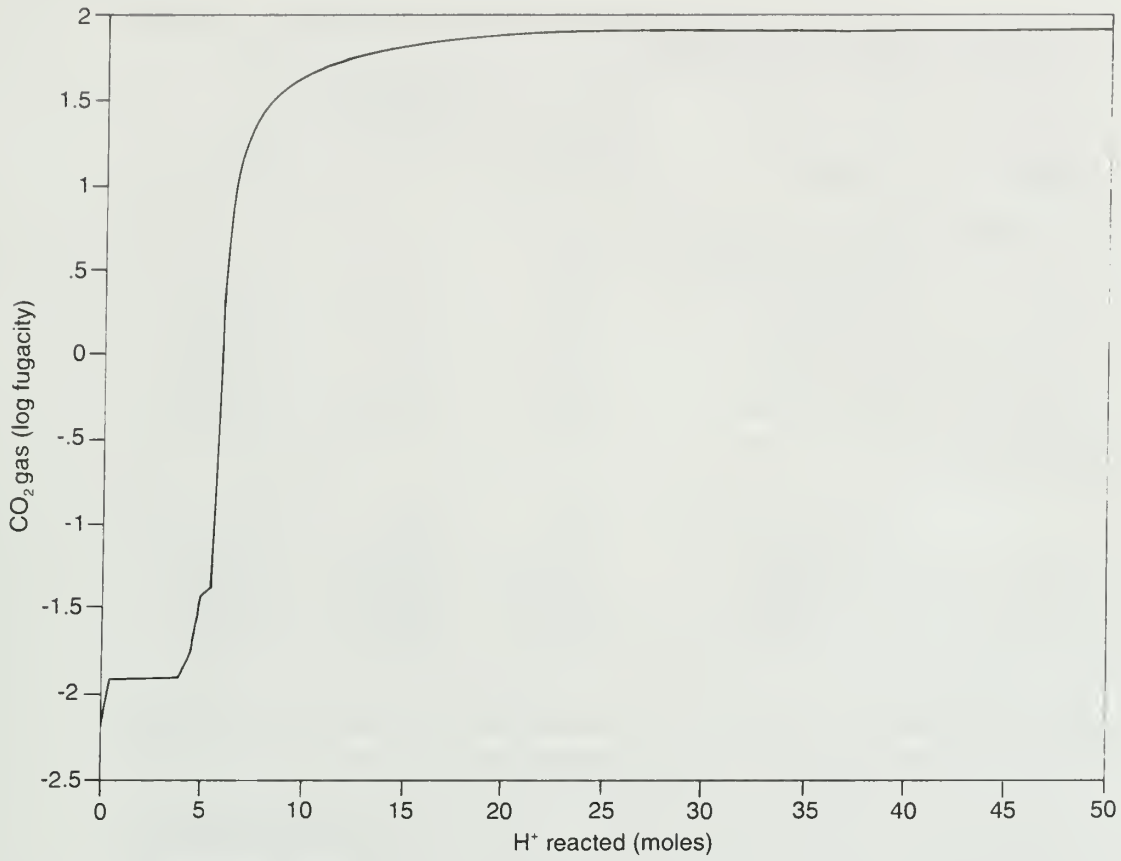

Figure 20 Predicted change in CO_2 fugacity along the reaction path when 1 part pore water is flushed with 10 parts 15% HCl-MCA in an Energy Field well.

expected, most of the calcite in the rock in zone 2 was dissolved. The clay minerals and K-feldspar were also totally dissolved, assuming that reactions for these minerals continued until the system attained equilibrium. In such a short reaction time (2 days), however, the system probably would not attain equilibrium with respect to these minerals. As a result, contrary to the prediction by the model, K-feldspar and clay minerals, perhaps with the exception of chlorite, would probably dissolve only in small amounts. Large amounts of kaolinite, mordenite, and siderite precipitated. A small amount of pyrite also precipitated as a result of the reaction of ferrous iron with H_2S. On the basis of mineral precipitation and dissolution reactions predicted by the model, a 47.1% increase in pore volume would be expected for zone 2 in response to treatment of the well with 15% HCl-MCA (table 3). The dissolution of calcite generated CO_2 gas (fig. 20, table 5), which would build a gas pressure barrier and reduce rock permeability to oil and water. This reduction in permeability would be a temporary event, however, because the CO_2 gas dissipates rather quickly because of its high solubility in water.

The amount of calcite dissolved when the well was treated with 7.5% HCl-MCA was predicted to be less than that dissolved when the well was treated with 15% HCl-MCA (compare tables 3, 4). Kaolinite, mordenite, and siderite were also predicted to form when the well was treated with 7.5% HCl-MCA. The predicted 16.9% increase in pore volume in response to treatment of the well with 7.5% HCl-MCA was considerable, but much less than that achieved by treatment with 15% HCl-MCA (compare tables 3, 4). Compared with the reaction of the reservoir

Table 5 Predicted pH, CO_2 gas, and dissolved iron species generated when a production well in Energy Field was treated with MCA.

		Concentration		
Treatment	Parameter	Zone 2	Zone 3	Zone 4
15% HCl-MCA				
	CO_2 gas fugacity	$10^{1.9}$	$10^{1.8}$	$10^{-1.9}$
	pH	4.21	4.29	6.51
	Fe^{++} (molal)	0.0072	0.0066	0.0012
	$FeCl_2$ (molal)	0.0114	0.0100	0.0010
	$FeCl^+$ (molal)	0.0161	0.0144	0.0020
	Total Fe (molal)	0.0340	0.0310	0.0042
7.5% HCl-MCA				
	CO_2 gas fugacity	$10^{1.5}$	$10^{1.3}$	$10^{-2.0}$
	pH	4.50	4.65	6.59
	Fe^{++} (molal)	0.0047	0.0041	0.0008
	$FeCl_2$ (molal)	0.0015	0.0015	0.0006
	$FeCl^+$ (molal)	0.0049	0.0046	0.0012
	Total Fe (molal)	0.0110	0.0100	0.0026

with 15% HCl-MCA, the reaction of the reservoir with 7.5% HCl-MCA generated less CO_2 gas, dissolved iron, and H^+ (higher pH) (table 5).

The higher the dissolved iron content and the lower the pH of the formation fluids, the higher the risk of precipitating asphaltenes that occur as colloidal particles in crude oil. The release of light hydrocarbons, such as methane, propane, and butane, due to a drop in pressure around well bores, also promotes agglomeration and subsequent precipitation of asphaltenes.

Zone 3 As far as minerals and porosity are concerned, the reactions in this zone yielded results generally similar to those in zone 2 (tables 3, 4). The amounts of CO_2 gas, dissolved iron, and H^+ (pH) generated by treating the well with 7.5% HCl-MCA were much less than those generated by treating the well with 15% HCl-MCA (table 5).

Zone 4 In this zone, no noticeable change in porosity was predicted when the well was treated with 15% or 7.5% HCl-MCA (tables 3, 4). The initial reduction in permeability due to the generation of CO_2 gas, and possible migration of clay minerals that would result from calcite dissolution in zones 2 and 3, could trap the fluid mixture and thus provide enough time for the reactions in zone 4 to proceed to the point predicted by the model. Again, the amount of dissolved iron generated in response to treatment of the well with 7.5% HCl-MCA was much less than that generated in response to treatment with 15% HCl-MCA (table 5).

In summary, the geochemical model predicted that the porosity in zone 2 would increase from 22% (table 2) to 32.4% (table 3) when the well was treated with 15% HCl-MCA and to 25.7% (table 4) when the well was treated with 7.5% HCl-MCA. Farther away from the well bore (zone 4), no noticeable increase in the pore volume was predicted. The excess acidity and dissolved iron species generated by treatment of the well with 15% HCl-MCA increased the chance of asphaltene precipitation, which would reduce the permeability. The amount of acidity and dissolved iron species generated when the well was treated with 7.5% HCl-MCA was predicted to be considerably less than those generated when the well was treated with 15%

HCl-MCA. The smaller the amount of acidity and dissolved iron, the smaller the chance of asphaltene precipitation. Considering the amount of acidity and dissolved iron predicted by the model and perhaps the amount of fine clay particles likely to be released as a result of calcite dissolution, one can argue that the plugging of pores with possible asphaltene precipitation and fine clay particles would appear to be less during treatment of the well with 7.5% HCl-MCA than treatment with 15% HCl-MCA. This argument is consistent with the field observations that indicated increased oil production (permeability) in response to well treatment with 7.5% HCl-MCA but not with 15% HCl-MCA. Both treatments generate a significant amount of CO_2 gas, which would initially reduce the permeability. The CO_2 gas pressure, however, would dissipate relatively quickly, allowing restoration of the permeability. The model did not predict the expected ferric oxide precipitation resulting from the dissolution of Fe-chlorite. Ferric oxide precipitation would require much more dissolved oxygen than the 8 mg/L assumed to be introduced with the MCA, which probably is not realistic under the conditions modeled.

Waterflood Operations in Dale Consolidated Field

Water produced from an average depth of about 2,959 feet in the Cypress Formation was injected into the deeper Aux Vases reservoir to increase oil production in Dale Consolidated Field, Franklin County, Illinois (Udegbunam et al. 1993). The chemical composition of the injection water is given in appendix B (sample EOR-B101). The composition of the Aux Vases formation water was assumed to be represented by that of water produced at an average depth of about 3,172 feet (appendix B, sample EOR-B107). The average mineralogical composition and porosity of a core sample from McCreery no.1 well (table 6) were assumed to represent those of the Aux Vases reservoir in this field.

Geochemical reactions of the waterflood operation were simulated to estimate the effect of the waterflood on the reservoir properties. For the Aux Vases formation water, the pH of 5.34 measured in the field had to be adjusted to 5.85 in the geochemical modeling input file to make the simulation run converge. The types of chlorite and smectite (smectite portion of illite/smectite) reported in table 6 were assumed to be ripidolite (Fe-Mg-chlorite) and beidellite, respectively.

The first step in modeling the waterflood operation was to compute the distribution of aqueous species in the injection and reservoir waters at reservoir temperature (37 °C). Then the reactions between injection water, formation water, and reservoir minerals were simulated. Two different scenarios were modeled: (1) a volume of injection water ten times the volume of pore water flushed out the pore water and reacted with the reservoir rock during waterflood operations, and (2) somewhere in the reservoir, the injection and pore waters mixed at a 1:1 ratio and then reacted with the reservoir rock. All reactions were assumed to continue until thermodynamic equilibrium was attained. This assumption is probably reasonable for most reactions, perhaps with the exception of feldspar reactions, because the time scale of waterflood operations is long enough (usually 10 years or more) for the system to reach or approach the equilibrium.

Replacement of pore water by flushing During the simulated flushing of pore water with injection fluid, the model predicted relatively small changes in the volumes of the major components (quartz, calcite, and illite) of the reservoir rock when compared with their original measured volumes (table 7, fig. 21). The volumes of minor mineralogical components were predicted to change as a result of the reaction of reservoir rock with the injection fluid. Feldspars were altered to illite, smectite, and kaolinite. Some of the silica released from the dissolution of feldspars

Table 6 Mineralogical composition and porosity of the producing sandstone interval in McCreery no. 1 well, Dale Consolidated Field.

	Minerals (wt. %, except the last row)							Porosity
Depth (ft)	Illite	Illite/smectite	Chlorite	Quartz	K-feldspar	Plagioclase	Calcite	(%)
-3190.5	3.2	1.4	0.7	84.5	1.3	2.5	6.4	20.4
-3191.5	2.8	1.5	0.7	81.6	1.7	3.2	8.6	23.4
-3192.7	2.5	1.1	0.6	84.9	1.5	3.7	5.6	25.6
-3194.0	3.4	2.5	0.9	79.5	1.2	4.3	8.1	23.6
-3195.7	2.6	1.5	0.7	88	1.9	3.2	2.0	19.8
-3197.9	3.1	1.7	0.8	80.7	2.6	2.6	8.5	24.8
-3199.4	2.1	1.5	0.6	82.5	2.7	3.7	6.8	24.3
-3201.0	3.1	2.3	0.9	82.3	2.6	3.3	5.5	21.4
-3203.0	2.1	2.1	0.4	77.8	1.5	1.9	14.2	18.6
-3205.8	2.4	2.1	0.5	83.7	1.2	2.4	7.6	21.4
-3207.1	3.1	4.2	0.7	67.8	0.8	1.5	21.8	14.5
-3208.4	1.7	1.9	0.5	82.9	1.7	2.8	8.4	13.1
-3209.9	5.2	4.7	1.9	68.4	1.2	1.8	16.8	11.5
Average (wt.%)	2.9	2.2	0.8	80.4	1.5	2.7	9.3	–
Average (vol.%)	2.9	2.1	0.8	80.8	1.6	2.7	9.1	20.0[a]

[a] 20.2 was rounded to 20 in geochemical modeling computations.

Table 7 Mineral volume corresponding to each kg (917 cm^3) of pore water (at a 50% water saturation), or 1834 cm^3 total pore volume, before and after flushing the pore volume ten times with injection water in Dale Consolidated Field.

	Original mineral volume (cm^3)		Predicted mineral volume (cm^3) after reaction path	Net change[a]
Minerals	Measured	Predicted by model		
Quartz	5853	5894	5937	+84
Albite	193	193	167	-26
Calcite	657	657	656	-1
Chlorite	58	22 (daphnite)	0	-58
Illite	290	176 (muscovite)[b]	331 (muscovite)[b]	+41
Smectite	77	71 (nontronite + saponite)	111 (nontronite + saponite)	+34
K-feldspar	116	116	0	-116
Kaolinite	0	131	38	+ 38
Pyrite	0	tr	1	+1
Strontianite	0	0.1	1	+1
Witherite	0	tr	tr	nd
Net change in total mineral volume				-2
% Change in total pore volume[c]				+0.1
Final porosity (%)[d]				20.0

[a] Difference between original measured values and values after reaction path ended.
[b] Model assumes muscovite is a proxy for illite.
[c] (net change in total mineral volume/original total pore volume) x 100.
[d] (1 + (% change in total pore volume/100)) x (original porosity).
tr = trace, nd = not detectable.

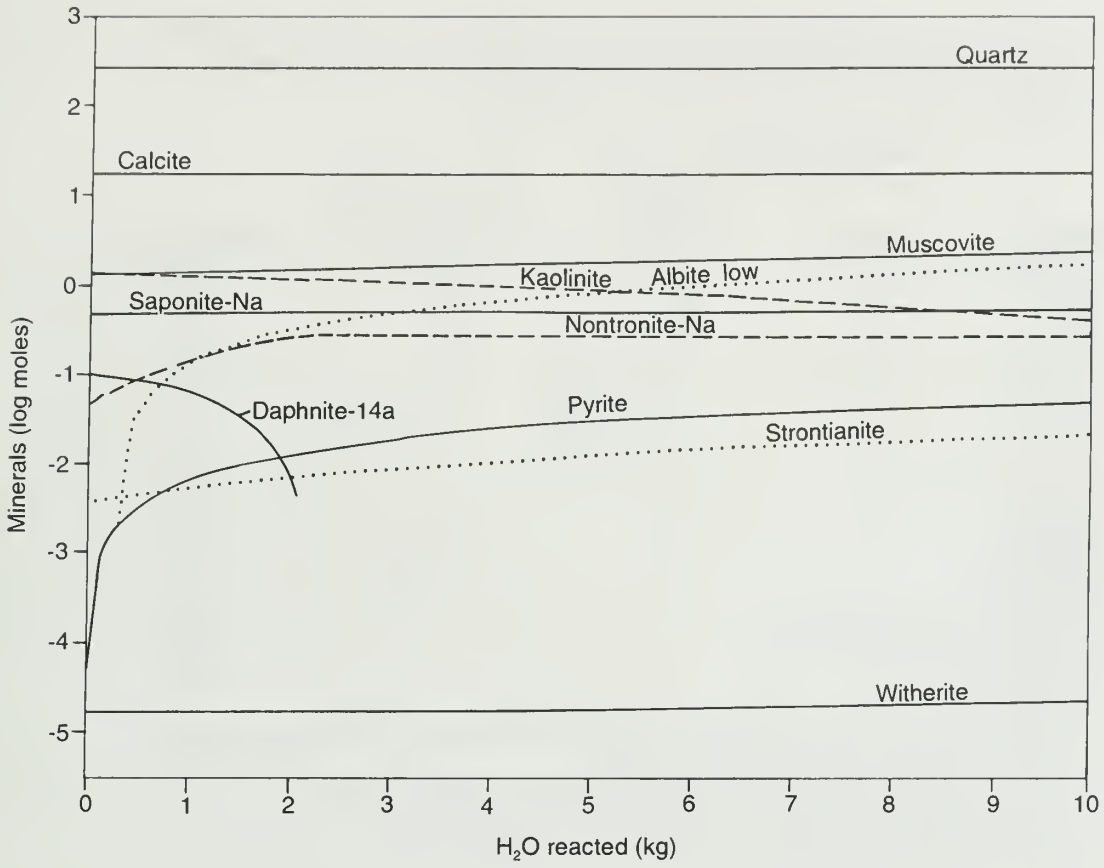

Figure 21 Predicted changes in mineral concentrations along the reaction path when 1 part pore water is flushed with 10 parts injection water in the Aux Vases reservoir, Dale Consolidated Field.

and chlorite apparently precipitated as quartz in the simulation. A small amount of pyrite was predicted to precipitate because of the reaction of ferrous iron with H_2S. The original measured volume of the reservoir rock (column 2, table 7) decreased by about 2 cm^3 (an increase of 0.1% in pore volume), which would not significantly change the original porosity of 20% (tables 6, 7).

Mixing formation and injection waters Mixing the injection and pore waters at a ratio of 1:1 resulted in a decrease of 20.4 cm^3 in total measured rock volume, which translates to an increase in average porosity from 20% (table 6) to 20.2% (table 8). Again, the changes in the volume of the major mineralogical components (quartz, calcite, and illite) of the reservoir rocks were small compared with their original measured volumes (columns 2 and 4, table 8).

The pH during both waterflooding scenarios (10× flush and 1:1 mixture) was predicted to remain about neutral during the reaction of the injection fluid with the reservoir (fig. 22). No change in the pH reduces the chance of asphaltene precipitation, which could take place in more acidic environments.

Overall, the computer simulation of the geochemical reactions of the waterflood operation in the Dale Consolidated Field predicted relatively small changes in the volume of the major reservoir minerals (quartz, calcite, and illite). The model also predicted that minor minerals (albite, chlorite, smectite, and K-feldspar) would react with the injection fluid and cause precipitation of some new minor minerals, such as kaolinite, pyrite, and strontianite. However, the resulting net change in the total

Table 8 Mineral volume corresponding to each kg (917 cm^3) of pore water (at a 50% water saturation), or 1834 cm^3 total pore volume, before and after mixing injection and formation waters at a 1:1 ratio in Dale Consolidated Field.

	Original mineral volume (cm^3)			
Minerals	Measured	Predicted by model	Predicted mineral volume (cm^3) after reaction path	Net change[a]
Quartz	5853	5894	5948	+95
Albite	193	193	184	-9
Calcite	657	657	657	0
Chlorite	58	22 (daphnite)	26	-32
Illite	290	176 (muscovite)[b]	327 (muscovite)[b]	+37
Smectite	77	71 (nontronite + saponite)	65 (saponite)	-12
				-12
K-feldspar	116	116	0	-116
Kaolinite	0	131	28	+28
Pyrite	0	tr	0.4	+0.4
Strontianite	0	0.1	0.2	+0.2
Witherite	0	tr	tr	nd
Net change in total mineral volume				-20.4
% Change in total pore volume[c]				+1.1
Final porosity (%)[d]				20.2

[a] Difference between original measured values and values after reaction path ended.
[b] Model assumes muscovite is a proxy for illite.
[c] (net change in total mineral volume/original total pore volume) x 100.
[d] (1 + (% change in total pore volume/100)) x (original porosity).
tr = trace, nd = not detectable.

mineral volume was very small, and, therefore, it was predicted that the porosity and permeability of the reservoir rock would not be affected significantly or would increase only slightly.

In summary, if the model assumptions and parameters were reasonable, the injection water used in the Dale Consolidated Field was compatible with the formation water and reservoir minerals, and thus should not result in any chemical damage to the formation. Furthermore, the TDS and chemical composition of the injection water were comparable to those of the formation water and should not cause serious clay mineral swelling problems.

Waterflood Operations in Tamaroa Field

Water produced from the Cypress Formation was reinjected into the reservoir to maintain pressure and increase production at Tamaroa Field, Perry County, Illinois (Grube 1992). The chemical composition of the injection water is given in appendix B (sample EOR-B23). The composition of the Cypress formation water was represented by that of water from the Gosper Stockton no. 1 well, which produces from an average depth of 1,159 feet in the Tamaroa Field (appendix B, sample EOR-B22). The average mineralogical composition and porosity of the Stockton no.1 well were assumed to be representative of those of the Cypress reservoir in the Tamaroa Field (table 9). The types of chlorite and smectite (smectite portion of illite/smectite) reported in table 9 were assumed to be ripidolite and beidellite, respectively. The concentrations of Br, I, and SO_4 in the injection water were arbitrarily set to 100, 5, and 20 mg/L, respectively; these values are within the ranges reported for Cypress formation waters (see appendix B).

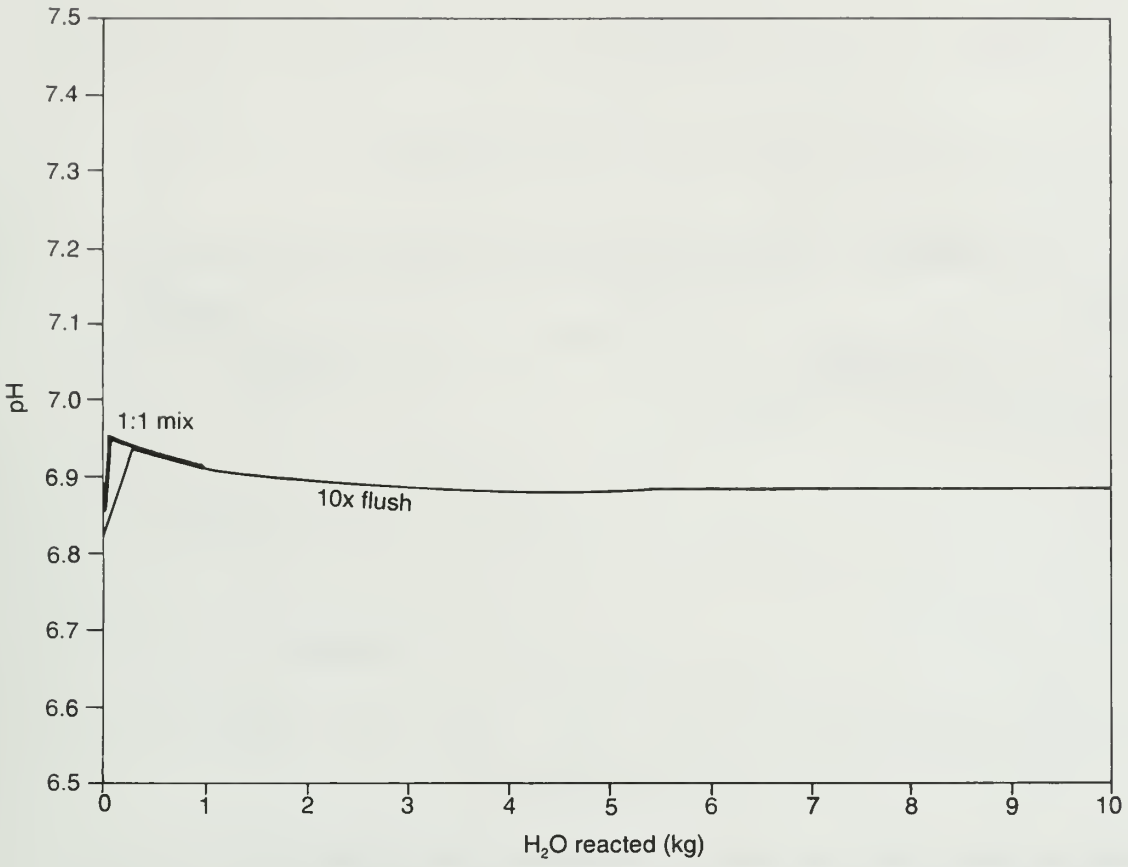

Figure 22 Predicted change in pH along the reaction path when 1 part of pore water is flushed with 10 parts of injection fluid and when pore and injection waters are mixed at a 1:1 ratio in the Aux Vases reservoir, Dale Consolidated Field.

Table 9 Mineralogical composition and porosity of producing sandstone interval in Stockton no. 1 well, Tamaroa Field.

	Minerals (wt. %, except the last row)							Porosity
Depth (ft)	Illite	Illite/smectite	Kaolinite	Chlorite	Quartz	Plagioclase	Calcite	(%)
-1155.5	tr	tr	0.6	0.2	98	0.5	0.4	21.5
-1160.5	0.3	0.2	3.5	1.6	90	4.1	0.1	20.7
-1163.5	0.5	0.8	3.7	3.1	77	9.8	4.6	15.8
-1165.5	tr	tr	0.5	0.3	97	1.8	0.2	19.3
Average (wt.%)	0.2	0.3	2.9	1.3	90.5	4.1	1.3	–
Average (vol.%)	0.3	0.3	2.9	1.1	90	4.2	1.3	19.0[a]

[a] In geochemical modeling computations 19.3 was rounded to 19.
tr = trace.

Scenarios of waterflood processes modeled for Tamaroa Field were similar to those modeled for Dale Consolidated Field.

Replacement of pore water by flushing The model predicted only small changes in the amounts of quartz, albite, calcite, and illite, compared with their original measured concentrations (table 10, fig. 23), in response to flushing the pore volume with the injection fluid. As a result of the reaction of the reservoir rock with

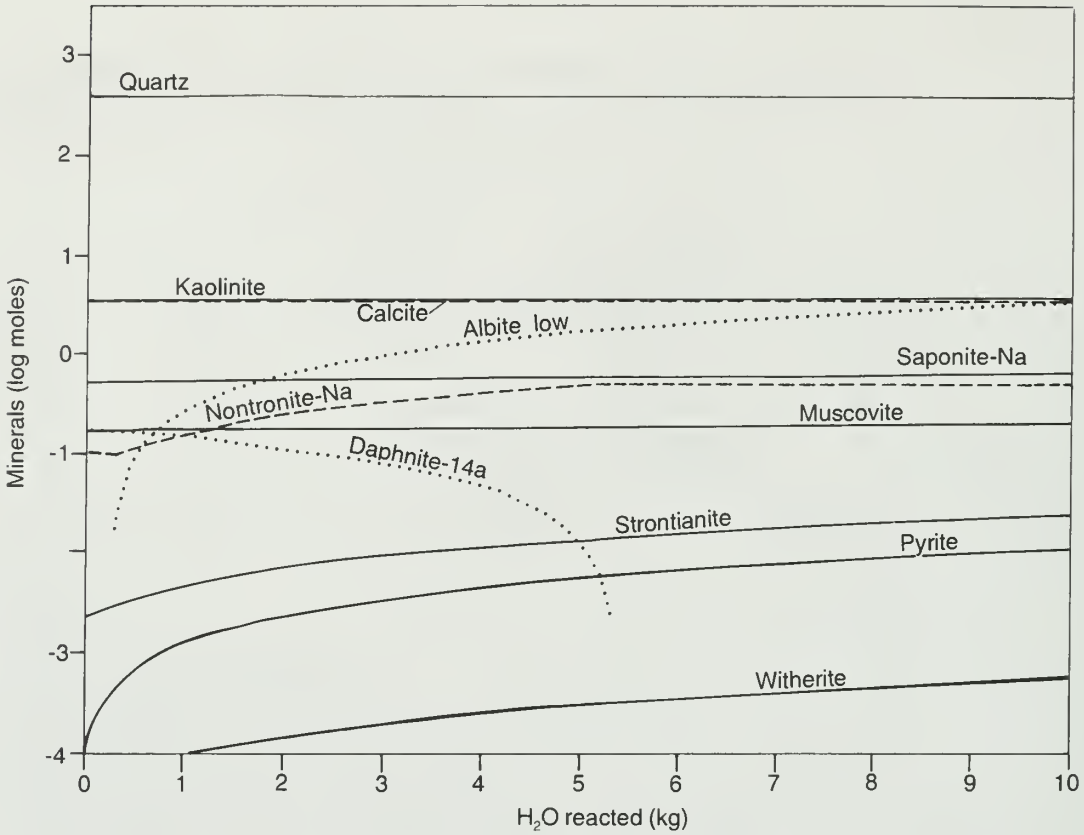

Figure 23 Predicted changes in mineral concentrations along the reaction path when 1 part pore water is flushed with 10 parts injection water in the Cypress reservoir, Tamaroa Field.

Table 10 Mineral volume corresponding to each 1 kg (943 cm^3) of pore water (at a 40% water saturation), or a total pore volume of 2358 cm^3, before and after flushing the pore volume ten times with injection water in Tamaroa Field.

	Original mineral volume (cm^3)			
Minerals	Measured	Predicted by model	Predicted mineral volume (cm^3) after reaction path	Net change[a]
Quartz	9045	9017	9018	-27
Albite	423	423	338	-85
Calcite	132	131	127	-5
Chlorite	106	40 (daphnite)	0	-106
Kaolinite	291	334	379	+88
Illite	39	24 (muscovite)[b]	28 (muscovite)[b]	-11
Smectite	13	86 (nontronite + saponite)	175 (nontronite + saponite)	+162
Pyrite	0	tr	0.3	+0.3
Strontianite	0	0.1	1	+1
Witherite	0	tr	tr	nd
Net change in total mineral volume				+17.3
% Change in total pore volume[c]				-0.7
Final porosity (%)[d]				18.9

[a] Difference between original measured values and values after reaction path ended.
[b] Model assumes muscovite is a proxy for illite.
[c] (net change in total mineral volume/original total pore volume) x 100.
[d] (1 + (% change in total pore volume/100)) x (original porosity).
tr = trace, nd = not detectable.

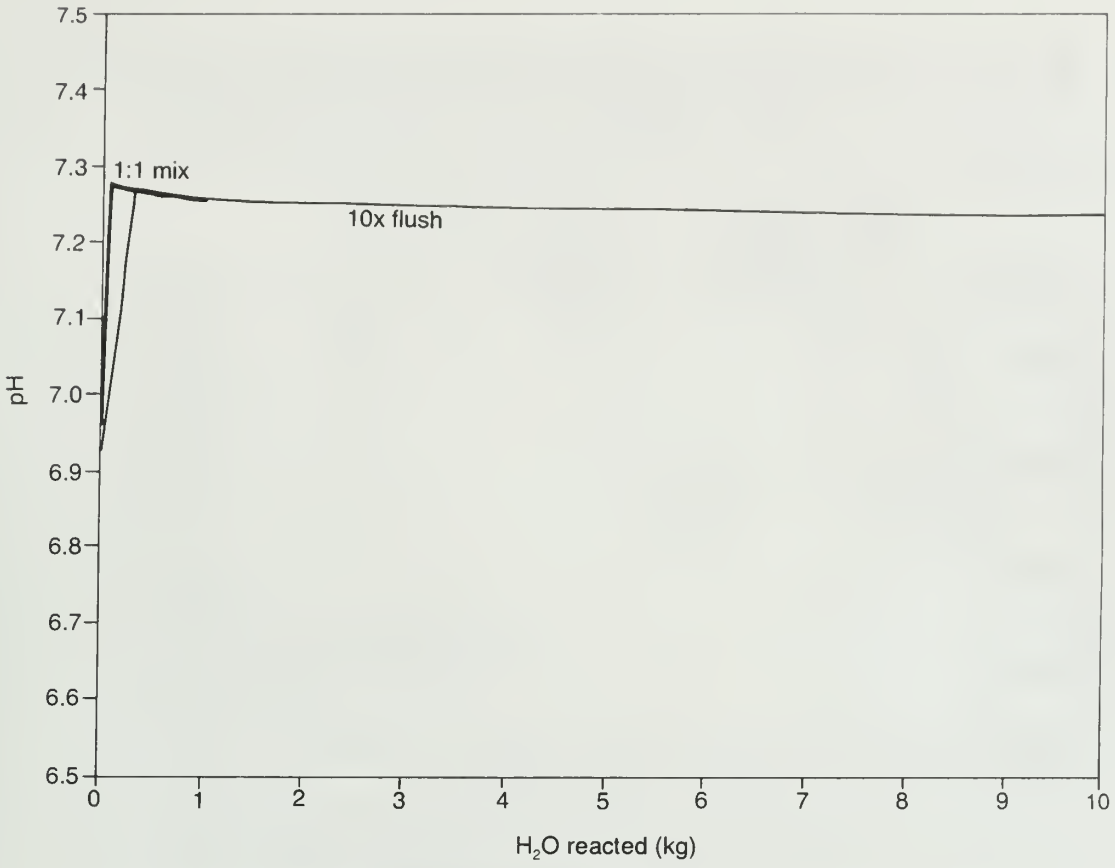

Figure 24 Predicted change in pH along the reaction path when 1 part pore water is flushed with 10 parts injection water and pore and injection waters are mixed at a 1:1 ratio in the Cypress reservoir, Tamaroa Field.

the injection fluid, some of the albite, all of the chlorite, and a relatively small amount of quartz were predicted to dissolve or to be altered. Dissolution or alteration of these minerals would lead to the precipitation of kaolinite and smectite. A small amount of pyrite was predicted to form from the reaction of ferrous iron with H_2S. Calcite was predicted to dissolve slightly, leading to the precipitation of a small amount of strontianite.

The volume of unit rock was predicted to increase by 17.3 cm^3 and, accordingly, pore volume was predicted to decrease by 0.7%, which would change the original porosity of 19% (table 9) to 18.9% (table 10).

The pH remained relatively neutral during the reaction path (fig. 24). Therefore, asphaltene precipitation (promoted by low pH) would not be expected during the waterflood operation. Although the formation of smectite (table 10) creates a potential clay swelling problem, this was not expected to be a concern because the TDS remained high during the reaction path (fig. 25). High TDS would reduce the electrical double layer around and in the interlayer regions of the smectite, and thus prevent clay swelling.

Mixing formation and injection waters Mixing the injection and pore waters in a 1:1 ratio resulted in the partial dissolution of quartz, albite, chlorite, and illite (table 11) and the formation of kaolinite and smectite. The original average porosity (19%) was predicted not to change (table 11). As in the case of flushing the pore volume with injection fluid, the change in pH was very small as a result of mixing the fluids in a 1:1 ratio (fig. 24); again, asphaltene precipitation should not be a concern. In

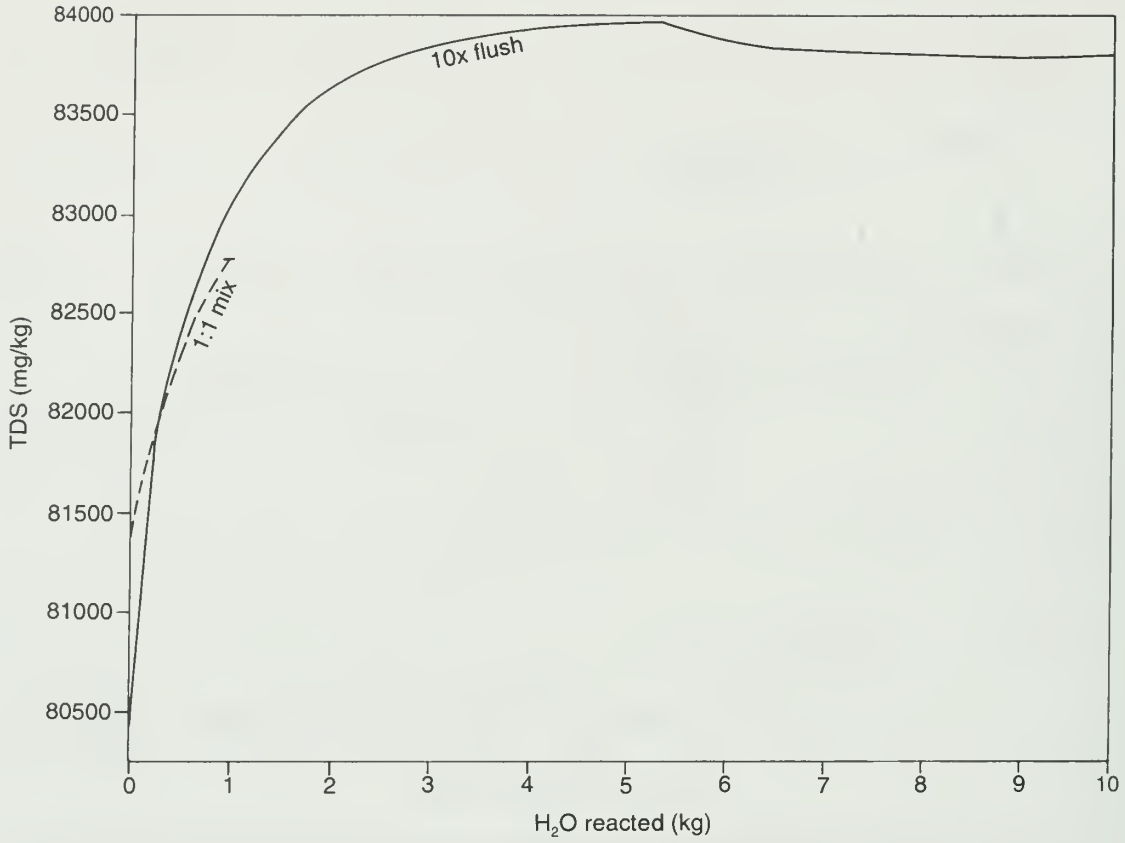

Figure 25 Predicted change in TDS along the reaction path when 1 part pore water is flushed with 10 parts injection water and pore and injection waters are mixed at a 1:1 ratio in Cypress reservoir, Tamaroa Field.

addition, TDS remained high during the reaction path (fig. 25) and reduced the chance of clay mineral swelling.

In summary, the modeling of the waterflood operation in Tamaroa Field predicted no significant change in reservoir porosity under the conditions modeled. If the model assumptions and parameters were reasonable, the injection water used in the Tamaroa South Field was compatible with the formation water and the reservoir minerals.

Carbon Dioxide-Flood Operations in Tamaroa Field

Carbon dioxide (CO_2) flooding, injected alone or alternately with water injection, is one of the enhanced oil recovery methods used to increase oil production in mature fields. The chemical composition of the Cypress formation water in Tamaroa Field was once again assumed to be represented by that of the water sample from the Gosper Stockton no. 1 well (appendix B, sample EOR-B22). The average mineralogical composition and porosity of the Stockton no.1 well were assumed to be representative of those of the Cypress reservoir in the Tamaroa Field (table 9).

The computer model simulated the heating of the formation water to the reservoir temperature (32 °C) and the subsequent reaction of CO_2 with the reservoir water and minerals at the reservoir temperature. The pH of the formation water had to be adjusted slightly, from 6.47 to 6.5, to make the computer simulation converge. Two scenarios were modeled: (1) reaction of 1 mol of CO_2 with the reservoir, and (2)

Table 11 Mineral volume corresponding to each kg (943 cm^3) of pore water (at a 40% water saturation), or a total pore volume of 2358 cm^3, before and after mixing injection and formation waters at a 1:1 ratio in Tamaroa Field.

Minerals	Original mineral volume (cm^3)		Predicted mineral volume (cm^3) after reaction path	Net change[a]
	Measured	Predicted by model		
Quartz	9045	9017	9030	-15
Albite	423	423	404	-19
Calcite	132	131	132	0
Chlorite	106	40 (daphnite)	44 (daphnite)	-62
Kaolinite	291	334	341	+50
Illite	39	24 (muscovite)[b]	24 (muscovite)[b]	-15
Smectite	13	86 (nontronite + saponite)	74 (nontronite + saponite)	+61
Pyrite	0	tr	0.2	+0.2
Strontianite	0	tr	0.2	+0.2
Witherite	0	tr	tr	nd
Net change in total mineral volume				+0.4
% Change in total pore volume[c]				<-0.1
Final porosity (%)[d]				19.0

[a] Difference between original measured values and values after reaction path ended.
[b] Model assumes muscovite is a proxy for illite.
[c] (net change in total mineral volume/original total pore volume) x 100.
[d] (1 + (% change in total pore volume/100)) x (original porosity).
tr = trace, nd = not detectable.

reaction of 5 mol of CO_2 with the reservoir. Albite, quartz, and amorphous silica were assumed to react according to a kinetic rate law (Rimstidt and Barnes 1980, Knauss and Wolery 1986) and all other minerals were assumed to react freely until thermodynamic equilibrium was achieved. The duration of the CO_2 flood was arbitrarily set to 30 days, which is within the time span commonly used in field applications of CO_2 flooding.

Reaction with 1 mol CO_2 The reaction of 1 mol of CO_2 with a unit volume of reservoir rock containing 1 kg of formation water was predicted to cause partial dissolution (or alteration) of chlorite and illite, and the formation of smectite, kaolinite, gibbsite, siderite, and dawsonite (table 12, fig. 26).The precipitation of siderite resulted from the reaction of ferrous iron with CO_3^{2-} or HCO_3^- and the precipitation of pyrite resulted from the reaction of ferrous iron with H_2S. The quantities of the two other minerals (strontianite and witherite) predicted to form were too small to warrant further discussion.

The predicted rock volume was about 14.3 cm^3 greater than the original measured rock volume. This change in rock volume yielded a 0.6% decrease in pore volume and, accordingly, a final average porosity of 18.9% (table 12), which was not significantly different from the original average porosity of 19% (table 9).

The pH along the reaction path (fig. 27) remained higher than the original pH (6.5). Asphaltene precipitation (promoted by low pH), therefore, would not be expected during treatment of the reservoir with 1 mol of CO_2. Although formation of additional smectite could create a potential for swelling of clay minerals, this would not be a concern because the relatively high TDS that remained after the reaction path ended (fig. 28) would prevent swelling of clays.

Table 12 Mineral volume corresponding to each kg (943 cm^3) of pore water (at a 40% water saturation), or a total pore volume of 2358 cm^3, before and after the reaction of 1 mol CO_2 gas with the Cypress reservoir in Tamaroa Field.

	Original mineral volume (cm^3)			
Minerals	Measured	Predicted by model	Predicted mineral volume (cm^3) after reaction path	Net change[a]
Quartz	9045	9045	9045	0
Albite	423	423	423	0
Calcite	132	132	133	+1
Chlorite[b]	103	47 (daphnite)	4 (daphnite)	-99
Kaolinite	291	273	303	+12
Illite[b]	22	13 (muscovite)[c]	13 (muscovite)[c]	-9
Smectite[b]	9	67 (nontronite	64 (saponite) + saponite)	+55
Gibbsite	0	33	23	+23
Dawsonite	0	0	5	+5
Siderite	0	0	26	+26
Pyrite	0	tr	0.2	+0.2
Strontianite	0	0.1	0.1	+0.1
Witherite	0	tr	tr	nd
Net change in total mineral volume				+14.3
% Change in total pore volume[d]				-0.6
Final porosity (%)[e]				18.9

[a] Difference between original measured values and values after reaction path ended.
[b] The original measured volumes of these minerals were adjusted somewhat to make the simulation runs converge (compare the first and second columns of this table to those of table 11).
[c] Model assumes muscovite is a proxy for illite.
[d] (net change in total mineral volume/original total pore volume) x 100.
[e] (1 + (% change in total pore volume/100)) x (original porosity).
tr = trace, nd = not detectable.

Reaction with 5 mol CO_2 The model predicted total dissolution or alteration of chlorite, illite, and smectite (table 13, fig. 29) during reaction of the reservoir with 5 mol of CO_2 gas. The model also predicted some of the calcite would dissolve. Increased concentrations of the aluminum and silica released by the dissolution of clay minerals resulted in the precipitation of clinoptilolite, dawsonite, and mordenite. The dissolution of the CO_2 gas and calcite provided excess carbonate, which was consumed as dawsonite, siderite, and magnesite precipitated. The average porosity was predicted on the basis of changes in the original measured mineral volumes to decrease from 19% (table 9) to 18.4% (table 13).

The reaction of the reservoir with 5 mol of CO_2 lowered the pH significantly along the reaction path relative to the original pH (fig. 27). The low pH has the potential of initiating asphaltene precipitation in some crude oils. Precipitation of asphaltene would probably be minimal in this reservoir because of the peptizing effect of resins, which are relatively high (about 10%–18%) in Tamaroa Field oils. Again, TDS increased significantly during the reaction path (fig. 28) and reduced the chance of swelling of clay minerals.

In summary, geochemical modeling of the CO_2-flood operation in Tamaroa Field predicted that, at thermodynamic equilibrium, the clay minerals chlorite, illite, and smectite in the reservoir rock would dissolve to varying degrees depending on the concentration of CO_2 gas. Increased concentrations of carbonate, aluminum, and

Table 13 Mineral volume corresponding to each kg (943 cm^3) of pore water (at a 40% water saturation), or a total pore volume of 2358 cm^3, before and after the reaction of 5 mol CO_2 gas with the Cypress reservoir in Tamaroa Field.

	Original mineral volume (cm^3)			
Minerals	Measured	Predicted by model	Predicted mineral volume (cm^3) after reaction path	Net change[a]
Quartz	9045	9045	9045	0
Albite	423	423	423	0
Calcite	132	132	121	-11
Chlorite[b]	103	47 (daphnite)	0	-103
Kaolinite	291	273	293	+2
Illite[b]	22	13 (muscovite)[c]	0	-22
Smectite[b]	9	67 (nontronite + saponite)	0	-9
Gibbsite	0	33	0	
Clinoptilolite	0	0	76	+76
Dawsonite	0	0	61	+61
Siderite	0	0	28	+28
Magnesite	0	0	30	+30
Mordenite	0	0	20	+20
Pyrite	0	tr	0.2	+0.2
Strontianite	0	0.1	0.1	+0.1
Witherite	0	tr	tr	nd
Net change in total mineral volume				+72.3
% Change in total pore volume[d]				-3.1
Final porosity (%)[e]				18.4

[a] Difference between original measured values and values after reaction path ended.
[b] The original measured volumes of these minerals were adjusted somewhat to make the simulation runs converge (compare the first and second columns of this table to those of table 11).
[c] Model assumes muscovite is a proxy for illite.
[d] (net change in total mineral volume/original total pore volume) x 100.
[e] (1 + (% change in total pore volume/100)) x (original porosity).
tr = trace, nd = not detectable.

silica in the formation water due to the dissolution of CO_2 gas, calcite, and clay minerals would lead to the precipitation of clinoptilolite, dawsonite, siderite, magnesite, gibbsite, and mordenite. Overall, changes in the mass and type of the reservoir minerals were predicted to result in a decrease of 0.6% or less in the reservoir porosity.

Alkali-Flood Operations in Tamaroa Field

When alkali solutions are introduced into an oil reservoir, they react with organic acids in the oil to generate organic salts that can act as surfactants (Jennings et al. 1974, Bethke 1992). The surfactants reduce the surface tension of water and thus increase the effective permeability of the reservoir to oil. This type of oil recovery process can be especially useful for old oil fields, such as most of the Illinois Basin fields, where during primary production lighter oils were preferentially extracted and relatively heavy oils were left in the reservoirs. The most commonly used alkali-flood agents are sodium hydroxide (NaOH), sodium carbonate (Na_2CO_3), and sodium silicate (Na_2SiO_3).

The reservoir mineralogy, formation water chemistry, and related assumptions for the computer simulation processes were the same as those for the waterflood and

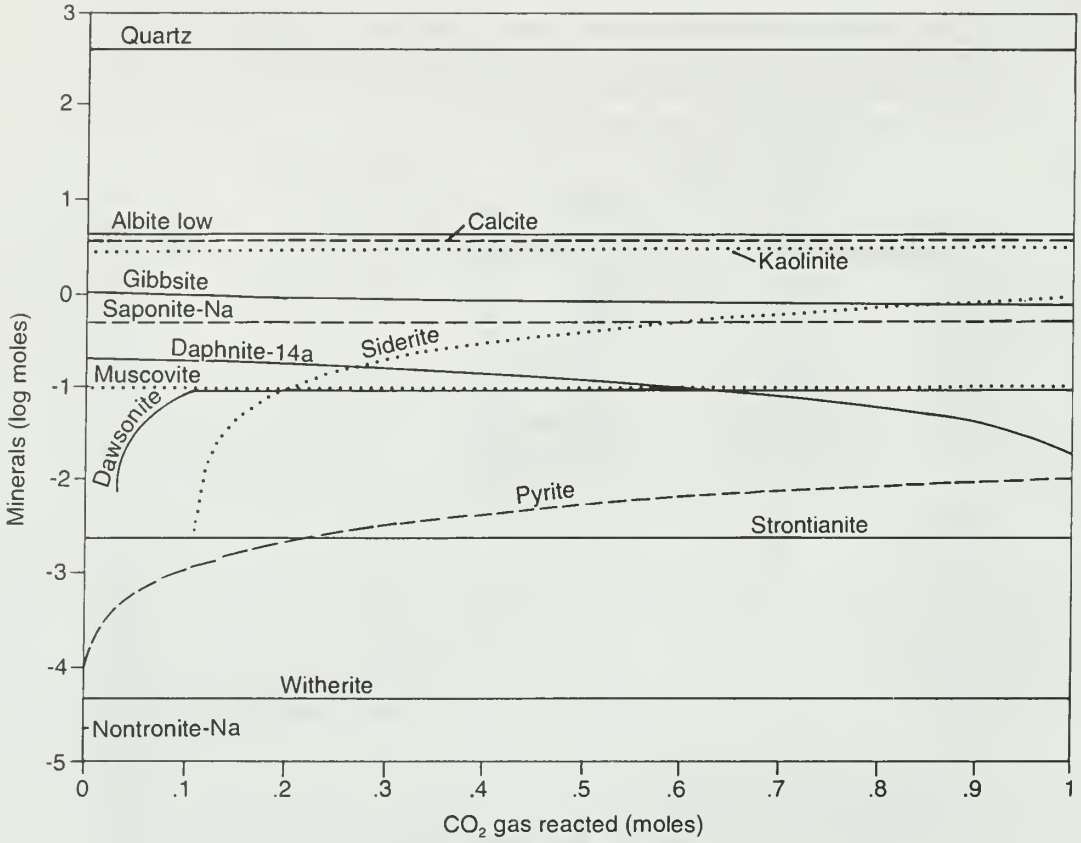

Figure 26 Predicted changes in mineral concentrations along the reaction path when the Cypress reservoir is flooded with 1 mol CO_2 solution in Tamaroa Field.

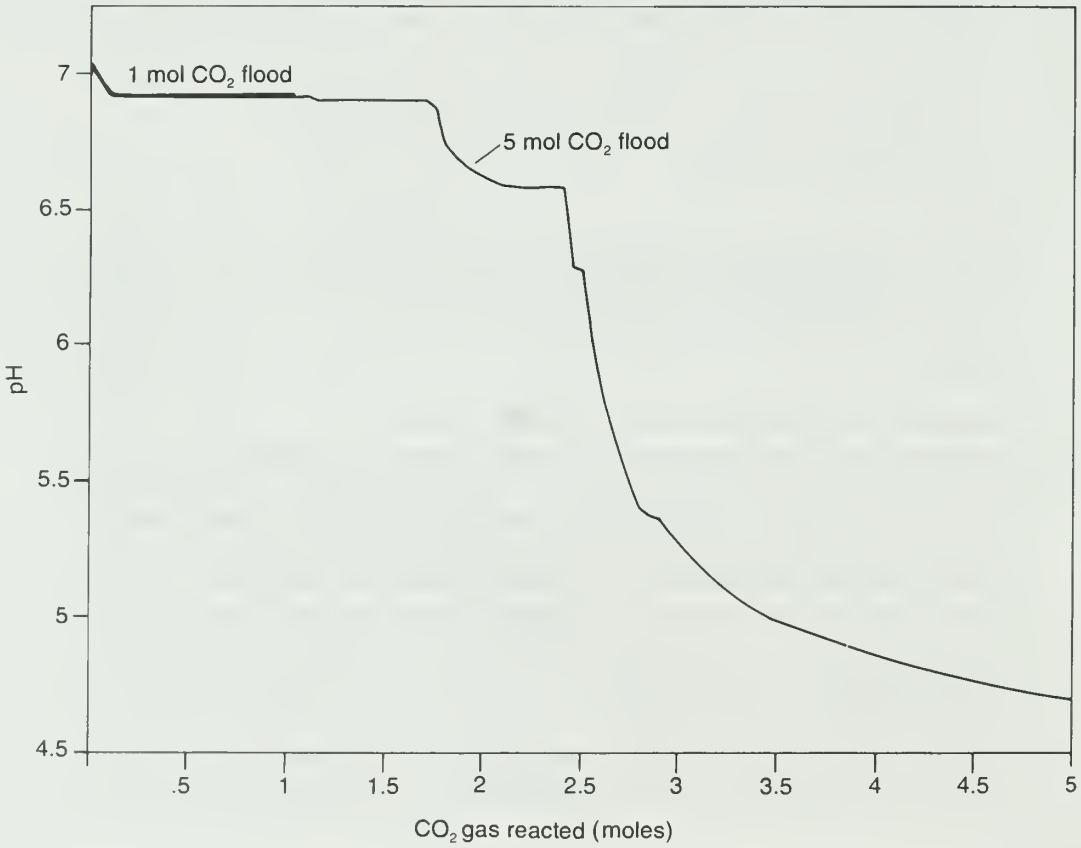

Figure 27 Predicted change in pH along the reaction path when the Cypress reservoir is flooded with 1 mol and 5 mol CO_2 solutions in Tamaroa Field.

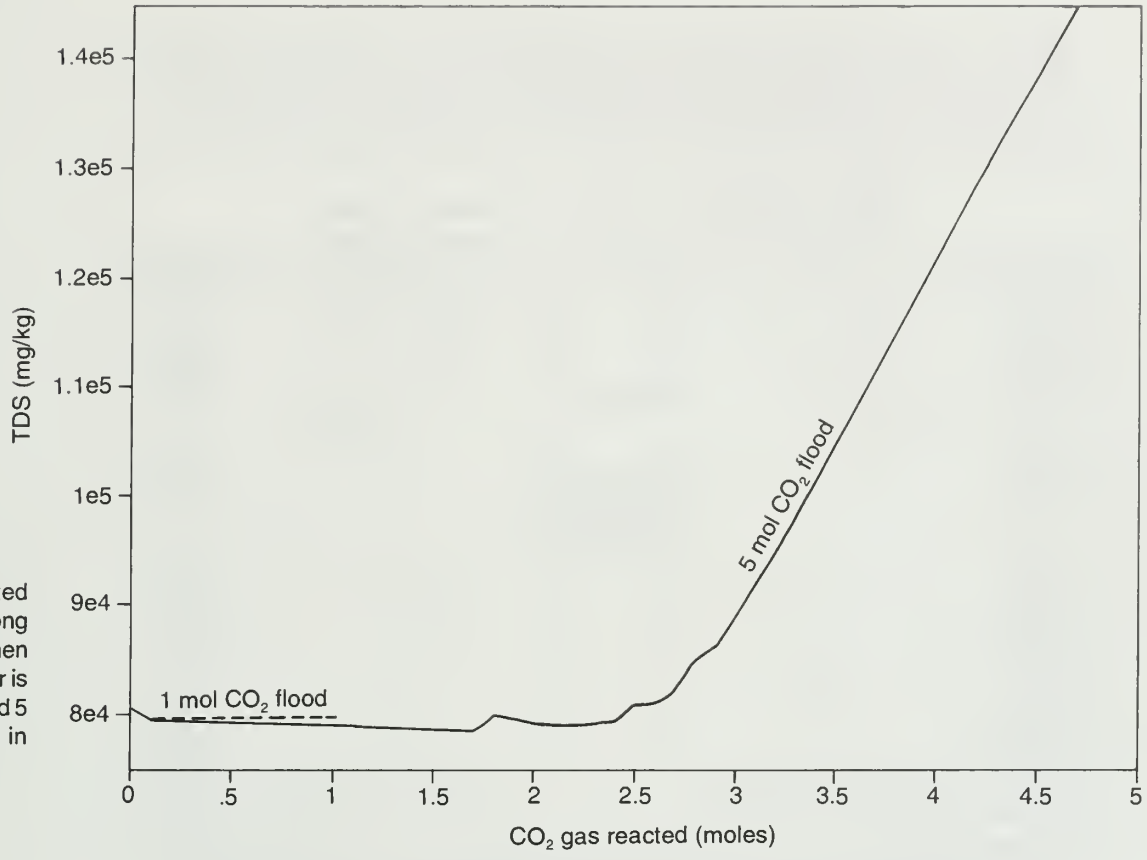

Figure 28 Predicted change in TDS along the reaction path when the Cypress reservoir is flooded with 1 mol and 5 mol CO_2 solutions in Tamaroa Field.

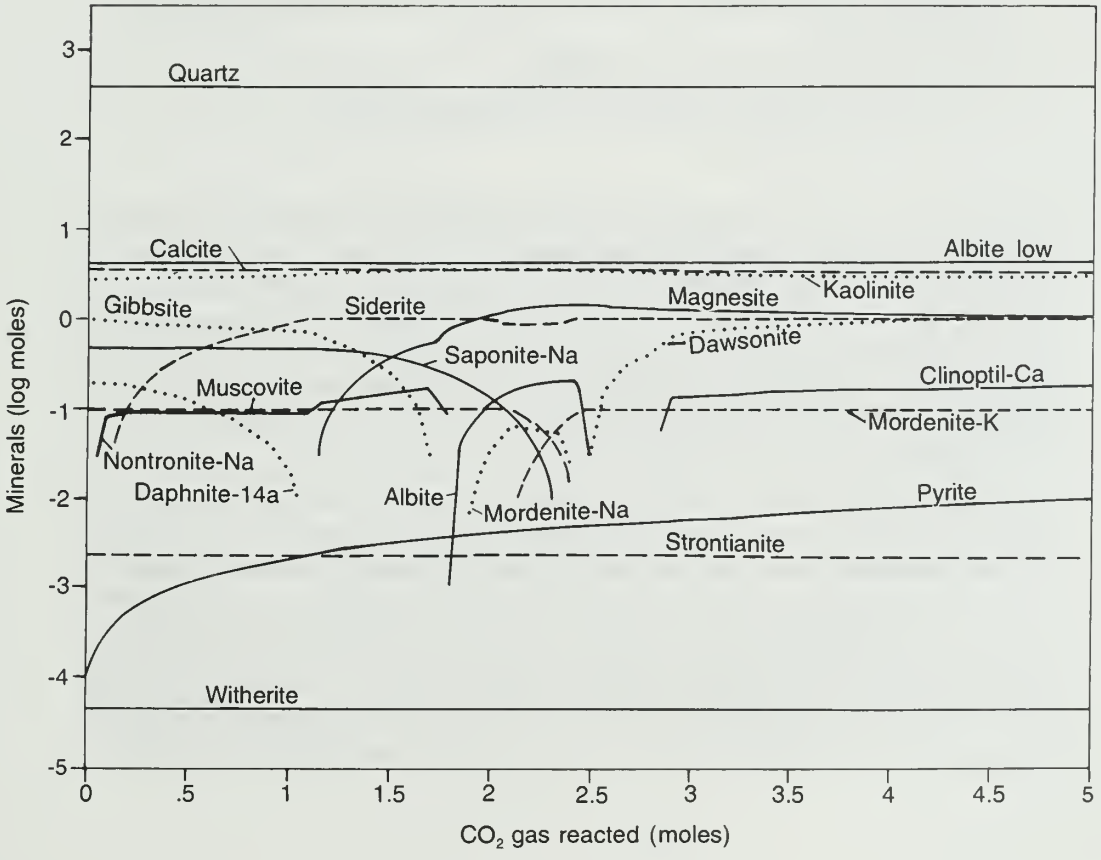

Figure 29 Predicted changes in mineral concentrations along the reaction path when the Cypress reservoir is flooded with 5 mol CO_2 solution in Tamaroa Field.

Table 14 Mineral volume corresponding to each kg (943 cm^3) of pore water (at a 40% water saturation), or a total pore volume of 2358 cm^3, before and after the reaction of 0.5 mol NaOH solution with the Cypress reservoir in Tamaroa Field.

	Original mineral volume (cm^3)			
Minerals	Measured	Predicted by model	Predicted mineral volume (cm^3) after reaction path	Net change[a]
Quartz	9045	9045	9045	0
Albite	423	423	423	0
Calcite	132	132	104	-28
Chlorite[b]	103	47 (daphnite)	93 (daphnite + ripidolite)	-10
Kaolinite	291	273	0	-291
Illite[b]	22	13 (muscovite)[c]	0	-22
Smectite[b]	9	67 (nontronite + saponite)	0	-9
Prehnite	0	0	53	+53
Analcime	0	0	261	+261
Phlogopite	0	0	14	+14
Gibbsite	0	33	82	+82
Pyrite	0	tr	0	
Strontianite	0	0.1	0.1	+0.1
Witherite	0	tr	tr	nd
Net change in total mineral volume				+50.1
% Change in total pore volume[d]				-2.1
Final porosity (%)[e]				18.6

[a] Difference between original measured values and values after reaction path ended.
[b] The original measured volumes of these minerals were adjusted somewhat to make the simulation runs converge (compare the first and second columns of this table to those of table 11).
[c] Model assumes muscovite is a proxy for illite.
[d] (net change in total mineral volume/original total pore volume) x 100.
[e] (1 + (% change in total pore volume/100)) x (original porosity).
tr = trace, nd = not detectable.

CO_2-flood operations. Alkali concentrations in the solutions used for the simulation runs were the same as those used by Bethke (1992): 0.5 mol of NaOH, 0.25 mol Na_2CO_3, and 0.25 mol Na_2SiO_3. A volume of alkali solutions ten times the volume of pore water was arbitrarily chosen to flush out the pore water for 30 days. Quartz, amorphous silica, and albite were allowed to precipitate or dissolve according to a kinetic rate law using the rate data of Rimstidt and Barnes (1980) and Knauss and Wolery (1986). Other minerals were allowed to react freely until they attained thermodynamic equilibrium with the solution.

Results Clay minerals reacted with the alkali flood to form zeolite minerals: analcime and prehnite during the NaOH and Na_2SiO_3 floods (tables 14, 15, figs. 30, 31) and analcime during the Na_2CO_3 flood (table 16, fig. 32). The precipitation of zeolites in the pore space of reservoir rock during alkali flooding may contribute to formation damage (Sydansk 1982, Bethke 1992). Quartz and albite did not react with the alkali solutions (tables 14–16, figs. 30–32). The model predicted that the reservoir's average porosity would decrease from 19% (table 9) to 18.6% during the NaOH flood, and to 17.7% during the Na_2SiO_3 and Na_2CO_3 floods (tables 14–16).

Table 15 Mineral volume corresponding to each kg (943 cm^3) of pore water (at a 40% water saturation), or a total pore volume of 2358 cm^3, before and after the reaction of 0.25 mol Na_2SiO_3 solution with the Cypress reservoir in Tamaroa Field.

	Original mineral volume (cm^3)			
Minerals	Measured	Predicted by model	Predicted mineral volume (cm^3) after reaction path	Net change[a]
Quartz	9045	9045	9045	0
Albite	423	423	423	0
Calcite	132	132	123	-9
Chlorite[b]	103	47 (daphnite)	93 (Ripidolite + clinochlore)	-10
Kaolinite	291	273	0	-291
Illite[b]	22	13 (muscovite)[c]	0	-22
Smectite[b]	9	67 (nontronite + saponite)	0	-9
Analcime	0	0	421	+421
Prehnite	0	0	17	+17
Phlogopite	0	0	14	+14
Gibbsite	0	33	54	+54
Pyrite	0	tr	0.2	+0.2
Strontianite	0	0.1	0.1	+0.1
Witherite	0	tr	tr	nd
Net change in total mineral volume				+165.3
% Change in total pore volume[d]				-7.0
Final porosity (%)[e]				17.7

[a] Difference between original measured values and values after reaction path ended.
[b] The original measured volumes of these minerals were adjusted somewhat to make the simulation runs converge (compare the first and second columns of this table to those of table 11).
[c] Model assumes muscovite is a proxy for illite.
[d] (net change in total mineral volume/original total pore volume) x 100.
[e] (1 + (% change in total pore volume/100)) x (original porosity).
tr = trace, nd = not detectable.

The consumption of alkali metal (Na^+) by mineral precipitation or dissolution is undesirable because the purpose of alkali flooding for improved oil recovery is to react the alkali metal with oil to form a surfactant. The NaOH flood was predicted to be the most efficient in delivering the alkali metal to the reservoir, because more Na^+ remained in the fluid at the end of the reaction paths to react with oil for the NaOH flood than for the other two floods (fig. 33). As expected, all three alkali floods raised the pH from 6.5 to more than 9, further reducing the chance of asphaltene precipitation. Because illite and smectite were predicted to dissolve during the NaOH and Na_2SiO_3 floods, swelling of clay minerals should not be a concern for these two floods. Potential formation damage from the swelling of clay minerals exists, however, during the Na_2CO_3 flood because of the predicted precipitation of smectite (table 16) and reduction of TDS to 2855 mg/kg, which is much lower than the original TDS in the formation water (appendix B, sample EOR-B22).

On the basis of change in pore volume, greater delivery of alkali metal to the formation fluid, and swelling of clay minerals discussed above, the NaOH flood appeared to be more efficient than Na_2CO_3 and Na_2SiO_3 floods for increasing oil production in the Tamaroa Field under the conditions modeled.

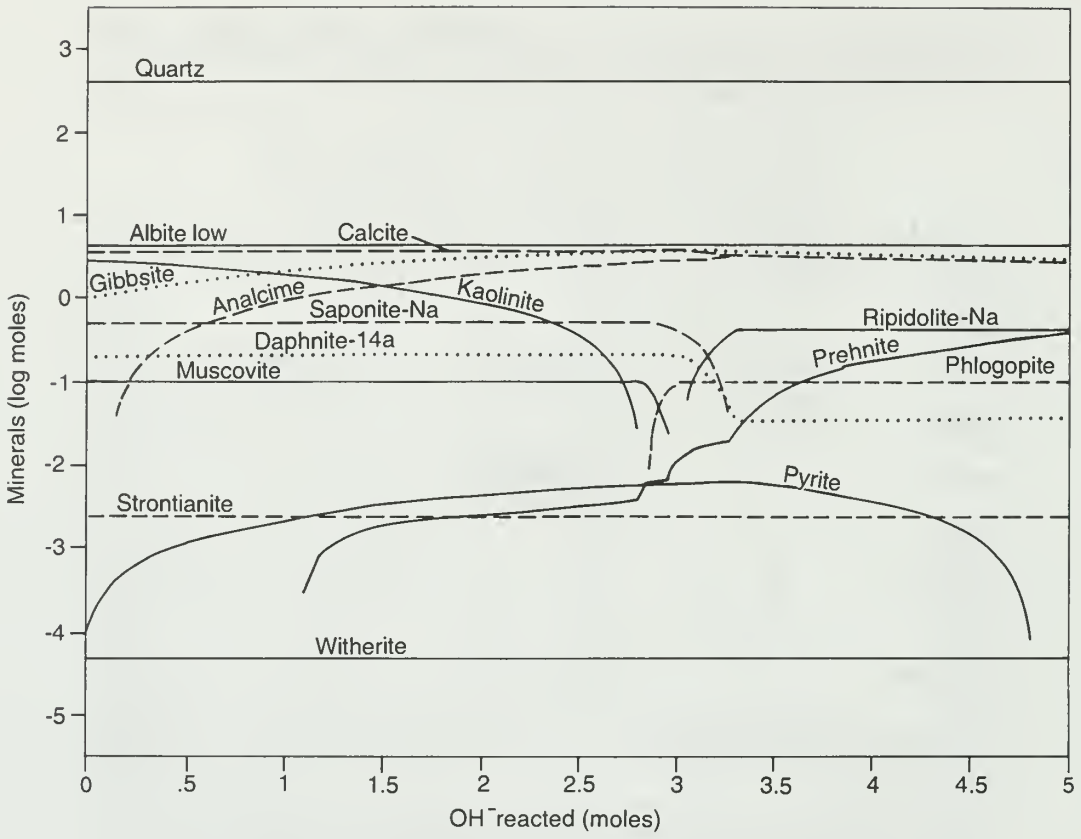

Figure 30 Predicted changes in mineral concentrations along the reaction path when the Cypress reservoir is flooded with 0.5 mol NaOH solution in Tamaroa Field.

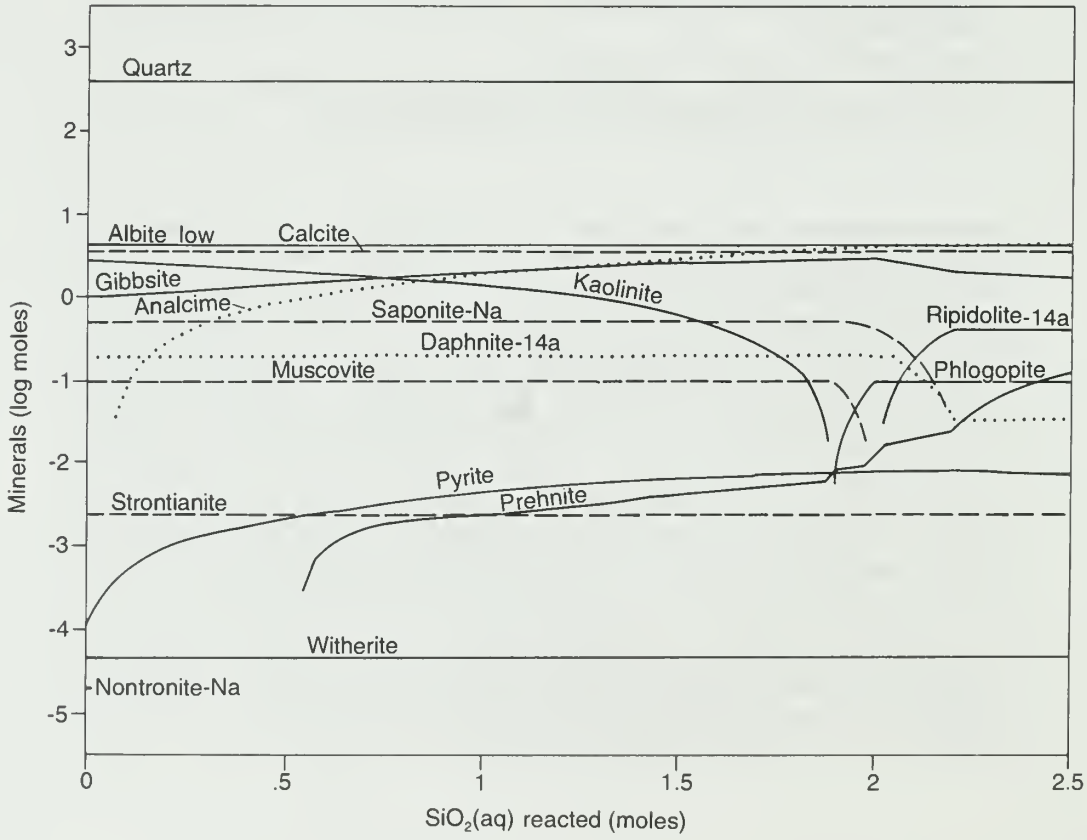

Figure 31 Predicted changes in mineral concentrations along the reaction path when the Cypress reservoir is flooded with 0.25 mol Na_2SiO_3 solution in Tamaroa Field.

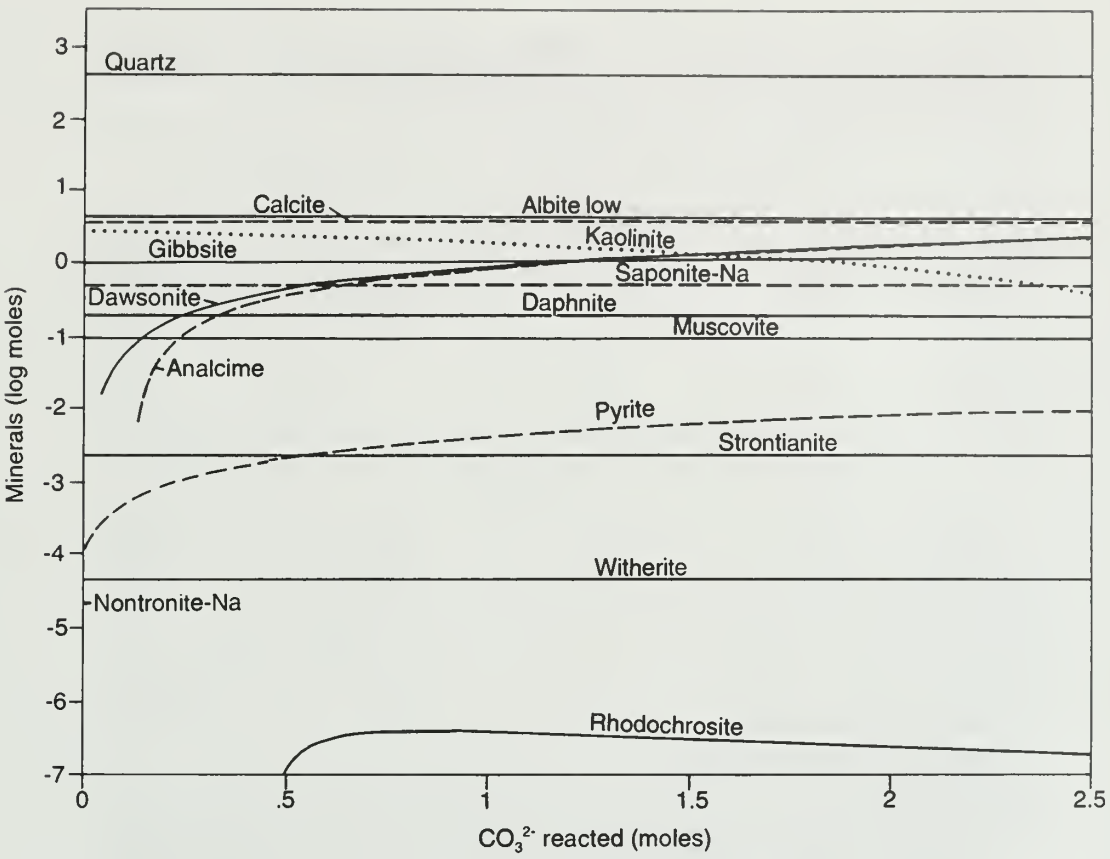

Figure 32 Predicted changes in mineral concentrations along the reaction path when the Cypress reservoir is flooded with 0.25 mol Na_2CO_3 solution in Tamaroa Field.

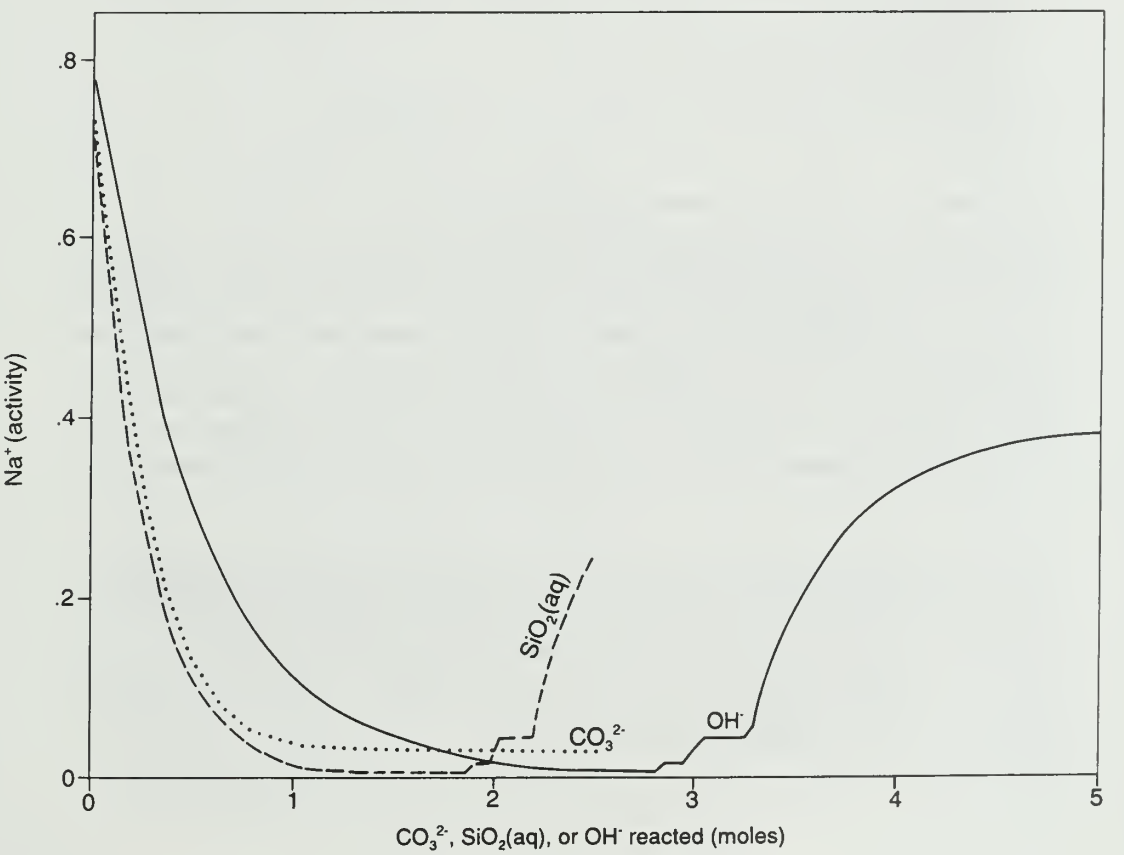

Figure 33 Predicted change in Na^+ activity along the reaction path when the Cypress reservoir is flooded with three types of alkali solutions (0.5 mol NaOH, 0.25 mol Na_2SiO_3, or 0.25 mol Na_2CO_3) in Tamaroa Field.

Table 16 Mineral volume corresponding to each kg (943 cm^3) of pore water (at a 40% water saturation), or a total pore volume of 2358 cm^3, before and after the reaction of 0.25 mol Na_2CO_3 solution with the Cypress reservoir in Tamaroa Field.

	Original mineral volume (cm^3)			
Minerals	Measured	Predicted by model	Predicted mineral volume (cm^3) after reaction path	Net change[a]
Quartz	9045	9045	9045	0
Albite	423	423	423	0
Calcite	132	132	134	+2
Chlorite[b]	103	47 (daphnite)	47 (daphnite)	-56
Kaolinite	291	273	38	-253
Illite[b]	2	13 (muscovite)[c]	13	+11
Smectite[b]	9	67 (nontronite + saponite)	69 (saponite)	+60
Dawsonite	0	0	130	+130
Analcime	0	0	226	+226
Gibbsite	0	33	39	+39
Rhodochrosite	0	0	tr	
Pyrite	0	tr	0.2	+0.2
Strontianite	0	0.1	0.1	+0.1
Witherite	0	tr	tr	tr
Net change in total mineral volume				+159.3
% Change in total pore volume[d]				-6.7
Final porosity (%)[e]				17.7

[a] Difference between original measured values and values after reaction path ended.
[b] The original measured volumes of these minerals were adjusted somewhat to make the simulation runs converge (compare the first and second columns of this table to those of table 11).
[c] Model assumes muscovite is a proxy for illite.
[d] (net change in total mineral volume/original total pore volume) x 100
[e] (1 + (% change in total pore volume/100)) x (original porosity)
tr = trace.

Limitations of Geochemical Modeling

The success of geochemical modeling depends on several conditions. First, the research question has to be posed correctly. This requires an adequate database and a knowledgeable user to describe the problem in precise terms. Secondly, geochemical modeling is a new field with gaps in both theory and data. The application of geochemical modeling will increase gradually as pertinent theories and data are refined and adequately formulated in a single piece of software. Until then, and only in the hands of an experienced and knowledgeable user, can geochemical modeling codes (simulators) now in existence provide reasonable solutions for simple problems, and serve only as a guide for complex problems.

The geochemical simulations discussed in this study required several assumptions that were considered reasonable, but have not been verified. These assumptions introduced uncertainty for the model predictions. Also, only a few scenarios were simulated. Furthermore, the models evaluated only chemical reactions in the reservoir. Physical changes, such as fracturing, also can affect the porosity and permeability. The results presented in this report should, therefore, be used with caution and only as a guide for subsequent work.

SUMMARY AND CONCLUSIONS

About 100 formation water samples were collected from oil wells producing from reservoirs in the Mississippian Aux Vases and Cypress Formations. The samples were analyzed in the field and laboratory for various geochemical parameters (pH, Eh, resistivity, and concentrations of aqueous species). The geochemical composition of the formation water samples, along with mineralogical compositions of core samples from the Aux Vases and Cypress Formations, were used to aid geological interpretation and reservoir analysis to improve oil recovery from these two formations. The findings and conclusions are summarized as follows:

- The Cl-Br relationship in waters from the Aux Vases and Cypress Formations suggest that these waters have a halite dissolution component and probably an evaporated seawater component. The formation waters were depleted of K and Mg relative to the seawater evaporation trajectory. Depletion of K and Mg suggests that the original trapped seawater was either replaced or mixed with waters containing low ratios of K/Br and Mg/Br, or modified by diagenetic reactions. The concentrations of dissolved K and Mg were generally higher in the Aux Vases Formation than in the Cypress Formation, which is relatively poor in K- and Mg-bearing clay minerals and K-feldspar relative to the Aux Vases Formation. The implications are that the K- and Mg-rich clay minerals and K-feldspars in the Aux Vase and Cypress are detrital and/or formed primarily prior to the emplacement of the present day subsurface waters. Ultimately these clay minerals and K-feldspars contributed K and Mg to the formation waters through dissolution. Dissolution and recrystallization of calcite appeared to significantly influence Ca and Sr concentrations in solution. The observed Ca concentrations in excess of amounts that would be provided by calcite dissolution were probably caused by albitization of detrital plagioclase and possibly by partial dolomitization of calcite.

- Variations in water chemistry in a given reservoir in the same field can indicate a lack of communication between different pools, or mineralogical heterogeneity within the reservoir. Therefore, formation water data provided in this study may be used to aid geological interpretations in relation to hydrocarbon production.

- The formation water resistivities and TDS data included in this report can be used to calculate water saturations and permeabilities in oil reservoirs in the Aux Vases and Cypress Formations. Empirical relationships were determined to calculate the electrical resistivity from the TDS or, vice versa, at any temperature encountered within the Aux Vases and Cypress Formations. The areal distributions of all available resistivity and TDS data for the two formations were mapped. These maps are useful for estimating TDS and resistivity in areas where data are unavailable.

- In oil reservoirs, disturbance produced in water-rock systems by changes in temperature or pressure and reactions with externally introduced fluids can result in serious formation damage, which reduces oil production. Minerals that commonly precipitate in reservoirs and boreholes during primary production and thus reduce production are calcite, aragonite, gypsum, anhydrite, celestite, barite, and various Fe-sulfide minerals. The saturation indexes of these minerals in randomly selected Aux Vases and Cypress formation waters were calculated under reservoir conditions. The results indicated that most of the samples were saturated or supersaturated with respect to calcite, barite, and Fe-sulfides. Saturation with

respect to these minerals suggests that they can potentially precipitate if geochemical parameters, such as pressure, temperature, ionic strength, and chemical composition of the reservoir water, change.

- Computerized geochemical models can help in predicting the results of fluid-rock interactions during improved oil recovery processes. The reaction path model REACT was used in this study to simulate the chemical aspects of improved oil recovery processes in three fields under selected scenarios. The volume of minerals that precipitated and/or dissolved and the accompanying changes in porosity were calculated.

    - Geochemical modeling predicted a consistent increase in pore volume in the zone adjacent to a well bore, if a production well in the Energy Field was treated with 15% or 7.5% HCl-MCA. The higher acidity and dissolved iron concentration caused by treatment with 15% HCl-MCA relative to those caused by treatment with 7.5% HCl-MCA were predicted to increase the chance of asphaltene precipitation.

    - The simulations of geochemical reactions of waterflood operations in the Dale Consolidated and Tamaroa Fields predicted little change in porosity. Therefore, injection waters used in these operations were judged to be compatible with the reservoirs.

    - In addition to waterflood operations, two other improved oil recovery processes, CO_2 and alkali (NaOH, Na_2CO_3, and Na_2SiO_3) floods, were simulated for the Tamaroa Field. Geochemical modeling of the CO_2-flood operation predicted a small or negligible decrease in reservoir porosity. Simulation of alkali-flood operations indicated that clay minerals reacted with the alkali to form zeolites, a special concern for formation damage. The purpose of alkali flooding is to allow the alkali metal (Na^+ in this case) to react with oil to form surfactants, which improve the effective permeability to oil. The NaOH flood was predicted to be the most efficient in delivering alkali metal to the reservoir and to have the least adverse effect on the reservoir porosity.

    - Because natural processes are complex, extreme caution should be taken when geochemical modeling is used for prediction purposes. The geochemical simulations discussed in this report were based on several unverified assumptions, and only a limited number of scenarios were modeled. Therefore, the results should serve only as an introduction and guide for future work in this area.

ACKNOWLEDGMENTS

I particularly thank R. T. Black for his technical assistance in contacting the oil companies and in collecting and processing the samples. I thank D. S. Beaty for his selfless assistance in sample collection and for providing, along with R. E. Hughes and D. M. Moore, the mineralogical data. I am grateful to J. D. Steele of the ISGS and D. S. Dickerson of ARDL, Mt. Vernon, Illinois, who produced the solute concentrations data for the formation water samples. I also thank W. R. Roy, W. T. Frankie, G. B. Dreher, D. M. Moore, and J. H. Goodwin for critically reviewing the

manuscript. Finally, I greatly appreciate the guidance, support, and good sense of humor of D. F. Oltz, the overall project leader.

This research was funded by the U.S. Department of Energy, Grant DE-FG22-89BC14250, and the Illinois Department of Energy and Natural Resources, Grant AE-45. This support is gratefully acknowledged.

REFERENCES

Allison, J.D., D.S. Brown, and K.J. Novo-Gradac, 1991, MINTEQA2/PRODEFA2, A Geochemical Assessment Model for Environmental Systems, Version 3.0 User's Manual: U.S. Environmental Protection Agency, EPA/600/3-91/021, Athens, GA.

Archie, G.E., 1942, The electrical resistivity log as an aid in determining some reservoir characteristics: Transactions of AIME, v. 146, p. 54–62.

ASTM, 1976, Water (Part 31): Annual Book of ASTM Standards, 956 p.

Ball, J.W., E.A. Jenne, and M.W. Cantrell, 1981, WATEQ3—A Geochemical Model with Uranium Added: U.S. Geological Survey, Open File Report 81-1183, 81 p.

Ball, J.W., and D.K. Nordstrom, 1991, User's Manual for WATEQ4F, with Revised Thermodynamic Data Base and Test Cases for Calculating Speciation of Major, Trace, and Redox Elements in Natural Waters: U.S. Geological Survey, Open File Report 91-183, 193 p.

Bethke, C.M., 1992, Geochemical Reaction Modeling Short Course Work Book: Hydrogeology Program, University of Illinois at Urbana–Champaign, 275 p.

Bethke, C.M., 1986, Hydrologic constraints on the genesis of the Upper Mississippi Valley mineral district from Illinois Basin brines: Economic Geology, v. 81, p. 233–249.

Bethke, C.M., and S. Marshak, 1990, Brine migration across North America—The plate tectonics of groundwater: Annual Review of Earth Planetary Science, v. 18, p. 287–315.

Blount, C.W., and F.W. Dickson, 1969, The solubility of anhydrite ($CaSO_4$) in $NaCl$-H_2O from 100 to 450 °C and 1 to 1000 bars: Geochimica Cosmochimica Acta, v. 33, p. 227–245.

Carothers, W.W., and Y.K. Kharaka, 1978, Aliphatic acid anions in oil field waters —Implications for origin of natural gas: Association of American Petroleum Geologists Bulletin, v. 62, p. 2441–2453.

Carpenter, A.B., 1978, Origin and chemical evolution of brines in sedimentary basins: Oklahoma Geological Survey Circular, v. 79, p. 60–77.

Choquette, P.W., and R.P. Steinen, 1980, Mississippian non-supratidal dolomite, Ste. Genevieve Limestone, Illinois Basin: Evidence for mixed-water dolomitization, *in* D. H. Zenger, J. B. Dunham, and R. L. Ethington, editors, Concept and Models of Dolomitization: Society of Economic Paleontologists and Mineralogists Special Publication 28, p. 163–196.

Clayton, N.R., I. Friedman, D.L. Graf, T.K. Mayeda, W.F. Meents, and N.F. Shimp, 1966, The origin of saline formation waters: I. Isotopic composition: Journal of Geophysical Research, v. 71, p. 3869–3882.

Collins, G.A.,1975, Geochemistry of Oil Field Waters: Elsevier, New York, p. 496.

Collins, G.A., and M.B. Kayser, 1985, Interaction, Compatibilities, and Long-Term Environmental Fate of Deep-Well-Injected EOR Fluids and/or Waste Fluids with Reservoir Fluids and Rocks—State of the Art: National Institute for Petroleum and Energy Research, Report NIPER-70 (DE85000146) 103 p.

Das, N., J. Horita, and H.D. Holland, 1990, Chemistry of fluid inclusions in halite from the Salina Group of Michigan Basin—Implications for Late Silurian seawater and origin of sedimentary brines: Geochimica et Cosmochimica Acta, v. 54, p. 319–327.

Davis, J.W., and A.G. Collins, 1971, Solubility of barium and strontium sulfates in strong electrolyte solutions: Environmental Science Technolology, v. 5, p. 1039–1043.

Dickinson, G., 1953, Geological aspects of abnormal reservoir pressure in Gulf Coast Louisiana: American Association of Petroleum Geologists Bulletin, v. 37, p. 4100–432.

Drever, J.I., 1988, The Geochemistry of Natural Waters: Prentice Hall, Englewood Cliffs, New Jersey 437 p.

Duan, Z.N. Moller, J. Greenberg, and J.H. Weare, 1992, The prediction of methane solubility in natural waters to high ionic strength from 0 to 250 °C and from 0 to 1600 bar: Geochimica et Cosmochimica Acta, v. 56, p. 1451–1460.

Felmy, A.R., D.C. Girvin, and E.A. Jenne, 1984, MINTEQ—A Computer Program for Calculating Aqueous Geochemical Equilibria: United States Environmental Protection Agency, EPA-600/3-84-032, Athens, GA, 86 p.

Fletcher, G.E., T.R. French, and A.G. Collins, 1981, A Method for Calculating Strontium Sulfate Solubility: U.S. Department of Energy, DOE/BETC/RI-80/10, 17 p.

Frape, S.K., P. Fritz, and R.H. McNutt, 1984, Water-rock interaction and chemistry of groundwaters from the Canadian shield: Geochimica et Cosmochimica Acta, v. 48, p. 1617–1627.

Fulford, R.S., 1968, Effects of brine concentration and pressure drop on gypsum scaling in oil wells: Journal of Petroleum Technology, v. 20, p. 559–564.

Garrels, R.M., and M.E. Thompson, 1962, A chemical model for seawater at 25 °C and one atmosphere total pressure: American Journal of Science, v. 260, p. 57–66.

Graf, D.L., W.F. Meents, and N.F. Shimp, 1966, The Origin of Saline Formation Waters, III—Calcium Chloride Waters: Illinois State Geological Survey, Circular 397, 60 p.

Grube, J.P., 1992, Reservoir Characterization and Improved Oil Recovery from Multiple Bar Sandstones, Cypress Formation, Tamaroa and Tamaroa South Fields, Perry County, Illinois: Illinois State Geological Survey, Illinois Petroleum Series 138, 49 p.

Haggerty, D.J., and B. Seyler, in preparation, Experimental Investigation of Formation Damage Caused by Mud Cleaning Acids and Injection Waters in Aux Vases Sandstone Reservoirs: Illinois State Geological Survey, Illinois Petroleum Series.

Hanor, J.S., 1987, Origin and Migration of Subsurface Sedimentary Brines: Society of Economic Paleontologists and Mineralogists Short Course No. 21, 247 p.

Helgeson, H.C., R.M. Garrels, and F.T. Mackenzie, 1969, Evaluation of irreversible reactions in geochemical processes involving minerals and aqueous solutions: II, Applications: Geochimica et Cosmochimica Acta, v. 33, p. 455–481.

Helgeson, H.C., T.H. Brown, A. Nigrini, and T.A. Jones, 1970, Calculation of mass transfer in geochemical processes involving aqueous solutions: Geochimica et Cosmochimica Acta, v. 34, p. 569–592.

Hitchon, B., G.K. Billings, and J.E. Klovan, 1971, Geochemistry and origin of formation waters in the western Canada sedimentary basin–Factors controlling chemical composition: Geochimica et Cosmochimica Acta, v. 35, p. 567–598.

ISGS Oil and Gas Section, 1993, Improved and Enhanced Oil Recovery in Illinois by Reservoir Characterization—Standard Operating and QA/QC Procedures: Illinois State Geological Survey, Open File Series 1993-13, 174 p.

Jennings, H.Y., Jr., C.E. Johnson, Jr., and C.D. McAuliffe, 1974, A caustic water flooding process for heavy oils: Journal of Petroleum Technology, v. 26, p. 1344–1352.

Kharaka, Y.K., and I. Barnes, 1973, SOLMINEQ: Solution—mineral—equilibrium Computations: U.S. Geological Survey Computer Contributions, NTIS no. PB215–899, 81 p.

Kharaka, Y.K., W.D. Gunter, P.K. Aggarwal, R.W. Hull, and E.H. Perkins, 1988, SOLMINEQ88: A Computer Program for Geochemical Modeling of Water-Rock Interactions: U.S. Geological Survey, Water Resources Investigations Report 88-4227, 420 p.

Kharaka, Y.K., L.M. Law, W.W. Carothers, W.W., and D.F. Goerlitz, 1986, Role of organic species dissolved in formation waters from sedimentary basins in mineral diagenesis, *in* D. Gautier, editor, Relationship of Organic Matter and Sediment Diagenesis: Society of Economic Paleontologists and Mineralogists Special Publication, v. 38, p. 111–122.

Knauss, K.J., and T.J. Wolery, 1986, Dependence of albite dissolution kinetics on pH and time at 25 °C and 70 °C: Geochimica et Cosmochimica Acta, v. 50, p. 2481–2497.

Land, L.S., 1983, Dolomitization: American Association of Petroleum Geologists, Education Course Note Series 24, 20 p.

Land, L.S., and G.L. Macpherson, 1992, Origin of saline formation waters, Cenozoic section, Gulf of Mexico Sedimentary Basin: American Association of Petroleum Geologists Bulletin, v. 76, p. 1344–1362.

Land, L.S., and D.R. Prezbindowski, 1981, The origin and evolution of saline formation water, Lower Cretaceous carbonates, south-central Texas, U.S.A.: Journal of Hydrology, v. 54, p. 51–74.

Land, L.S., and D.R. Prezbindowski, 1985, Chemical constraints and origins of four groups of Gulf Coast reservoir fluids—Discussion: American Association of Petroleum Geologists Bulletin, v. 69, p. 119–121.

Leetaru, H.E., 1990, Application of Old Electrical logs in the Analysis of Aux Vases Sandstone (Mississippian) Reservoirs in Illinois: Illinois State Geological Survey, Illinois Petroleum 134, 21 p.

Lico, M.S., Y.K. Kharaka, W.W. Carothers, and V.A. Wright, 1982, Methods for Collection and Analysis of Geopressured Geothermal and Oil Field Waters: U.S. Geological Survey, Water Supply Paper 2194, 21 p.

Macpherson, G.L., 1992, Regional variations in formation water chemistry: Major and minor elements, Frio formation fluids, Texas: American Association of Petroleum Geologists Bulletin, v. 76, p. 740–757.

Mattes, B.W., and E.W. Mountjoy, 1980, Burial dolomitization of the Upper Devonian Miette Buildup, Jasper National Park, Alberta, *in* D. H. Zenger, J. B. Dunham, and R. L. Ethington, editors, Concept and Models of Dolomitization: Society of Economic Paleontologists and Mineralogists Special Publication 28, p. 259–297

Moldovanyi, E.P., and L.M. Walter, 1992, Regional trends in water chemistry, Smackover formation, Southwest Arkansas—Geochemical and physical controls: American Association of Petroleum Geologists Bulletin, v. 76, p. 864–894.

Morton, R.A., and L.S. Land, 1987, Regional variations in formation water chemistry, Frio formation (Oligocene), Texas Gulf Coast: American Association of Petroleum Geologists Bulletin, v. 71, p. 191–206.

Nesbitt, H.W., 1980, Characterization of mineral-formation water interactions in carboniferous sandstones and shales of the Illinois Sedimentary Basin: American Journal of Science, v. 280, p. 607–630.

Nesbitt, H.W., 1985, A chemical equilibrium model for the Illinois Basin formation waters: American Journal of Science, v. 285, p. 436–458.

Parkhurst, D.L., D.C. Thorstenson, and L.N. Plummer, 1980, PHREEQE—A Computer Program for Geochemical Calculations: U.S. Geological Survey, Water Resources Investigation Report 80-96, 210 p.

Plummer, L.N., B.F. Jones, and A.H. Truesdell, 1976, WATEQF—A FORTRAN IV Version of WATEQ, A Computer Program for Calculating Chemical Equilibrium of Natural Waters: U.S. Geological Survey, Water Resources Investigation Report 76-13, 310 p.

Plummer, L.N., D.L. Parkhurst, G.W. Fleming, and S.A. Dunkle, 1988, A Computer Program Incorporating Pitzer's Equations for Calculation of Geochemical Reactions in Brines, U.S. Geological Survey, Water Resources Investigation Report 88-4153.

Pollack, H.N., and D. Watts, 1976, Thermal profile of the Michigan Basin: EOS, v. 57, 595 p.

Reed, M.H., 1982, Calculation of multicomponent chemical equilibria and reaction processes in systems involving minerals, gases, and aqueous phase: Geochimica et Cosmochimica Acta, v. 46, p. 513–528.

Rimstidt, J.D., and H.L. Barnes, 1980, The kinetics of silica-water reactions: Geochimica et Cosmochimica Acta, v. 44, p. 1683–1699.

Rittenhouse, G., 1967, Bromine in oil field waters and its use in determining possibilities of origin of these waters: American Association of Petroleum Geologists Bulletin, v. 51, p. 2430–2440.

Sanders, L.L., 1991, Geochemistry of formation waters from the Lower Silurian Clinton formation (Albion Sandstone), Eastern Ohio: American Association of Petroleum Geologists Bulletin, v. 75, p. 1593–1609.

Schlumberger Log Interpretation Charts for 1989: Schlumberger Education Services, Houston, TX, 150 p.

Sibley, D.F., R.E. Dedoes, and T.R. Bartlett, 1987, Kinetics of dolomitization: Geology, v. 15, p. 1112–1114.

Spycher, N.F., and M.H. Reed, 1989a, SOLVEQ—A Computer Program for Computing Aqueous-Mineral-Gas Equilibria (Revised Preliminary Edition): Department of Geological Sciences, University of Oregon, Eugene, 36 p.

Spycher, N.F., and M.H. Reed, 1989b, CHILLER—A Program for Computing Water-Rock Reactions, Boiling, Mixing and Other Reaction Processes in Aqueous-Mineral-Gas Systems (Revised Preliminary Edition): Departmental of Geological Sciences, University of Oregon, Eugene, 64 p.

Stoessell, R.K., and A.B. Carpenter, 1986, Stoichiometric saturations tests of $NaCl_{1-x}Br_x$ and $KCl_{1-x}Br_x$: Geochimica et Cosmochimica Acta, v. 50, p. 465–1474.

Stueber, A.M., and L.M. Walter, 1991, Origin and chemical evolution of formation waters from Silurian-Devonian strata in the Illinois Basin: Geochimica et Cosmochimica Acta, v. 55, p. 309–325.

Stueber, A.M., L.M. Walter, T.J. Huston, and P. Pushkar, P., 1993, Formation waters from Mississippian-Pennsylvanian reservoirs, Illinois Basin, USA—Chemical and isotopic constraints on evolution and migration: Geochimica et Cosmochimica Acta, v. 57, p. 763–784.

Sydansk, R.D., 1982, Elevated-temperature caustic/sandstone interaction—Implications for improving oil recovery: Journal of the Society of Petroleum Engineers, p. 453–462

Templeton, C.C., 1960, Solubility of barium sulfate in sodium chloride solutions from 25 °C to 95 °C: Journal of Chemical Engineering Data, v. 5, p. 514–516.

Truesdell, A.H., and B.F. Jones,1974, WATEQ, a computer program for calculating chemical equilibria of natural waters: Journal of Research, U. S. Geological Survey, v. 2, p. 233–248.

Udegbunam, E.O., D.S. Beaty, and J.P. Fagan, Jr., 1993, Strategies for Improved Oil Recovery from Aux Vases Reservoirs in McCreery and McCullum Waterflood Units, Dale Consolidated Field, Franklin County, Illinois: Illinois State Geological Survey, Illinois Petroleum 143, 39 p.

U.S. Environmental Protection Agency, 1975, Standard Method for Examination of Water and Waste Water, 14th edition: American Public Health Association, American Water Works Association, and American Pollution Control Federation, Washington, DC, 11,093 p.

U.S. Environmental Protection Agency, 1985, Standard Method for Examination of Water and Waste Water, 16th edition: American Public Health Association, American Water Works Association, and American Pollution Control Federation, Washington, DC, 1,268 p.

Walter, L.M., A.M. Stueber, and T.J. Huston, 1990, Br-Cl-Na systematics in Illinois Basin fluids: Constraints on fluid origin and evolution: Geology, v. 18, p. 315–318.

Westall, J.C., J.L. Zachary, and F.M.M. Morell, 1976, MINEQL, A Computer Program for Calculation of Chemical Equilibrium Composition of Aqueous Systems, Technical Note 18: Ralph M. Parson Laboratory for Water Resources and

Environmental Engineering, Department of Civil Engineering, Massachusett Institute of Technology, Cambridge, 91 p.

Wolery, J.T., 1979, Calculation of Chemical Equilibrium between Aqueous Solutions and Minerals—The EQ3/6 Software Package: Lawrence Livermore National Laboratory Report UCRL-52658, 41 p.

Wolery, J.T., 1992a, EQ3NR, A Computer Program for Geochemical Aqueous Speciation Solubility Calculations—Theoretical Manual, User's Guide, and Related Documentation (Version 7.0): Lawrence Livermore National Laboratory Report UCRL-MA-1100662 PT III, 246 p.

Wolery, J.T., 1992b, EQ3/6, A Software Package for Geochemical Modeling of Aqueous Systems—Package Overview and Installation Guide (Version 7.0): Lawrence Livermore National Laboratory Report UCRL-MA-1100662 Pt I, 66 p.

APPENDIX A Procedure for Sampling Formation Waters

1 Collect the samples in a carboy (a polyethylene container with a bottom spigot). Attach PVC tubing to the bleed line at the well head, open the bleed valve slowly, and rinse the tubing and the carboy at least once with the formation fluid (oil-brine mixture).

2 Insert the other end of the tubing down to the bottom of the carboy through a hole in a modified carboy cap (collection cap). Fill the carboy with formation fluid, and quickly replace the collection cap with an air-tight cap to minimize oxidation and degassing.

3 Allow sufficient time for the oil and water to separate. This step usually takes 5 to 30 minutes.

4 Connect the spigot of the carboy to a polyethylene column (filled with glass wool) using Tygon tubing. Connect the other end of the column to the inlet of a portable, battery operated pump, and connect the outlet of the pump to the inlet of a multiprobe monitoring chamber using Tygon tubing.

5 Place pH and Eh electrodes, conductivity cell, and temperature probe in the multiprobe monitoring chamber. Open the valve of the carboy spigot, and pump the formation water through the glass wool column into the multiprobe chamber. The glass wool removes any solids and oil droplets. When the brine begins overflowing from the chamber, start monitoring the conductivity (or resistivity), pH, Eh, and temperature under continuous flow conditions. Record the pH under slow and Eh under fast flow conditions. Record the values on the field data form (ISGS 1993) when the readings are stable, and then close the carboy spigot valve.

6 Disconnect the Tygon tubing from the multiprobe monitoring chamber, and connect it to the inlet of an in-line filter assembly containing a 0.1-μm membrane filter. Pump and discard about 250 mL of formation water from the carboy to rinse the in-line filter, and then collect about 750 mL in a 1-L clean polyethylene bottle. Rinse all the sampling bottles twice with the collected formation water. Then pump 250 mL of formation water into the 1-L polyethylene bottle and close the carboy spigot valve. Acidify 125 mL of the sample with HNO_3 to pH 1.5 in a 125 mL polyethylene bottle, label it as filtered-acidified (FA), and store it for metals analysis. Make 1:4 and 1:1 dilutions with the rest of the sample, using deionized water, and label them as such, and store them in 125-mL polyethylene bottles for silica analysis.

7 Replace the 0.1-μm filter in the in-line filter assembly with a 0.45-μm filter. Open the carboy spigot valve, pump about 250 mL of brine to rinse the filter, and then collect 1 L of formation water sample. Label this as filtered (F) and store for anions and ammonium analyses.

8 To prepare for collection of the next sample, rinse the multiprobe chamber, Tygon tubing, and the in-line filter holder thoroughly with deionized water. Use clean carboy and new and clean sample bottles, glass wool columns, PVC tubing, and filter papers for each sample and repeat steps 1 to 8.

9 Transport all the field samples to the laboratory in an ice box.

Appendix B Well Identification and Chemical Composition of Formation Waters

Sample no.	API no.	Field name	Strat. Unit	Average depth (ft)	Resis. (ohm-m)	Eh (mV)	pH	TDS (mg/l)	Anions and major cations (mg/L) Cl	Br	I	SO_4	NO_3	CO_3	HCO_3	Na	Ca	Mg
EOR-B115	120552391900	AKIN	Cypr.	2825	0.0601	-186	6.44	145333	87000	160	3.50	270	0.62	0.04	140	52100	4010	1370
EOR-B92	121913194800	BARNHILL	Aux V.	3360	0.0639	-234	6.89	132780	78000	110	13.00	1300	0.08	0.10	110	46400	5170	1310
EOR-B17	120270314300	BARTELSO	Cyp.	987	0.1382	-318	7.01	49667	29000	84	5.60	2.5	0.10	0.86	460	18160	892	601
EOR-B18	120270156000	BARTELSO	Cyp.	955	0.1389 *	-197	7.05	49352	29750 +							17870	936	556
EOR-B19*	120270417500	BARTELSO	Cyp.	991	0.1364	-111	6.95	51519	31067 +							18620	1013	586
EOR-B28*	120270115700	BARTELSO	Cyp.	985	0.1401 *	-271	6.9	48809	29366 +							17650	935	545
EOR-B29	120270112700	BARTELSO	Cyp.	980	0.1427	-275	7.2	49715	29977 +							18000	980	585
EOR-B30	120270110600	BARTELSO	Cyp.	973	0.1425	-142	6.87	48698	29000	85	4.70	7.5	0.10	0.24	290	17480	991	592
EOR-B31	120270110600	BARTELSO	Cyp.	979	0.1346 *	-335	6.87	51339	30935 +							18550	995	590
EOR-B98	120652505500	BUNGAY C.	Aux V.	3317	0.0627	-280	6.93	137213	82000	170	7.80	990	0.28	0.39	130	47300	4790	1460
EOR-B70	121932941500	CARMI NORTH	Aux V.	3236	0.0676	-150	5.92	125460	74000	180	7.00	304	0.60	0.05	60	43830	5340	1210
EOR-B72	121932955300	CARMI NORTH	U. Cyp	2936	0.0689	-128	6.26	122960	72000	180	6.40	64	0.32	0.28	93	43740	5230	1180
EOR-B50	121913164700	CLAY CITY C.	Aux V.	3169	0.0606	-300	6.74	145056	85000	180		660	0.62	0.16	110	50950	5920	1750
EOR-B51	121913099200	CLAY CITY C.	Aux V.	3234	0.0782	-335	7.24	100768	59000	130		690	<0.04	1.00	170	35560	3770	1040
EOR-B78	121592444800	CLAY CITY C.	Aux V.	2819	0.0689	-279	6.06	126899	76741 +							44830	3300	1280
EOR-B79	121592447000	CLAY CITY C.	Aux V.	2824	0.0667	-270	6.46	132062	79000		5.70	1.1	0.23	0.09	94	46770	3550	1430
EOR-B80	120252804100	CLAY CITY C.	Aux V.	2918	0.0728	-277	6.99	115063	66000		6.30	1500	0.27	0.32	170	42020	3740	1260
EOR-B81	120250299100	CLAY CITY C.	Aux V.	2911	0.0614	-283	6.92	144656	85000		8.80	510	0.27	0.38	160	52030	5170	1350
EOR-B86	120792465900	CLAY CITY C.	Aux V.	2743	0.0636	-202	6.8	138339	81000	150	7.70	1800	0.19	0.11	190	48800	4750	1210
EOR-B93	121910790600	CLAY CITY C.	Aux V.	3102	0.0692	-287	6.56	116926	68000	140	7.70	1200	<0.01	0.13	180	42100	3750	1180
EOR-B52	121913114900	CLAY CITY C.	Cyp.	2940	0.0670	-285	7.24	124254	72000	140		990	0.27	0.34	230	45940	3490	1140
EOR-B65	120252769800	LAY CITY C.	Cyp.	2628	0.0751	-288	6.37	104855	61000	140	4.40	870	4.70	0.19	260	38080	2740	1400
EOR-B69	121590326100	CLAY CITY C.	Cyp.	2555	0.0796	-280	6.82	101462	60000	98	4.40	1100	1.40	0.81	690	36280	1990	1030
EOR-B97	121592532000	CLAY CITY C.	Cyp.	2490	0.0907	-99	7.71	84594	51000	94	3.90	1.4	0.28	0.14	230	30600	1670	772
EOR-B102	121592532000	CLAY CITY C.	Cyp.	2490	0.0901	-103	6.16	83707	50000	96	3.90	4.8	0.27	0.14	190	30690	1730	782
EOR-B11	120552345700	DALE CONS.	Aux V	3182	0.0664 *	-226	7.06	125875	74684 +							43650	5230	1740
EOR-B12	120552345500	DALE CONS.	Aux V	3159	0.0676 *	-329	8.02	123181	72506 +							42400	5540	2190
EOR-B13	120552487700	DALE CONS.	Aux V	3232	0.0585	-135	6.03	136549	78000	220	15.00	700	0.25	0.01	30	48310	6350	2180
EOR-B62	120652487700	DALE CONS.	Aux V	3219	0.0635	-280	7.03	130049	77000	190	11.00	140	1.30	0.02	100	44080	6170	1810
EOR-B107	120552347200	DALE CONS.	Aux V	3172	0.0615	-134	5.34	137444	84000	160	9.90	9.5	0.41	0.00	64	44850	5820	1950
EOR-B108	120552348700	DALE CONS.	Aux V	3176	0.0636	-124	7.08	129440	78000	150	12.00	19	0.43	0.01	94	42990	5830	1740
EOR-B101	120552272100	DALE CONS.	Cyp.	2959	0.0621	-270	6.24	140537	83000	150	2.40	930	0.36	0.05	90	50700	4050	1270
EOR-B114	120652507900	DALE CONS.	Cyp.	2724	0.0625	-173	5.68	137161	81000	140	3.10	920	0.60	0.04	160	49530	3870	1260
EOR-B85	120812435900	DIVIDE CONS.	Aux V.	2670	0.0624	-206	5.76	137875	83000		8.80	460	0.06	0.06	94	46970	5380	1490
EOR-B56	120812468600	DIX SOUTH	Aux V.	2044	0.0664	-104	6.17	125882	76000	140	6.40	130	<0.04	0.02	67	42460	4910	1660
EOR-B99	121652490500	ELDORADO W.	Aux V.	2864	0.0746	-213	6.56	108598	65000	180	10.20	430	0.24	0.39	210	36200	4030	1960
EOR-B4	121992345600	ENERGY	Aux V.	2400	0.0633	-205	7.02	122431	72453 +							42370	4630	2200
EOR-B5	121992345500	ENERGY	Aux V.	2371	0.0633	-202	7.12	124000	73377 +							42900	4510	2360
EOR-B6	121992345700	ENERGY	Aux V.	2400	0.0623	-106	5.79	131352	79000	190	9.70	2.1	0.29	0.04	85	43350	5300	2580
EOR-B7	121992346600	ENERGY	Aux V.	2389	0.0639	-146	7.26	123629	73063 +							42720	4700	2290
EOR-B60	121992347700	ENERGY	Aux V.	2364	0.0632	-102	6.63	132040	79000	180	10.00	1.8	0.25	0.01	60	44210	5370	2510
EOR-B100	121993348100	ENERGY	Aux V.	2369	0.0632	-152	6.51	131711	79000	170	10.20	<1	0.36	0.19	100	43900	5410	2450
EOR-B90	121913142200	GOLDEN GATE C.	Aux V.	3296	0.0635	-305	6.87	133970	79000	160	9.20	1300	0.25	0.27	230	46600	5030	1290
EOR-B91	120472428600	GOLDEN GATE C.	Aux V.	3179	0.0685	-98	6.55	122271	73000	190	13.00	1500	0.23	0.10	170	39600	6060	1420
EOR-B109	121652581700	HARCO	Cypr.	2584	0.0656	-270	7	124101	74000	150	6.80	480	0.46	0.20	170	43020	4840	1150
EOR-B77	121933050200	HERALD CONS.	Aux V.	2886	0.0673	-288	6.38	125828	72000	200	11.00	1400	0.26	0.41	140	46980	3260	1420
EOR-B84	121910515800	JOHNSONVILLE W.	Aux V.	2973	0.0593	-275	6.31	151399	89000		8.20	290	0.19	0.10	160	54660	5260	1550
EOR-B8*	120810049800	KING	Aux V	2720	0.0648 *	-238	6.35	129783	78815 +							46020	3260	1260
EOR-B9	120810016700	KING	Aux V.	2744	0.0621	-287	6.81	141529	85000	180	3.90	720	0.06	0.11	120	48540	4710	1720
EOR-B67	121012359300	LAWRENCE	Cyp.	1593	0.1447	-228	5.67	48460	28000	60	4.40	830	0.81	<0.01	20	18400	633	378
EOR-B53	121912918100	MAPLE GROVE C.	Aux V.	3148	0.0617	-210	6.28	142269	85000	180		1200	0.13	<0.01	30	47000	6750	1700
EOR-B89	120472231600	Bennington S.	Aux V.	3156	0.0714	-201	6.84	116670	67000	190	8.50	1800	0.55	0.04	83	41700	4450	1150
EOR-B14	120292300800	MATTOON	L. Cyp.	1868	0.0752 *	-298	7.52	107508	64959 +							38070	3100	1114
EOR-B15*	120290182200	MATTOON	Cyp.	1784	0.0785	-284	7.35	98074	59276 +							34810	2790	913
EOR-B16	120292310100	MATTOON	Cyp.	1882	0.0715	-333	7.4	110214	66475 +							38940	3400	1113
EOR-B34	120290054300	MATTOON	Cyp.	1752	0.0700	-95	6.3	113311	67000	140	13.00	280	0.15	0.15	100	40290	3890	1290
EOR-B36	120292340200	MATTOON	Cyp.	1820	0.0692	-276	6.85	117069	69000	140	4.70	600	0.10	0.26	140	41050	4490	1330
EOR-B37	120292316200	MATTOON	Cyp.	1971	0.0708	-157	6.06	120678	72680 +							42500	3785	1365
EOR-B63	120292322100	MATTOON	Cyp.	1809	0.0869	-132	6.35	88781	52000	100	3.90	630	0.13	0.08	170	31980	2780	863
EOR-B64	120290082400	MATTOON	Cyp.	1780	0.0727	-290	7.17	110591	65000	120	4.30	820	<0.02	0.59	200	38990	3940	1210
EOR-B35	120290127300	MATTOON	Aux V.	1808	0.1252	-314	7.36	56100	33000	71	2.00	31	<0.02	1.30	170	20450	1580	564
EOR-B73	121932575700	NEW HARMONY C.	Cyp.	2611	0.0707	-156	5.92	116603	67000	190	8.20	30	0.29	0.45	120	42990	4340	1310
EOR-B74	121933100800	NEW HARMONY C.	Aux V	2873	0.1603	-53	6.06	43325	25000	65	3.20	13	0.44	0.09	75	16290	1140	452
EOR-B110	121852666700	NEW HARMONY C.	U+M. Cypr.	2475	0.071	-178	5.98	115473	70000	160	6.60	47	0.93	0.01	88	38350	5150	1300
EOR-B38	120812389600	OAKDALE	Aux V.	2870	0.0601	-140	6.98	148028	89000	190	8.60	590	<0.04	0.02	70	50280	5650	1640
EOR-B39	120472246900	PARKERSBURGH	M.Cyp+Bet	2842	0.0707 *	-347	7.09	116201	69000		130.00	310	0.40	0.03	92	39980	5130	1270
EOR-B40	120472418300	PARKERSBURGH	M.+L.Cyp.	2893	0.0703 *	-329	6.9	117119	70000	150	24.00	470	1.20	0.11	153	39480	5280	1230
EOR-B41	120472399500	PARKERSBURGH	L.Cyp.	2804	0.0723	-284	6.74	116429	71000	140	7.00	510	0.90	0.21	110	37810	5200	1340
EOR-B42*	121592517100	PARKERSBURGH	M.Cyp.	2798	0.0715	-131	6.71	117205	71000	170	12.00	150	0.10	0.03	92	39210	4470	1640
EOR-B43	121592506000	PARKERSBURGH	L.Cyp.	2890	0.0673 *	-261	7.37	123766	76000	180	<10.00	390	0.10	0.18	153	39820	5600	1280
EOR-B44	121592509000	PARKERSBURGH	M.Cyp.	2960	0.0703	-150	6.28	120911	74000	140	6.60	510	1.70	0.16	130	39170	5380	1290
EOR-B87	121592531400	PASSPORT N.	Aux V.	2959	0.0799	-324	6.31	102798	59000	100	7.70	1900	0.19	0.19	410	34800	5300	999
EOR-B116	120812474400	RADOM SOUTHEAST	Cypr.	1791	0.0669	-95	5.46	121464	72000	140	3.20	42	0.50	0.01	59	41450	5340	1920
EOR-B24*	121890191900	RICHVIEW	Cyp.	1532	0.0719 *	-99	7.02	113766	67712 +							39650	4125	1760
EOR-B25*	121890182700	RICHVIEW	Cyp.	1482	0.0771 *	-193	6.56	104202	62658 +							36750	3070	1270
EOR-B26*	121890183600	RICHVIEW	Cyp.	1474	0.0788	-131	6.76	106491	63878 +							37450	3345	1390
EOR-B27	121892407200	RICHVIEW	Cyp.	1530	0.0676	-209	6.91	122964	75000	150		<1	<0.04	0.03	88	40010	5120	2040
EOR-B76	121933102400	ROLAND CONS.	Cyp.	2788	0.0729	-250	6.54	108815	63000	140	4.40	32	0.29	0.18	120	39000	4880	1180
EOR-B68	121013012400	RUARK	Cyp.	2015	0.1225	-209	5.53	56431	33000	96	7.40	<0.1	0.97	0.04	150	21430	1010	480
EOR-B82	120252756000	SAILOR SPRING C.	Aux V.	2924	0.0615	-150	6.79	143686	84000		8.80	670	0.19	0.07	190	51870	5110	1380
EOR-B83	120252742400	SAILOR SPRING C.	Aux v.	2909	0.0613	-144	6.13	146456	85000		7.00	660	0.38	0.03	79	53780	5120	1360
EOR-B96	120252743700	SAILOR SPRING C.	Cyp.	2568	0.0722	-250	6.2	106577	62000	120	3.10	860	0.40	0.16	220	39600	2400	1080
EOR-B1*	121730113900	STEWARDSON	Aux V.	1949	0.0693	-248	6.52	114740	69194 +							40500	3250	1500
EOR-B2*	121732247300	STEWARDSON	Aux V.	1953	0.0706	-194	6.12	114833	68000	150	3.50	3.5	0.20	0.10	88	41180	3540	1550
EOR-B3*	121730128800	STEWARDSON	Aux V.	1946	0.0696	-274	6.43	108844	65603 +							38440	3140	1350
EOR-B106	121933111200	STORMS C.	Aux V	2963	0.0639	-237	6.1	127744	76000	160	12.00	750	0.24	0.19	130	45010	3600	1540
EOR-B111	121930609600	STORMS C.	Cypr.	2660	0.073	-150	7.06	108343	64000	140	6.90	47	0.52	0.02	100	40090	2830	889
EOR-B113	Injec. Water	STORMS C.	Waltersbrg		0.1406	-59	7.22	44320	25000	64	3.50	36	0.51	0.36	300	17450	892	468
EOR-B75	121933110800	SUMPTER EAST	Aux V.+S.M.	3027	0.0652	-320	6.54	133882	78000	200	10.00	740	0.29	0.60	160	46220	6450	1700
EOR-B20*	121450294600	TAMAROA S.	Cyp.	1160	0.0953	-100	6.76	83457	50178 +					<1	156	29590	2025	1150
EOR-B21*	121450302300	TAMAROA S.	Cyp.	1148	0.0911 *	-81	6.7	84255	50596 +					<1	164	29830	2114	1194
EOR-B22	121450237300	TAMAROA	Cyp.	1159	0.0877	-178	6.47	87529	52000	140	6.30	18	0.10	0.07	180	30910	2450	1430
EOR-B23	Injec. water	TAMAROA	Cyp.	NA	0.0877	-73	6.68	85236	51276 +					<1	156	30220	2058	1164
EOR-B45*	120552370200	THOMPSONVIL. N.	Aux V	2991	0.0633	-102	5.78	131732	77508 +							45270	6660	1760
EOR-B46*	120552370100	THOMPSONVIL. N.	Aux V.	3020	0.0620 *	-148	6.65	137264	82000	200	12.00	750	0.60	0.02	79	45190	6780	1720
EOR-B47*	120552357400	THOMPSONVIL. N.	Aux V.	2988	0.0598 *	-38	6.53	143646	91000	200	16.00	240	0.30	0.01	46	43620	6140	1830
EOR-B49*	120552372500	THOMPSONVIL. N.	Aux V.	2946	0.0610 *	-236	5.65	140189	83000	210	16.00	1500	0.60	0.02	61	46610	6390	1850
EOR-B48*	120552374500	Logan	Aux V	2938	0.0581 *	-235	6.43	149184	94000	260	12.00	340	0.60	0.04	92	45860	6320	1760
EOR-B32*	120550209000	ZEIGLER	Aux V.	2623	0.0675	-260	6.37	123391	73813 +							43150	4395	1515
EOR-B33*	120550206100	ZEIGLER	Aux V	2627	0.0684	-118	6.8	121168	72419 +							42350	4390	1490
EOR-B59	120552387700	ZEIGLER	Aux V	2629	0.0610	-111	6.24	137329	82000	190	10.00	490	0.29	0.03	120	45950	6020	1900

* Water-flooded, ** Estimated from TDS, + Estimated from Na

Sample no.	Minor and Trace Constituents (mg/L)																						
	K	Sr	NH_4	Ba	Li	Fe	Mn	B	Si	Al	Pb	Ti	V	Co	Ni	Cu	Zn	Zr	Cd	Be	Cr	As	Se	Mo	Sb
EOR-B115	105	130	31	0.66	3.90	3.00	0 43	2.89	1.60	0.2	<0 4	<0.04	<0.08	<0.07	<0.1	<0.06	<0.02	<0.08	<0.05	<0.003	<0.07	<0.5	<0.7	<0 08	<0 3
EOR-B92	182	145	23	0.22	6.86	0.40	0.73	4.10	4.80	0.1	<0.4	0.03	<0.07	<0.07	<0.1	<0.05	<0.02	<0.07	<0.05	<0.003	<0.07	<0.5	<0.7	<0.08	<0.3
EOR-B17	69	101	23	252.00	4.90	0.10	1.07	2.60	4.90	<0 4	<0.4	0.02	<0.08	0.15	<0.1	<0.05	<0.02	0.08	<0.05	<0.003	<0.07	<0.5	0.7	<0.08	1.2
EOR-B18	62	96		65.40		6.41	0.80	2.87	3.90		<0.4	0 07		<0 07	<0.15	<0.06	<0.02	0.05	<0.05	0 0018			1.5	<0 08	1.3
EOR-B19*	66	103		26.10		37.60	1.07	2.82	3.81		<0.4	0.07		<0.07	<0.15	<0.06	<0.02	0.05	<0.05	0.0028			1.3	<0.08	1.2
EOR-B28*	70	92		140.00		0.25	0.25	2.97	5.10	1.45	<0.4	0.09		<0.05	<0.15	0.11	<0.02	0.05	<0.05					<0.05	<0.3
EOR-B29	70	92		3.15		0.20	0.33	2.62	4 65		<0.4	0.09		<0.05	<0.15	0.11	<0.02	0.05	<0.05					<0.05	<0.3
EOR-B30	65	90	21	36.10	4.72	22.70	0.79	2.30	4.90	<0.4	<0.4	0.03	<0.08	<0.07	0.10	<0.05	<0.02	<0.08	<0.05	0.003	<0.07	<0.5	<0.7	<0.08	<0.3
EOR-B31	70	97		92.00		0.25	0.18	3.43	5.35		<0.4	0.09		<0.05	<0.15	0.10	<0.02	0.05	<0.05					<0.05	<0.3
EOR-B98	174	150	24	0.51	6.44	0.20	0.50	4.30	4.30	0.1	<0.4	0.05	<0.07	<0.07	<0.1	<0.05	<0.02	<0.07	<0.05	<0.003	0.1	<0.5	<0.7	0.11	<0.3
EOR-B70	170	313	21	2.19	7.10	6.10	1.25	3.70	3.20	<0.1	<0.4	<0.04	<0.07	<0.07	<0.1	0.04	<0.02	<0.07	<0.05	<0.003	<0.07	<0.5	0.6	<0.08	<0.3
EOR-B72	140	267	17	8.54	6.10	10.40	3.59	3.10	10.70	<0.1	<0.4	<0.04	<0.07	<0.07	<0.1	0.05	<0.02	<0.07	<0.05	<0.003	<0.07	<0.5	<0.7	<0.08	<0.3
EOR-B50	239	195	31	0.75	10.70	0.06	0.61	3.40	4.30	<0.4	<0.4	0.04	<0.08	<0.07	<0.1	<0.05	<0.02	<0.08	<0.05	<0.003	<0.07	<0.5	<0.7	<0.08	<0.3
EOR-B51	173	192	26	0.51	6.27	<0.06	0.34	3.00	5.70	0.2	<0.4	0.03	<0.08	<0.07	<0.1	<0.05	<0.02	<0.08	<0.05	<0.003	<0.07	<0.5	<0.7	<0.08	<0.3
EOR-B78	184	542		7.50	5.40	<0.06	0.60	3.30	4.70	<0 4	<0.4	<0.04	<0.07	<0.07	<0.1	<0.06	<0.02	<0.07	<0.05	<0.003	<0.07	<0.5	<0.7	<0.08	<0.3
EOR-B79	193	958	37	9.00	5.20	0.50	0.33	3.40	4.10	0.2	<0.4	<0.04	<0.07	<0.07	<0.1	<0.06	<0.02	<0.07	<0.05	<0.003	<0.07	<0.5	<0.7	<0.08	<0.3
EOR-B80	180	133	36	0.50	8.10	<0.06	0.51	4.00	4.20	<0.4	<0.4	<0.04	<0.07	<0.07	<0.1	<0.06	<0.02	<0.07	<0.05	<0.003	<0.07	<0.5	<0.7	<0.08	<0.3
EOR-B81	214	175	23	0.90	7.10	0.40	0.34	3.70	2.40	<0.4	<0.4	<0.04	<0.07	<0.07	<0.1	<0.06	<0.02	<0.07	<0.05	<0.003	0.06	<0.5	<0.7	<0.08	<0.3
EOR-B86	256	117	37	0.17	7.61	1.94	0.86	4.10	5.70	0.2	<0.4	0.05	<0.07	<0.07	<0.1	<0.05	<0.02	<0.07	<0.05	<0.003	0.09	<0.5	<0.7	<0.08	0.1
EOR-B93	187	133	30	0.77	5.93	0.60	0.52	5.40	5.20	0.1	<0.4	0.04	<0.07	<0.07	<0.1	<0.05	<0.02	<0.07	<0.05	<0.003	<0.07	<0.5	<0.7	<0.08	<0.3
EOR-B52	174	106	28	0.26	6.77	0.17	0.87	2.20	5.20	0.2	<0.4	0.03	<0.08	<0.07	<0.1	<0.05	<0.02	<0.08	<0.05	0.009	<0.07	<0.5	<0.7	<0.08	<0.3
EOR-B65	213	77	41	1.30	15.60	0.10	0.43	2.70	4.70	0.2	<0.4	0.03	<0.07	<0.07	<0.15	<0.05	<0.02	<0.07	<0.05	<0.003	<0.07	<0.5	<0.7	<0.08	<0.3
EOR-B69	158	75	17	0.14	6.40	0.10	1.36	2.72	5.90	0.3	<0.4	<0.04	<0.07	<0.07	<0.15	<0.05	<0.02	<0.07	<0.05	<0.003	<0.07	<0.5	<0.7	<0.08	<0.3
EOR-B97	124	55	15	2.56	3.53	12.40	0.93	2.50	6.40	0.1	<0.4	0.02	<0.07	<0.07	<0.1	<0.05	<0.02	<0.07	<0.05	<0.003	<0.07	<0.5	<0.7	<0.08	<0.3
EOR-B102	100	54	26	2.47	2.80	12.00	1.28	2.62	7.80	0.3	<0.4	<0.04	<0.08	<0.07	0.15	<0.05	<0.02	<0.08	<0.05	<0.003	<0.07	<0.5	<0.7	<0.08	<0.3
EOR-B11	255	274	29	0.74		1.20	0.69	4.88	4 46		<0.4	0.21		<0.01	<0.15	0.09	<0.02	0.10	<0.05					<0.01	0.6
EOR-B12	356	145	29	0.06		0.97	0.34	9.21	4.21		<0.4	0.21		<0.05	<0.15	0.09	<0.02	0.10	<0.05					<0.01	0.6
EOR-B13	354	312	46	0.57	15.00	6.40	0.73	4.05	4.50	0.2	<0.4	0.05	<0.08	<0.07	<0.15	0.01	<0.02	0.01	<0.05	0.03	<0.07	<0.5	<0.8	<0.08	<0.3
EOR-B62	247	247	29	4.13	11.10	<0.06	0.41	3.80	4.30	<0.2	<0.4	0.05	<0.08	<0.07	<0.15	0.02	<0.02	<0.08	<0.05	<0.003	<0.07	<0.5	<0.8	<0.08	<0.3
EOR-B107	175	322	26	2.77	7.10	34.90	1.43	3.94	6.70	0.3	<0.4	<0.04	<0.08	<0.07	<0.1	<0.05	<0.02	<0.08	<0.05	<0.003	<0.07	<0.5	<0.7	<0.08	<0.3
EOR-B108	241	251	32	8.28	6.70	52.30	2.25	3.45	7.40	0.3	<0.4	<0.04	<0.08	<0.07	<0.1	<0.05	<0.02	<0.08	<0.05	<0.003	<0.07	<0.5	<0.7	<0.08	<0.3
EOR-B101	149	149	26	0.29	5.82	5.00	1.20	2.30	4.00	0.1	<0.4	0.03	<0.07	<0.07	<0.1	<0.05	<0.02	<0.07	<0.05	<0.003	<0.07	<0.5	<0.7	<0.08	1.6
EOR-B114	112	118	31	0.29	3.70	5.80	1.10	3.21	1.90	0.2	<0.4	<0.04	<0.08	<0.07	<0.1	<0.06	<0.02	<0.08	<0.05	<0.003	<0.07	<0.5	<0.7	<0.08	<0.3
EOR-B85	171	268	18	0.60	7.40	0.80	0.66	3.30	2.70	0.1	<0.4	<0.04	<0.07	<0.07	<0.1	<0.06	<0.02	<0.07	<0.05	<0.003	<0.07	<0.5	<0.7	<0.08	<0.3
EOR-B56	182	272	31	1.88	8.51	5.40	0.84	2.80	3.90	0.3	<0.4	0.05	<0.08	<0.07	<0.1	<0.05	<0.02	<0.08	<0.05	<0.003	<0.07	<0.5	<0.7	<0.08	<0.3
EOR-B99	210	321	23	0.81	12.90	1.40	0.52	2.80	4.40	0.1	<0.4	0.03	<0.07	<0.07	<0.1	<0.05	<0.02	<0.07	<0.05	<0.003	<0.07	<0.5	<0.7	<0.08	<0.3
EOR-B4	173	559	26	6.63		5.70	0.68	3.79	2.47		<0.4			<0.07	<0.15	0.19	<0.02	0.10	<0.05					<0.08	
EOR-B5	174	631	24	5.59		10.40	0.92	4.06	2.17		<0.4			<0.07	<0.15	0.19	0.04	0.10	<0.05					<0.08	
EOR-B6	181	574	36	17.40	13.60	2.80	0.71	4.02	3.80	0.1	<0.4	0.04	<0.08	<0.07	<0.15	<0.05	0.02	0.03	<0.05	<0.003	<0.07	<0.5	<0.8	<0.08	0.9
EOR-B7	180	614	21	4.63		21.80	1.02	4.00	8.91		<0.4			<0.07	<0.15	0.19	<0.02	0.10	0.02					<0.08	
EOR-B60	190	441	31	12.50	12.00	6.00	0.74	1.80	3.30	<0.2	<0.4	0.04	<0.08	<0.07	<0.15	<0.05	<0.02	<0.08	<0.05	<0.003	<0.07	<0.5	<0.8	<0.08	<0.3
EOR-B100	168	452	29	3.92	9.91	0.60	0.94	2.20	3.80	0.1	<0.4	0.02	<0.07	<0.07	<0.1	<0.05	<0.02	<0.07	<0.05	<0.003	<0.07	<0.5	<0.7	<0.08	<0.3
EOR-B90	176	133	25	0.26	7.00	0.06	0.76	3.60	4.50	0.1	<0.4	0.03	<0.07	<0.07	<0.1	<0.05	<0.02	<0.07	<0.05	<0.003	<0.07	<0.5	<0.7	<0.08	<0.3
EOR-B91	149	125	26	0.17	5.77	2.30	0.55	3.30	5.50	0.1	<0.4	0.05	<0.07	<0.07	<0.1	<0.05	<0.02	<0.07	<0.05	<0.003	<0.07	<0.5	<0.7	<0.08	<0.3
EOR-B109	130	247	23	3.17	5.60	0.30	0.39	2.16	6.40	0.4	<0.4	<0.04	<0.08	<0.07	<0.1	<0.05	<0.02	<0.08	<0.05	<0.003	<0.07	<0.5	<0.7	<0.08	<0.3
EOR-B77	219	157	18	0.17	11.70	0.30	0.28	6.90	2.80	<0.1	<0.4	<0.04	<0.07	<0.07	<0.1	0.03	<0.02	<0.07	<0.05	<0.003	<0.07	<0.5	<0.7	<0.08	<0.3
EOR-B84	211	218	23	2.20	7.10	0.30	1.15	3.30	3.70	0.2	<0.4	<0.04	<0.07	<0.07	<0.1	<0.06	<0.02	<0.07	<0.05	<0.003	0.1	<0.5	<0.7	<0.08	<0.3
EOR-B8*	205	173	33	0.49		5.70	0.62	3.80	4.68		<0.4	0.15		<0.07	<0.15	0.11	<0.02	0.08	<0.05					<0.08	1
EOR-B9	280	199	36	0.75	10.70	<0.06	0.56	3.40	4.40	0.3	<0.4	0.04	<0.08	<0.07	<0.1	<0.05	<0.02	<0.02	<0.05	<0.003	<0.07	<0.5	<0.7	<0.08	<0.3
EOR-B67	70	32	10	0.15	1.70	12.70	4.42	2.72	<0.5	<0.4	<0.4	<0.04	<0.07	<0.07	<0.15	<0.05	<0.02	<0.07	<0.05	<0.003	<0.07	<0.5	<0.7	<0.08	<0.3
EOR-B53	184	145	40	0.27	10.40	20.20	1.77	2.80	4.40	0.3	<0.4	0.06	<0.08	<0.07	<0.1	<0.05	<0.02	<0.08	<0.05	0.009	<0.07	<0.5	<0.7	<0.08	<0.3
EOR-B89	146	95	27	0.13	5.83	3.00	1.30	4.20	4.70	0.1	<0.4	0.04	<0.07	<0.07	<0.1	<0.05	<0.02	<0.07	<0.05	<0.003	<0.07	<0.5	<0.7	<0.08	<0.3
EOR-B14	98	130	26	2.28		0.78	0.32	2.94	3.83		<0.4	0.15		<0.07	<0.15	0.04	<0.02	0.08	<0.05					<0.08	0 6
EOR-B15*	86	141	33	15.30		0.69	0.50	2.66	5.08		<0.4	0.14		<0.07	0.14	0.02	<0.02	0.08	<0.05					<0.08	0.4
EOR-B16	97	151	28	0.90		0.74	0.25	3.01	3.97		<0.4	0.15		<0.07	<0.15	0.03	<0.02	0.08	<0.05					<0.08	0.7
EOR-B34	112	144	33	2.83	4.50	4.00	1.02	2.54	3.30	<0 4	<0.4	0.03	<0.07	<0.07	<0.15	<0.05	<0.02	<0.08	<0.05	<0.003	<0.07	<0.5	<0.7	<0.08	<0.3
EOR-B36	102	175	25	0.52	5.20	0.19	0.89	1.67	3.50	0.1	<0.4	0.03	<0.07	<0.07	<0.15	<0.05	<0.02	<0.08	<0.05	<0.003	<0.07	<0.5	<0.7	<0.08	<0.3
EOR-B37	105	191		0.39		36.80	2.61	3.05	9.15		<0.4	0.19		<0.07	<0.15		<0.02		<0.05					<0.08	<0.3
EOR-B63	84	120	24	0.46	3.00	12.80	1.73	1.78	6.10	0.2	<0.4	<0.04	<0.07	<0.07	<0.15	<0.05	<0.02	<0.08	<0.05	<0.003	<0.07	<0.5	<0.7	0.1	<0.3
EOR-B64	101	168	25	0.79	4.40	0.12	1.08	1.91	3.50	0.2	<0.4	<0.04	<0.07	<0.07	<0.15	<0.05	<0.02	<0.08	<0.05	<0.003	<0.07	<0.5	<0.7	<0.08	<0.3
EOR-B35	61	132	17	10.90	1.90	<0.06	0.15	1.95	5.70	0.1	<0.4	<0.04	<0.07	<0.07	<0.15	0.03	<0.02	<0.08	<0.05	<0.003	<0.07	<0.5	<0.7	<0.08	<0.3
EOR-B73	80	315	16	183.00	3.70	5.40	2.63	2.90	5.20	<0.1	<0.4	<0.04	<0.07	0.11	<0.1	0.06	<0.02	<0.07	<0.05	<0.003	<0.07	<0.5	<0.7	<0.08	<0.3
EOR-B74	79	165	6	16.30	2.20	9.50	1.92	4.40	0.60	0.1	<0.4	<0.04	<0.07	<0.07	0.40	<0.05	<0.02	<0.07	<0.05	<0.003	<0.07	<0.7	<0.7	<0.08	<0.3
EOR-B110	90	202	11	22.20	2.50	18.70	4.84	3.46	15.40	0.3	<0.4	<0.04	<0.08	<0.07	<0.1	<0.06	0.02	<0.08	<0.05	<0.003	<0.07	<0.5	<0.7	<0.08	<0.3
EOR-B38	282	242	46	0.55	13.90	5.50	0.58	4.00	5.30	<0.4	<0.4	0.04	<0.08	<0.07	<0.1	<0.05	<0.02	<0.02	<0.08	0.008	<0.07	<0.5	<0.7	<0.08	<0.3
EOR-B39	96	158	18	3.18	4.81	<0.06	1.50	2.20	4.70	0.3	<0.1	0.05	<0.08	<0.07	<0.15	<0.5	<0.02	<0.08	<0.05	<0.003	<0.07	<0.5	<1	<0.08	<0.3
EOR-B40	130	167	18	1.71	5.56	<0.06	1.10	2.20	4.40	0.4	<0.1	0.05	<0.08	<0.07	<0.15	<0.5	<0.02	<0.08	<0.05	<0.003	<0.07	<0.5	<1	<0.08	<0.3
EOR-B41	131	147	17	1.15	5.00	<0.06	1.89	2.76	4.20	0.2	<0.4	0.03	<0.07	<0.07	<0.15	0.02	<0.02	<0.07	<0.05	<0.003	<0.07	<0.5	0.8	<0.08	<0.3
EOR-B42*	143	268	22	9.36	6.77	2.60	1.60	2.40	4.80	0.2	<0.1	0.04	<0.08	<0.07	<0.15	<0.5	<0.02	<0.08	<0.05	<0.003	<0.07	<0.5	<1	<0.08	<0.3
EOR-B43	127	174	22	1.21	5.40	<0.06	2.50	2.00	8.80	0.2	<0.1	0.05	<0.08	<0.07	<0.15	<0.5	<0.02	<0.08	<0.05	<0.003	<0.07	<0.5	<1	<0.08	<0.3
EOR-B44	87	164	14	0.89	5.50	1.60	2.25	2.69	4.20	0.2	<0.4	0.03	<0.07	<0.07	<0.15	<0.05	<0.02	<0.07	<0.05	<0.003	<0.07	<0.5	<0.7	<0.08	<0.3
EOR-B87	133	99	27	0.32	4.64	0.09	3.20	4.10	9.10	0.1	<0.4	0.04	<0.07	<0.07	<0.1	<0.05	<0.02	<0.07	<0.05	<0.003	0.11	<0.5	<0.7	<0.08	<0.3
EOR-B116	108	306	36	34.20	3.00	15.50	2.54	2.47	0.90	0.3	<0.4	<0.04	<0.08	<0.07	<0.1	<0.06	<0.02	<0.08	<0.05	<0.003	<0.07	<0.5	<0.7	<0.08	<0.3
EOR-B24*	186	302		11.80		8.00	2.57	3.28	4.14		<0.4	0.21		<0.05	<0.15	0.24	<0.02	0.10	<0.05					<0.05	<0.3
EOR-B25*	153	195		90.50		5.70	1.69	2.98	4.84		<0.4	0.71		<0.05	<0.15	0.20	<0.02	0.09	<0.05					<0.05	<0.3
EOR-B26*	160	216		26.50		16.10	1.67	3.02	4.51		<0.4	0.18		<0.05	<0.15	0.18	<0.02	0.09	<0.05					<0.05	<0.3
EOR-B27	172	302	46	14.20	6.31	5.70	3.22	1.60	3.30	<0.4	<0.4	0.04	<0.08	<0.07	<0.1	<0.05	<0.02	<0.08	<0.05	0.011	<0.07	<0.5	<0.7	<0.08	1.2
EOR-B76	113	301	18	6.73	5.70	2.30	3.26	2.50	5.00	0.2	<0.4	<0.04	<0.07	<0.07	<0.1	0.02	<0.02	<0.07	<0.05	<0.003	<0.07	<0.5	<0.7	<0.08	<0.3
EOR-B68	103	50	18	7.26	2.70	65.30	1.78	2.77	6.00	0.2	<0.4	<0.04	<0.07	<0.07	<0.15	<0.05	<0.02	<0.07	<0.05	<0.003	<0.07	<0.5	<0.7	<0.08	<0.3
EOR-B82	229	164	34	0.60	7.90	12.90	1.87	3.40	3.00	<0.4	<0.4	<0.04	<0.07	<0.07	<0.1	<0.06	<0.02	<0.07	<0.05	<0.003	<0.07	<0.5	<0.7	<0.08	<0.3
EOR-B83	216	180	27	1.90	7.10	7.00	0.89	3.80	5.60	0.1	<0.4	<0.04	<0.07	<0.07	<0.1	<0.06	<0.02	<0.07	<0.05	<0.003	0.05	<0.5	<0.7	<0.08	<0.3
EOR-B96	151	100	24	0.29	5.49	4.80	0.50	2.30	5.00	0.1	<0.4	0.04	<0.07	<0.07	<0.1	<0.05	<0.02	<0.07	<0.05	<0.003	<0.07	<0.5	<0.7	<0.08	<0.3
EOR-B1*	125	133	25	3.45		0.92	0.43	4.55	3.05		<0.4			<0.05	<0.15	0.19	<0.02	0.08	0.02					<0.08	
EOR-B2*	122	131	27	15.80	12.10	0.47	0.71	2.82	3.50	0.7	<0.4	<0.04	<0.07	<0.07	<0.15	<0.05	<0.02	<0.08	<0.05	<0.003	0.07	<0.05	<0.7	<0.08	1.8
EOR-B3*	118	144	24	15.60		1.34	0.53	4.21	2.66		<0.4			<0.05	<0.15	0.16	<0.02	0.08	<0.05					<0.08	
EOR-B106	216	263	38	0.90	8.20	0.40	0.69	7.95	6.20	0.3	<0.4	<0.04	<0.08	<0.07	<0.1	<0.05	<0.02	<0.08	<0.05	<0.003	<0.07	<0.5	<0.7	<0.08	<0.3
EOR-B111	71	117	17	11.60	3.80	12.00	0.77	4.25	2.20	0.3	<0.4	<0.04	<0.08	<0.07	<0 1	<0.06	<0.02	<0.08	<0.05	<0.003	<0.07	<0.5	<0.7	<0.08	<0.3
EOR-B113	41	39	9	6.60	1.70	1.50	0.38	3.42	2.30	0.1	<0.4	<0.04	<0.08	<0.07	<0.1	<0.06	<0.02	<0.07	<0.05	<0.003	<0.07	<0.5	<0.7	<0.08	<0.3
EOR-B75	168	197	20	0.53	7.40	<0.1	0.55	4.90	3.00	0.2	<0.4	<0.04	<0.07	<0.07	<0.1	<0.05	<0.02	<0.07	<0.05	<0.003	<0.07	<0.7	<0.7	<0.08	<0.3
EOR-B20*	136	191		9.75		13.70	0.56	2.71	3.40		<0.4	0.12		<0.05	<0.15	<0.06	<0.02	0.07	<0.05	0.014				<0.08	1.2
EOR-B21*	137	201		6.55		4.03	0.79	2.78	3.30		<0.4	0.12		<0.05	<0.15	<0.06	<0.02	0.07	<0.05	0.014				<0.08	1.1
EOR-B22	128	204	29	6.42	5.51	15.30	0.44	1.20	3.70	0.2	<0.4	0.03	<0.08	<0.07	<0.1	<0.05	<0.02	<0.08	<0.05	0.003	<0.07	<0.5	<0.7	<0.08	0.8
EOR-B23	134	195		7.10		18.00	0.72	2.79	3.19		<0.4	0.12		<0.07	<0.15	<0.06	<0.02	0.07	<0.05	0.014				<0.08	0.7
EOR-B45*	201	309		0.38	13.10	3.30	0.50	2.80	4.10	<0.4	<0.4	0.06	<0.08	<0.07	<0.1	0.09	<0.02	<0.08	<0.05	<0.003	<0.07	<0.5	<0.8	<0.08	<0.3
EOR-B46*	190	294	22	0.31	13.00	6.00	0.50	2.60	3.80	0.3	<0.4	0.07	<0.08	<0.07	<0.1	0.10	<0.02	<0.08	<0.05	<0.003	<0.07	<0.5	<0.8	<0.08	<0.3
EOR-B47*	199	308	21	4.66	12.40	0.80	0.50	2.60	3.60	0.2	<0.4	0.04	<0.08	<0.07	<0.1	<0.05	<0.02	<0.08	<0.05	<0.003	<0.07	<0.5	<0.8	<0.08	0.9
EOR-B49*	199	304	21	6.47	12.00	0.60	0.50	2.50	4.70	0.3	<0.4	0.04	<0.08	<0.07	<0.1	<0.05	<0.02	<0.08	<0.05	<0.003	<0.07	<0.5	<0.8	<0.08	<0.3
EOR-B48*	198	297	21	2.42	12.40	0.90	0.50	2.70	4.30	0.3	<0.4	0.05	<0.08	<0.07	<0.1	<0.05	<0.02	<0.08	<0.05	<0.003	<0.07	<0.5	<0.8	<0.08	<0.3
EOR-B32*	190	315		0.67		0.68	0.79	4.22	6.10		<0.4	0.21		<0.05	<0.15	0.24	<0.02	0.10	<0.05					<0.05	<0.3
EOR-B33*	190	304		0.38		14.80	0.65	4.31	5.00		<0.4	0.21		<0.05	<0.15	0.21	<0.02	0.10	<0.05					<0.05	<0.3
EOR-B59	196	381	35	0.44	10.60	17.20	1.04	2.19	3.40	0.2	<0 4	0.05	<0.08	<0 07	<0.15	<0.05	0.49	<0.08	<0.05	<0.003	<0.07	<0.5	<0.8	<0.08	1.2

APPENDIX C Identification of Core Samples for Which Mineralogical Data Were Available

Sample API no.	Well name	Field name	Formation	Average depth (ft)
01120	Mattoon no. 1	Mattoon	Aux Vases	1902.0
00312	Bates no. 1	Mattoon	Aux Vases	1882.0
23465	Morgan Coal no. 2	Energy	Aux Vases	2391.4
23491	Burr Oak no. 3	Energy	Aux Vases	2406.3
00392	L. M. Compton no. 1	Mode	Aux Vases	1813.0
23456	McCreery no. 1	Dale Consol.	Aux Vases	3204.9
23744	Mack no. 1 (020*4)	Zeigler	Aux Vases	2623.0
23750	Mack no. 2	Zeigler	Aux Vases	2617.3
23753	Mack no. 3	Zeigler	Aux Vases	2642.5
23768	Mack no. 5	Zeigler	Aux Vases	2623.4
23769	Mack no. 6	Zeigler	Aux Vases	2625.6
	Misc. Mack Sample	Zeigler	Aux Vases	2626.0
01070	Novak no. 4	Oakdale	Aux Vases	2880.0
01543	Horrell no. 3	Oakdale	Aux Vases	2915.0
23499	Breeze no. 1	Oakdale	Aux Vases	2880.6
00078	G. D. Chaffee no. 1	Stewardson	Aux Vases	1954.0
01862	Chaffee no. 8	Stewardson	Aux Vases	1970.0
01972	Price no. 1	Boyd	Aux Vases	2133.0
01950	Sanders no. 7	Boyd	Aux Vases	2148.0
01935	F. High no. 2	Boyd	Aux Vases	2130.0
00496	E. W. Hale	King	Aux Vases	2740.0
00488	Ford no. 1	King	Aux Vases	2738.0
00490	L. Wallace no. 1	King	Aux Vases	2732.0
00090	I. W. Mace no. 1	King	Aux Vases	2752.0
00459	St. Game Farm no. 1	King	Aux Vases	2748.5
01301	Eugene Tnan no. 1	Mattoon	Cypress	1803.0
01131	Anna Strong no. 8	Mattoon	Cypress	1778.0
00795	Ruth Uphoft no. 6	Mattoon	Cypress	1821.0
01319	Strong-Seamen no. 1	Mattoon	Cypress	1831.0
01169	Kuehne Mfg. no. 1	Mattoon	Cypress	1813.0
00291	Joshua Akers no. 1	Mattoon	Cypress	1860.0
01330	Elizabeth Strong no. 7	Mattoon	Cypress	1872.0
00788	N. D. Rick no. 9	Mattoon	Cypress	1866.0
00325	A. G. Carnine no. 1	Mattoon	Cypress	1736.0
02187	Stockton Lease no. 1	Tamaroa	Cypress	1160.5
00551	Kampwerth no. 1	Bartelso	Cypress	1002.0
01266	Hempen no. 1	Bartelso	Cypress	1063.0
01812	Droege Unit no. 2	Richview	Cypress	1498.5
01165	Campbell Lease no. 3	Xenia East	Cypress	2538.0